To be submitted to Meteoritics & Planetary Sciences, version 12/24/2013

# Fall, Recovery and Characterization of the Novato L6 Chondrite Breccia

Peter JENNISKENS[1,2*], Alan E. RUBIN[3], Qing-Zhu YIN[4], Derek SEARS[2,5], Scott A. SANDFORD[2], Michael E. ZOLENSKY[6], Alexander N. KROT[7], Leigh BLAIR[1], Darci KANE[8], Jason UTAS[9], Robert VERISH[10], Jon M. FRIEDRICH[11,12], Josh WIMPENNY[4], Gary R. EPPICH[13], Karen ZIEGLER[14], Kenneth L. VEROSUB[4], Douglas J. ROWLAND[15], Jim ALBERS[1], Peter S. GURAL[1], Bryant GRIGSBY[1], Marc D. FRIES[6], Robert MATSON[16], Malcolm JOHNSTON[17], Elizabeth SILBER[18], Peter BROWN[18], Akane YAMAKAWA[4], Matthew E. SANBORN[4], Matthias LAUBENSTEIN[19], Kees C. WELTEN[20], Kunihiko NISHIIZUMI[20], Matthias M. M. MEIER[21,22], Henner BUSEMANN[23], Patricia CLAY[23], Marc W. Caffee[24], Phillipe SCHMITT-KOPPLIN[25,26], Norbert HERTKORN[25], Daniel P. GLAVIN[27], Michael P. CALLAHAN[27], Jason P. DWORKIN[27], Qinghao WU[28], Richard N. ZARE[28], Monica GRADY[29], Sasha VERCHOVSKY[29], Vacheslav EMEL'YANENKO[30], Sergey NAROENKOV[30], David CLARK[18], Beverly GIRTEN[2], and Peter S. WORDEN[2]
(Novato Meteorite Consortium)

[1] SETI Institute, Carl Sagan Center, Mountain View, CA 94043, USA.
[2] NASA Ames Research Center, Moffett Field, CA 94035, USA.
[3] Institute of Geophysics and Planetary Physics, UCLA, Los Angeles, CA 90095-1567, USA.
[4] Department of Earth and Planetary Sciences, University of California at Davis, One Shields Avenue, Davis, CA 95616-8605, USA.
[5] BAER Institute, Mountain View, CA, USA.
[6] Astromaterials Research and Exploration Sci., NASA Johnson Space Center, Houston, TX 77801, USA.
[7] Hawai'i Institute of Geophysics and Planetology, University of Hawai'i at Manoa, Honolulu, HI 96822
[8] Buck Institute, 8001 Redwood Blvd., Novato, CA 94945, USA.
[9] UCLA, Los Angeles, CA, USA.
[10] Meteorite Recovery Lab., P. O. Box 463084, Escondido, CA 92046, USA.
[11] Department of Chemistry, Fordham University, Bronx, New York 10458, USA.
[12] Dep. of Earth and Plan. Sciences, American Museum of Natural History, New York, NY 10024, USA.
[13] Glenn Seaborg Institute, Lawrence Livermore National Laboratory, Livermore, CA 94550, USA
[14] Institute of Meteoritics, University of New Mexico, Albuquerque, NM 7131-0001, USA.
[15] Center for Molecular and Genomic Imaging, University of California at Davis, One Shields Avenue, Davis, CA 95616, USA.
[16] S.A.I.C., San Diego, CA 92121, USA.
[17] US Geological Survey, 345 Middlefield Road, Menlo Park, CA 94025, USA.
[18] Department of Physics & Astronomy, Univ. of Western Ontario, London, Ontario, N6A 3K7, Canada
[19] Inst. Naz. di Fiscia Nucleare, Lab. Naz. del Gran Sasso, S.S. 17/bis, I-67010 Assergi (AQ), Italy.
[20] Space Sciences Laboratory, University of California, Berkeley, CA 94720, USA.
[21] Department of Earth Sciences, ETH Zürich, Clausiusstrasse 25, CH-8092 Zürich, Switzerland.
[22] Department of Geology, Lund University, SE-22362 Lund, Sweden.
[23] School of Earth, Atmospheric and Environmental Sciences (SEAES), University of Manchester, Oxford Road, Manchester M13 9PL, UK.

[24] Department of Physics, Purdue University, West Lafayette, Indiana 47907, USA
[25] B.G.C., Helmholtz Zentrum München, D-85764 München, Germany.
[26] A.L.C., Technische Universität München-TUM, Freising, Germany.
[27] Solar System Exploration Division, NASA Goddard Space Flight Center, Greenbelt, MD 20771, USA.
[28] Department of Chemistry, Stanford University, Stanford, CA 94305-5080, USA.
[29] Planet. and Space Sci. Res. Inst., Open University, Milton Keynes MK7 6AA, UK.
[30] Institute of Astronomy of the Russian Academy of Sciences (INASAN), Pyatnitskaya 48, Moscow 119017, Russia.

*Corresponding author. Email: Petrus.M.Jenniskens@nasa.gov

*Submitted to MAPS, 12.24.2013 / Revised XX.XX.2014*

**Abstract –** The Novato L6 chondrite fragmental breccia fell in California on 17 October 2012, and was recovered after the Cameras for Allsky Meteor Surveillance (CAMS) project determined the meteor's trajectory between 95 and 45 km altitude. The final fragmentation at 33–21 km altitude was exceptionally well documented by digital photographs. The first sample was recovered before rain hit the area. First results from a consortium study of the meteorite's characterization, cosmogenic and radiogenic nuclides, origin and conditions of the fall are presented. Some meteorites did not retain fusion crust and show evidence of spallation. Before entry, the meteoroid was 35±5 cm in diameter (mass 80±35 kg) with a cosmic ray exposure age of 9±1 Ma, if it had a one-stage exposure history. However, based on the cosmogenic nuclide inventory, a two-stage exposure history is more likely, with lower shielding in the last few Ma. Thermoluminescence data suggest a collision event within the last ~0.1 Ma. Novato likely belonged to the class of shocked L chondrites that have a common shock age of 470 Ma, based on the U,Th-He age of 460±220 Ma. The measured orbits of Novato, Jesenice and Innisfree are consistent with a proposed origin of these shocked L chondrites in the Gefion asteroid family, but leave open the possibility that they came to us directly from the 5:2 mean motion resonance with Jupiter. Novato experienced a stronger compaction than did other L6 chondrites of shock-stage S4. Despite this, a freshly broken surface shows a wide range of organic compounds.

## INTRODUCTION

In the evening of Wednesday 17 October 2012, a bright fireball was widely observed and photographed from locations in and around the San Francisco Bay Area. Following the fireball sighting, six meteorites were recovered in the town of Novato (Fig. 1a). The meteorite is an L6 ordinary chondrite breccia of shockstage S4, composed of dark and light lithologies (Fig. 1b).

Initial reports in the media put the impact location erroneously in the hills north of Martinez, CA. Fortunately, the fireball crossed the camera fields of NASA's Cameras for Allsky Meteor Surveillance (CAMS) program. This video surveillance of the night sky measures meteoroid trajectories over California in order to map the meteor showers throughout the year (Jenniskens et al., 2011). The calculated downward projected path predicted that 1 g fragments fell near Bolinas, 100 g fragments near Novato, and 1 kg fragments near Sonoma.

The CAMS-derived trajectory was published in the San Francisco Chronicle, initially on-line on Friday evening 19 October (See Fig. 6 below). Novato resident Lisa Webber read the article and remembered hearing the sound of an object hitting the roof of her garage multiple times ("tok-tok-tok-tok") that previous Wednesday night. At the time, she entered the garage thinking raccoons were knocking over objects, but no such disturbance was found. After reading the newspaper article, she searched her yard for possible meteorites on Saturday 20 October. She examined the roof and while climbing down the ladder, she noticed a dense 61.9 g stone near the foot of the ladder (now called Novato N01), which reacted strongly to a permanent magnet.

This Novato meteorite was difficult to distinguish from weathered terrestrial rocks, because the dark lithology did not retain its fusion crust (Fig. 1a). Searching for corroborating evidence of an impact at the Webber residence that evening, neighbor Luis Rivera identified an impact divot. That divot had a shape and location consistent with a meteorite from this fall first hitting the roof above the study room on one side of the U-shaped building, being deflected to the roof over the garage on the other side, where it bounced into the air and fell back several times before landing next to it. Indeed, a second divot was found later, on the side of the garage roof opposite to the study.

A second 65.8 g stone was found in Novato (N02) by Brien Cook on Monday 22 October. It was initially discarded, but subsequent to reports of the Webber find, it was retrieved, cut, and recognized as a meteorite on 24 October. Four more individual meteorites were recovered on pavement in the following weeks (Fig. 1a). An overview of these finds is given in Table 1.

An airship search was commenced along a line from Novato to the geometric impact point, and then back to Sonoma. Deployed from NASA Ames Research Center, the airship Eureka travelled at a 300 m altitude. Two spotters searched the terrain for impact

scars from falling 1–10 kg meteorites over a region ±1 km from the path. After consultation with the local landowners, some potential sites were investigated, but no confirmed impact sites were located.

This exceptionally well observed fall and fresh meteorite recovery led us to assemble a Novato Meteorite Consortium to further the recovery of the meteorites and do the preliminary analysis reported here (http://asima.seti.org/n/). This analysis is focused on characterization and aspects that might forge a link between L-group chondrites and the asteroid family of their parent body.

## METEORITE PROPERTIES AND CLASSIFICATION

### Mechanical and Properties and Magnetic Susceptibility

Of key interest were mechanical and physical properties that play a role in the fragmentation during entry. Parts of Novato N01 (type specimen) and N06 were made available for destructive analysis, while samples N02–N05 were available for nondestructive analysis. Sample N01 was broken in a controlled break (Fig. 1a), using a Southwark-Emery Tensile Machine at NASA Ames, measuring a quasi-static compressive strength of 1,100 ± 250 MPa. This value is much higher than the typical 100–200 MPa measured for ordinary chondrites (Slyuta, 2010). The uncertainty reflects the irregular loading of the surface area that was evident from the meteorite imprint on aluminum foil between sample and pressure surface.

At the Buck Institute, the density of N06 was measured in water at 3.4 ± 0.2 g/cm$^3$. Volumes of samples N06 (mostly dark lithologies) and N05 (light) were measured by High-Resolution X-Ray Computed Tomography at the Center for Molecular and Genomic Imaging at the University of California, Davis (UC Davis) (Fig. 2). Total volumes were calculated to be 4.46 and 7.12 cm$^3$ for N05 and N06, respectively. The samples did not have significant fusion crust. The corresponding densities are 3.21 ± 0.02 and 3.32 ± 0.02 g/cm$^3$, which is in good agreement with the average bulk density of 3.35 ± 0.16 g/cm$^3$ for ordinary L chondrites (Britt and Consolmagno, 2003). Porosity in L chondrites is primarily in the form of microcracks, whose sizes are below the 15–40 micron resolution of the CT volumes collected here. Most other shocked L chondrites have microporosities in the 3–5% range (Britt and Consolmagno, 2003; Friedrich and Rivers, 2013).

Magnetic susceptibility was measured on five samples at UC Davis (Table 1). To some extent the measured values of individual samples varied with their orientation in the susceptibility bridge, suggesting that the susceptibility is somewhat anisotropic. For the five samples, values of log $\chi$ ranged from 4.08 to 4.46 (where $\chi$ is measured in units of $10^{-9}$ m$^3$/kg). This range is below the range (4.75 to 4.95) for L6 meteorites as reported by Rochette et al. (2003).

## Petrography and Mineralogy

A slice of Novato N02 (Fig. 1a) examined at UCLA contained ~55 vol.% chondritic clasts and ~45 vol.% shock-darkened material. Fig. 1b shows details of the morphology. Fig. 3 (a-h) shows backscattered electron (BSE) images and combined X-ray elemental maps of a slab from Novato N06 (Fig. 1b), taken at the University of Hawai'i at Manoa.

The fragment initially examined for petrography at UCLA was from Novato N01. Silicates exhibit weak mosaic extinction, characteristic of a moderate shock-stage S4, corresponding to an equilibrium shock pressure of ≥10–15 GPa (Stöffler et al., 1991). Plagioclase grains range from 50–200 μm, consistent with petrologic type 6 (Van Schmus and Wood, 1967).

There are many troilite veins that transect large portions of the rock causing silicate darkening (Rubin, 1992; Simon et al., 2004). Most chromite grains are fractured; many are transected by troilite veins as is common in S3–S6 chondrites (Rubin, 2003). Also common in such chondrites are chromite-plagioclase assemblages (Rubin, 2003), a few of which occur in Novato (Fig. 3f). One 12×20-μm-size grain of metallic Cu was found. Some of the troilite grains are polycrystalline, consistent with shock stage S4–S5 (Schmitt et al., 1993; Bennett and McSween, 1996). There are regions of localized plagioclase melting, especially around metal and sulfide grains. A few silicate shock melt veins are present that contain small metal and sulfide blebs, consistent with shock stage S4–S6 (Stöffler et al., 1991).

The light-colored chondritic clasts have far fewer troilite veins and contain moderately large, highly recrystallized barred olivine (BO) (Fig. 3b-c) and porphyritic olivine-pyroxene (POP) chondrules that are well integrated into the matrix, consistent with petrologic type 6. These chondritic clasts are much lighter colored in transmitted light than the matrix of the rock.

The mineral compositions of olivine ($Fa_{24.1\pm0.4}$, n=21) and low-Ca pyroxene ($Fs_{20.7\pm0.5}\,Wo_{1.5\pm0.2}$, n=22) are characteristic of L-group chondrites (Rubin, 1990; Brearley and Jones, 1998). Also present among the mafic silicates is high-Ca pyroxene ($Fs_{8.0\pm0.7}\,Wo_{44.7\pm0.8}$, n=5). Chromite grains (n=11) are somewhat richer in $Al_2O_3$ (6.4 wt.%) and MgO (3.4 wt.%) than unshocked ordinary chondrite chromite (Bunch et al., 1967), but are more characteristic of shocked and shock-melted chromite grains (Rubin, 2003). Most of the metallic Fe-Ni is taenite with 21.4±5.4 wt.% Ni and 0.51±0.18 wt.% Co (n=18). Only one kamacite grain was identified (7.2 wt.% Ni and 1.1 wt.% Co). The Co content of this single grain is intermediate between the ranges for L (0.70–0.95 wt.% Co) and LL (1.42–37.0 wt.% Co) chondrites (Rubin, 1990), but is closer to L chondrites. Plagioclase, which has a mean composition of $Ab_{86.0\pm0.6}\,Or_{7.0\pm0.4}$ (n=14), is richer in alkalis than typical ordinary chondrite plagioclase (Van Schmus and Ribbe, 1968), and probably reflects shock melting (Rubin, 1992). Troilite (n=10) is essentially pure FeS; it contains no detectable Cr, Co or Ni.

**Bulk Chemical Composition**

Chemically, the Novato chondrite is a typical L chondrite. A slice of whole rock sample of Novato N06 (Fig. 1b) was analyzed for major element concentration using a Bruker S8 WD-XRF at Lawrence Livermore National Laboratory. These analyses were performed on two flat cut surfaces on both dark and light lithologies. In general, the results (Table 2) suggest that both light and dark portions of the fragment have very similar major element chemistry, with the following caveat. The XRF at Livermore has a minimum sample size of 8 mm round, which is bigger than the light lithology tip of the Novato 06 fragment (Fig. 1b). This means that the 'light' analyses are a mixture of both light and dark material (a ratio of about 70:30).

The abundances of 45 trace elements in the Novato meteorite were measured at Fordham University, using the acid dissolution and quadrupole inductively coupled plasma mass spectrometer (Q-ICP-MS) analysis methodology described in Friedrich et al. (2003). Samples analyzed were Novato N01-2b-4e (three aliquots 90.4 mg, 57.6 mg, 74.7 mg), all dark lithology, N01-2b-6, an aliquot with dark lithology, and a combined aliquot of N01-2b-11, 12 and 17, which consisted of 55% dark and 45% light lithology. Trace element abundances of averaged values are listed in Table 3. The mean lithophile, siderophile, and moderately volatile abundances are presented in Fig. 4a and Table 3. Most important for distinguishing between LL, L, and H chondrites is the mean siderophile abundance. This abundance in Novato is most like that of L chondrites. The apparent enrichment in uranium is often seen in chondrites, probably because of some sample enrichment in phosphate materials, for which U and Th have an affinity.

Using analytical procedures described in Jenniskens et al. (2012) and Popova et al. (2013), we have performed additional wet chemical analyses using the *Element XR* magnetic sector, high-resolution ICP-MS at UC Davis, which offers the possibility to run some elements at higher resolution to avoid potential isobaric interferences. Measured were predominantly light and dark lithology fragments from both N01-1b and N06, and a pure light lithology of Novato N05. Details of the method used and results for Novato and Orgueil are listed in Table 4, and compared with the averaged Q-ICP-MS data obtained at Fordham University.

The rare earth element (REE) patterns of Novato samples normalized to CI chondrites are presented in Fig. 4b. The pure light lithologies from N05 and N06 have positive Eu anomalies, with a lower overall rare earth elements (REE) pattern of 0.8-0.9 compared to CI chondrite (Lodders 2003), whereas the pure dark lithologies from N01 and N06 have negative Eu anomalies and an overall REE enrichment over CI chondrites by 1.4–1.8 (Lodders, 2003). Note that the sample “N01 Light” is not a pure light lithology, but made of mostly dark lithologies. “N01 Ave (F)” is an averaged value of seven larger fragments obtained at Fordham.

The observed pattern is often seen in equilibrated ordinary chondrites (*e.g.,* Haas and Haskin, 1991; Friedrich et al., 2003) and has been attributed to an inhomogeneous distribution of plagioclase (carrier of positive Eu anomalies) and apatites (and pyroxene,

to a lesser extent, as major REE carriers) formed during thermal metamorphism in equilibrated ordinary chondrites, with olivine, metal, and sulfide acting as diluting agents for REE concentration (Mason and Graham, 1970). The melting and mobilization of plagioclase and apatites due to their low impedance to shock compression during shock events is likely limited to a scale of at most 1 mm (Fig. 3f). A gram-sized sample would be required to obtain a representative sampling of Novato given the observed heterogeneous distribution of phosphates and plagioclase (Fig. 3g). Hence, compositional differences that deviate from the "chondritic norm" should be evaluated critically.

### Oxygen and Chromium Isotopes

Oxygen isotopes were measured at the University of New Mexico (Table 5a). Four aliquots derived from Novato N01-2b-1 were all of the dark lithology and provided an average $\delta^{17}O$ = 3.67±0.102‰, $\delta^{18}O$ = 4.812±0.206‰ and $\Delta^{17}O$ = 1.131±0.014‰. Four aliquots from N01-2b-15 were 50% light and 50% dark lithology and had average $\delta^{17}O$ = 3.654±0.034‰, $\delta^{18}O$ = 4.724±0.093‰ and $\Delta^{17}O$ = 1.159 ±0.025‰. Three aliquots from N05-1 provided an average $\delta^{17}O$ = 3.804±0.090‰, $\delta^{18}O$ = 5.010±0.193‰ and $\Delta^{17}O$ = 1.159±0.013‰. These values are not significantly different. Taken together, the oxygen isotope values were $\delta^{17}O$ = 3.701±0.098‰, $\delta^{18}O$ = 4.834 ±0.193‰, and $\Delta^{17}O$ 1.149±0.022‰ (n=8), respectively. These values plot in the overlapping area of the L- and LL-chondrite fields in Fig. 5 (Clayton et al., 1991). The distinction of Novato being L chondrite rather than LL chondrite is more apparent in the $\Delta^{17}O$ *vs.* Fa value of olivine plot (Fig. 5b).

Further evidence for an L chondrite classification comes from the high precision $\varepsilon^{54}Cr$ isotope composition of Novato (Table 5b), which was measured for both dark and light lithologies at UC Davis, following procedures similar to that applied to pieces of the Sutter's Mill carbonaceous chondrite (*c.f.,* Jenniskens et al., 2012). Whereas the dark lithology of Novato is typical of most other ordinary chondrites, the light lithology appears to have an elevated $\varepsilon^{54}Cr$ value (Fig. 5c). We note that $\Delta^{17}O$ values for the light lithology are also higher than that of the dark lithology (Fig. 5d). This is a consistent with the parallel positive trend of $\Delta^{17}O$ vs. $\varepsilon^{54}Cr$ shown for carbonaceous chondrites (Fig. 5d). The underlying cause for such a trend is not well understood.

## CONDITIONS OF THE FALL AND PRE-ATMOSPHERIC ORBIT

### Trajectory and Pre-Atmospheric Orbit

It was quite fortuitous that the fireball traveled through the video camera fields of the CAMS project (Jenniskens et al., 2011). The goal of CAMS is to measure meteor trajectories by triangulation of +4 magnitude meteors and brighter, in order to map meteor showers throughout the year. The project consists of three stations, each equipped with 20 Watec Wat 902H2 Ultimate low-light level video security cameras with 20º × 30º field of view pointed at different directions in the sky so that all elevations above 30º are covered. The stations are located at Fremont Peak Observatory, Lick Observatory and in Sunnyvale, CA. In addition, single cameras with the same specifications are operated by

participating amateur astronomers at several other locations in the San Francisco Bay area.

Five CAMS cameras filmed the first 11.1 seconds of the meteoroid trajectory from three locations (Fig. 6). The Lick Observatory station captured the beginning of the entry trajectory in camera #164. It then emerged behind a tree at the Sunnyvale station, where it was tracked by three video cameras (#152, #51, and #11, respectively). The final part was also captured by the single camera of the College of San Mateo station (#210 in Fig. 7).

To keep the astrometric precision high, each 8 seconds of video is compressed in four frames that contain the peak, average, and standard deviation of brightness at each pixel and the frame number in which peak brightness occurred (Jenniskens et al., 2011). The reconstructed video shows a point-like meteor image in cameras 164 and 152, but a speckled disc due to blooming in later cameras. The centroid of each image was carefully determined and while the centroid may be off-center due to optical distortions, the meteor's path is well recorded in the average image due to integration of the more persistent fireball's wake. The time averaged frame preserves this wake plus a rich (N > 100) star field, which is used for astrometry.

The trajectories calculated using methods described in Jenniskens et al. (2011) based on the two early, unsaturated, records and those for all camera solutions combined, are given separately in Table 6a. Fig. 6 shows the trajectory solutions by combining the first 2, 3, 4, 5 and 6 cameras. The 2-camera solution is hampered by a small convergence angle and large distance from meteor to stations. Solutions with 3 or 4 cameras converge on a solution that aligns with the majority of Novato meteorite finds (Q = 9.5º), labeled N02 to N06 in Fig. 6. The solutions that include the bloomed video of cameras 11 and 51 (Q = 21.4º) tend to produce slightly lower velocities and align closer to the N01 find, passing about 0.7 km east of it (Fig. 6). None of the solutions shows evidence of deceleration due to atmospheric drag above 46 km. Fitting a deceleration curve described in Jenniskens et al. (2011) results in a small value for the deceleration parameter $a_1 < 4\times10^{-7}$ km (and $a_2$ = 1.31±0.04 /s).

Using the Schiaparelli equation to approximate the influence of Earth's gravity on the orbit (columns A–C in Table 6a) results in an orbit that is defined as Earth not being at that location. Such an approximate orbit is not suitable for backward integrations. To create a suitable description of the pre-atmospheric orbit, the entry state vector needs to be integrated backwards to two months before entry, resulting in the orbital elements listed in column D of Table 6a.

**Light Curve and Initial Mass**

For photometry of the fireball, other images were also available. The CAMS videos stop at 46 km, just prior to a set of two bright flares at around 43 km altitude that briefly lit up the sky. A 30-s exposed all-sky image was obtained by Wesley Jones from Belmont, CA, but covers about the same part of the trajectory as the CAMS cameras. From a larger distance, James D. Wray in Foresthill captured the fireball near the horizon, providing a

global view of the brighter parts. The final part of the fireball trajectory was documented in a narrow field digital image by Phil Terzain from a location in the Santa Cruz Mountains (Fig. 6). This photograph shows the very end of the fireball track against stars of the asterism of the Big Dipper. Lick Observatory also captured the final part of the fireball in two security camera videos focused on the near field.

The resulting photometric lightcurve is shown in Fig. 8. The curve is relatively flat over most of the trajectory, with two nearly coincidental flares near the center. The peak brightness, uncertain by at least one visual magnitude, would correspond to a kinetic energy of about 1.4 (0.6–3.6) t of TNT for a luminous efficiency of 7% (ReVelle and Ceplecha, 2001). This would correspond to a meteoroid diameter of 33±10 cm and a mass of 60 (30-160) kg, if the meteoroid had the same density as the recovered meteorites.

**Dark Flight and Source Energy**

Based on upper atmosphere wind sounding data from station 72493 OAK in Oakland at 0h UT on October 18 (http://weather.uwyo.edu/upperair/sounding.html), prevailing winds below 30 km were blowing predominantly from the west over much of the dark flight trajectory, gradually changing to a more northerly and north-easterly direction below 9 km. So, meteorites would have fallen just east of the calculated trajectory, but only by about 430 m perpendicular to the trajectory for a 100 g meteorite and 120 m for a 1 kg meteorite (sphere, density 3.3 g/cm$^3$, fall from 43 km altitude, and drag coefficient $C_d = 0.43$ for Mach number Ma < 0.5, $C_d = 1.00$ for Ma > 1.4, and $C_d = 0.715 + 0.285$ *sin* [3.1415 (Ma/0.9 – 1.05) *rad.*] in between). A 61.9-g stone would have hit the Webber residence at 54 m/s after having broken off at about 35 km altitude.

The falling meteorites may have been detected by the nearest Doppler weather radar KMUX - San Francisco (37º09'18"N, 121º53'52"W) for elevation 3.62º at 2:39:44 UT (Fig. 9). Multiple returns were located over Marin County where meteorites of ~1–10 g were expected to fall. This is a similar size range as thought to have been responsible for the Sutter's Mill radar return signal (Jenniskens et al., 2012).

Audible sounds were reported in Marin County. Low-frequency sound waves emanating from the Novato fireball were detected at I57US, the closest of five infrasonic stations of the International Monitoring System (Christie and Campus, 2010). Located just over 300 km from the event, two arrivals were detected that are consistent with the propagation timing of a typical fireball at such ranges. Utilizing the standard method of cross-correlating the output between each sensor and performing beam forming of the signals across the array (Evers and Haak, 2001), the arrival azimuth corresponds to the predicted azimuth associated with the fireball. Table 7 summarizes the properties of both signal arrivals recorded by I57US. The blast wave coupled to the ground and created a weak seismic signature centered on Mount Tamalpais (+37º55'49"N, 122º36'01"W). No seismic signal from impacting meteorites was detected on high-resolution 3-component borehole strain and seismic instrumentation near Novato and Sonoma.

The infrasound records provide a measure of the source energy, which is derived using several empirical relations. These employ either the period at maximum amplitude or the range and signal amplitude (Ens et al., 2012). Both the dominant period and high frequency content of the signal clearly point to a low-energy source. The yield estimate, based on both of these methodologies, is several tons of TNT equivalent (with the lower range of 1 t, and the upper range of ~10 tons). That would put the pre-atmospheric mass between 45 and 450 kg (nominally 140 kg) and the diameter (if a sphere, using the measured density of 3.4 g/cm$^3$) at around 20-44 cm (nominally 30 cm).

**Fragmentation and Ablation**

A particularly nice set of photographic records of the meteoroid fragmentation was obtained by Robert P. Moreno in Santa Rosa (Fig. 10). During the final 6.2 seconds, when the train of fragments was descending from 33 to 20 km, photographic images were taken with a Canon EOS 7D camera a rate of 4 per second. Only two stars (ψ and ω Cap) are identified in the images. The positions of individual fragments relative to the leading fragment are shown in Fig. 10. Several discrete episodes of breakup are readily visible. The distribution of fragment sizes is determined at each discrete fragmentation, and is not further modified by a subsequent continuous cascading process, as often assumed in meteor models (ReVelle, 2002; Brown et al., 2004). For Novato, discrete episodes of fragmentation continued until the very end, when even the largest masses continue to fall apart. Hence, it is likely that no 10-kg-sized fragments landed on the ground.

Ablation proceeded differently for light and dark materials. A close examination of the exterior of the Novato N01 and N06 stones shows a fine distribution of tiny patches of fusion crust over most of its dark shock-melted surface (Fig. 1a). Those patches show layers (Fig. 11a–b), suggesting discontinuous ablation. In contrast, centered on the light lithology of Novato N04 is a well defined ~2×2-cm-wide fusion crust patch (Fig. 1a).

Both types of fusion crust were derived locally from the melting of the immediate, underlying lithology, with no evidence of mixing of these different melts prior to the crust solidifying. The patches of fusion-crust in contact with the light chondritic material are thicker and look more similar to the fusion-crust seen on other fresh chondrites (*e.g.,* Sears, 1979, pages 34–38; Brown et al., 2004), the thickness caused in part by materials with higher melting points withstanding the heating process longer (Sears and Mills, 1973; Schneider et al., 2000). In contrast, the smaller patches of fusion-crust in contact with the black, shock-darkened lithology appear to have been more viscous before they solidified (Fig. 11a,b). These melts appear to have had more difficulty adhering to that portion of the meteorite due to the lack of low melting point phases (like metal-sulfide eutectics) and the low porosity of the underlying lithology.

**Spallation**

Spallation played a role in the ablative process. One side of Novato N03, a fragment displaying both light and dark lithologies (Fig. 1a), displays a 1–2 mm deep depression with sharp, vertical edges (Fig. 11c–d). A thin flake of dark, impact-melted material 3 × 2

× 0.1–0.2 cm, detached itself from the stone immediately prior to the stone's entering dark flight. Sub-millimeter patches of fusion crust are visible on the exposed surface. As the stone is well-rounded, with traces of fusion crust on all sides, it can be assumed that mechanical spallation occurred while the meteorite was still in ablative flight. Only ~5% of its surface was retained long enough to leave well-developed primary fusion crust.

Pre-entry fractures were dismissed as a potential cause of the spallation. Novato N03 had been run over numerous times by automobiles; it was found sitting amongst ~25 fresh divots in the paved road where it was found. White marks from small amounts of crushed road surface were visible on all sides of the meteorite. Had the stone been internally fractured, it would have fragmented from this maltreatment. However, less than 1 g of fragments (mostly as a single chip) was found in the road ~5 m from the stone, and only a few small fragments were found when the road was systematically searched with a magnet.

It is likely that the brittle nature of the dark impact-melted chondritic material is to blame for the observed exterior spallation. The shock-hardened and impact-melted chondritic material may be more susceptible to fracturing caused by high thermal gradients. The thermal gradient experienced by the outer 3 mm of a stony meteorite can reach approximately 5,000K (Ceplecha et al., 1998).

Spallation as a significant contributor to meteoroid mass loss has been seldom noted in literature, except in the case of carbonaceous chondrites, where it was equated with meteoroid porosity (Baldwin and Shaeffer, 1971). Spallation of fragments with a diameter less than 1/10th of that of the meteoroid can increase the ablating surface area by a factor of ten, if spallation is occurring at a mass loss rate rivaling that of ablation. Theoretical models of the lightcurve and deceleration of the Park Forest meteoroid, another equilibrated chondrite that could have undergone mechanical spallation, suggested a 40% initial porosity (Brown et al., 2004). In contrast, the recovered meteorite fragments' observed average porosity was less than 5%. Subsequent work revisited the luminous efficiency for given mass loss and estimated the meteoroid porosity at only 20%, corresponding to a ~50% lower mass (ReVelle, 2007). Similar lightcurve modeling for Novato is not possible due to the lack of deceleration information for the leading fragment at the end of the trajectory. However, rapid late-stage or continuous mechanical surface spallation of otherwise intact fragments, as observed for Novato, could account for the anomalous luminous efficiency of Park Forest.

## COSMIC RAY EXPOSURE AGE AND ASTEROID FAMILY ORIGINS

### Meteoroid Diameter

To determine the pre-atmospheric size of the meteoroid, the concentrations of short-lived cosmogenic radionuclides, as well as longer-lived cosmogenic $^{26}$Al and natural radioactivity, were measured using non-destructive gamma-ray spectroscopy. The complete stone Novato N01 was measured in the STELLA (SubTErranean LowLevel Assay) facility of underground laboratories at the Laboratori Nazionali del Gran Sasso

(LNGS) in Italy, using a high-purity germanium (HPGe) detector of 518 $cm^3$ (Arpesella, 1996). The specimen was measured at the LNGS 21 days after the fall, so that also very short-lived radionuclides such as $^{52}$Mn (half-life = 5.9 d), $^{48}$V (half-life = 16 d) and $^{51}$Cr (half-life = 27.7d) could be detected.

Table 8a shows the measured activity for the cosmogenic radionuclides. For $^{60}$Co and $^{44}$Ti only upper detection limits can be reported. The given activities are calculated to the date of fall. The counting time was 8.5 days. The uncertainties in the radionuclide activities are dominated by the uncertainty in the counting efficiency, which is conservatively estimated at 10%. The counting efficiencies were calculated using a Monte Carlo code. This code is validated through measurements and analyses of samples of well-known radionuclide activities and geometries. The average density and composition were taken from Britt and Consolmagno (2003) and Jarosewich (1990), respectively.

The activity data of $^{60}$Co, $^{22}$Na and $^{54}$Mn were used to derive a meteoroid size and the approximate depth from where N01 originated in the meteoroid. As the $^{60}$Co concentration in Novato can be given only as an upper detection limit, N01 was either part of a small meteoroid with < 20 cm radius, or originally located very close to the surface of a meteoroid with a radius bigger than 30 cm. The $^{22}$Na data were compared to the calculations of Bhandari et al. (1993) for H chondrites, taking renormalizing to L chondrite elemental concentrations into account, and calculations of Eberhardt et al. (1963) and Spergel et al. (1986). If the measured activity is a saturation value, the resulting possible range in the radius is 15–95 cm. If it is not, and the sample originated from anywhere in the meteoroid, then the possible radius is 15–100 cm. Finally, the concentration of $^{54}$Mn was normalized to the concentration of its main target Fe, and compared to the calculations of Kohman and Bender (1967). This resulted in a radius of 15–70 cm if it came from the central part of the meteoroid, or 10–75 cm if it came from anywhere inside the meteoroid.

A conservative size for a spherical meteoroid, if the sample was derived from the central part of the body, is obtained by combining the results of all three radionuclides. This results in a diameter of 30 to 40 cm (45 to 115 kg mass).

The activities of the short-lived radionuclides are affected by solar modulation, which affects the galactic cosmic ray flux by up to a factor of 2 within a solar cycle. The fall of the Novato L6 chondrite occurred during the end of a solar minimum that preceded the current solar cycle 24. The galactic cosmic ray flux was therefore still high in the six months before the fall. Indeed, the $^{22}$Na/$^{26}$Al ratio of 1.77±0.23 in Novato is on the high end of the range observed for other chondrites (Evans et al., 1982).

The long-lived cosmogenic radionuclides $^{10}$Be ($t_{1/2}$ = 1.36 × $10^6$ yr), $^{26}$Al (7.05 × $10^5$ yr), and $^{36}$Cl (3.01 × $10^5$ yr) were measured by accelerator mass spectrometry (AMS) at PRIME Lab, Purdue University (Sharma et al., 2000). A sample of 89.5 mg N01, taken adjacent from the sample used for noble gas analysis, was dissolved in a mixture of $HF/HNO_3$ in the presence of Be and Cl carriers. After complete dissolution, a small

aliquot of the dissolved sample was taken for chemical analysis by ICP-OES. From the remaining solution, the Be, Al and Cl fractions were separated and purified for analysis by AMS. The measured $^{10}$Be/Be, $^{26}$Al/Al and $^{36}$Cl/Cl ratios are corrected for blank levels and normalized to AMS standards (Nishiizumi et al., 2004; Nishiizumi et al., 2007; Sharma et al., 1990). A $^{26}$Al concentration of 51.4±2.2 dpm/kg for Novato was found, while $^{10}$Be and $^{36}$Cl measurements are still in progress. This compares to 61.1±5.4 dpm/kg measured by non-destructive γ-ray spectrometry (Table 8a). The measured values deviate by 2 σ, but both are in good agreement with the expected activity for a 30–40 cm size range. If we assume the production rates in L chondrites for $^{26}$Al to be that of Leya and Masarik (2009), the expected saturation value for a 20 cm meteoroid is 49 dpm kg$^{-1}$, while for a 40 cm meteoroid it is 63 dpm kg$^{-1}$.

**Cosmic Ray Exposure Age**

In order to measure how long the meteoroid was exposed to cosmic rays, and when it was last heated, all noble gases (He–Xe) were measured at the noble gas laboratory of ETH Zurich. Two samples, N01-2b-7 and N01-2b-14 were measured for He, Ne and Ar. The former consisted exclusively of the light lithology, while the latter was a mixture of about 70% dark and 30% light. Three more samples, N01-2b-x (light lithology), N01-2b-y (dark), and N01-2b-3 (~90% dark) have been measured (as five fragments) for He-Xe, but mainly to determine the trapped Kr and Xe content. The measurement was based on an established protocol described by Wieler et al. (1989) and Busemann et al. (2000), and is identical to the one used in Meier et al. (2012).

Results in Table 9 show that Neon in all samples has a purely cosmogenic (cosmic-ray spallation induced) isotopic composition. The $^{22}$Ne/$^{21}$Ne-ratio of ~1.09 suggests moderate shielding. The smallest meteoroid size compatible with that number, according to the model by Leya and Masarik (2009), has a shielding depth of 20 cm and a diameter of 60 cm, which is a larger than the 20–44 cm size derived from infrasound and optical measurements. For these shielding conditions, we derived production rates for the cosmogenic nuclides $^{3}$He, $^{21}$Ne and $^{38}$Ar from the Leya and Masarik (2009) model for L-chondrite chemistry, resulting in cosmic-ray exposure (CRE) ages of in average 5.1, 6.4 and 5.8 Ma, respectively (Table 9). Using the older Eugster (1988) semi-empirical formulae for L chondrites, would suggest 6.2, 6.7 and 5.9 Ma, instead. The He-based CRE age is 8–23% lower than the Ne and Ar-based CRE ages. However, the $^{3}$He/$^{21}$Ne vs. $^{22}$Ne/$^{21}$Ne ratios plot only slightly (~5 %) below the general trend-line for ordinary chondrites in the "Bern-plot" (Eberhardt et al., 1966; Nishiizumi et al., 1980). The lower $^{3}$He/$^{21}$Ne ratio could be due to loss of He or due to high shielding conditions (Masarik et al., 2001).

However, the larger apparent size may reflect an earlier shielding condition than when the meteoroid impacted Earth. If we assume that the Novato meteorite had a simple (one-stage) exposure history, we can calculate a shielding-independent CRE age from the measured $^{21}$Ne/$^{26}$Al ratio. Since the production rates of cosmogenic $^{26}$Al and $^{21}$Ne in chondrites show very similar shielding dependency, the $^{26}$Al/$^{21}$Ne production rate ratio is relatively constant, independent of shielding conditions (Graf et al. 1990). The semi-

empirical model of Graf et al. (1990) suggest a $^{26}Al/^{21}Ne$ production rate ratio of 0.40 atom/atom for a $^{22}Ne/^{21}Ne$ ratio of 1.09, while the model calculations of Leya and Masarik suggest that the production ratio varies from 0.35 in large objects to 0.41 in small objects. Adopting an average $^{26}Al/^{21}Ne$ production rate ratio of 0.38±0.03 atom/atom, we calculate a shielding independent CRE age of 9±1 Ma for Novato. The 9 Ma exposure age overlaps with a well-defined peak at ~10 Ma in the CRE age histogram of L chondrites with low radiogenic $^{40}Ar$ contents (Marti and Graf, 1992). This $^{21}Ne/^{26}Al$ age is much longer than the $^{21}Ne$ age of 6.4 Ma, which was calculated using a $^{21}Ne$ production rate of $0.39 \times 10^{-8}$ $cm^3$ STP/g/Myr based on model calculations of Leya and Masarik (2009). Such a high production rate only occurs in or near the center of objects 60–90 cm in diameter, while the low $^{26}Al$ and absence of neutron-capture $^{60}Co$ in Novato clearly indicate that Novato N01 experienced much lower shielding conditions in the last ~1 Ma of CRE age, so there appears to be some discrepancy between the shielding conditions derived from the $^{22}Ne/^{21}Ne$ ratio and those derived from radionuclides.

The data suggest a scenario in which some of the cosmogenic Ne in Novato was produced under higher shielding conditions (leading to a low $^{22}Ne/^{21}Ne$ ratio) than the meteorite experienced in the last 1 Ma. Based on the current dataset, we cannot constrain the first-stage exposure conditions of Novato, but it seems likely that the change in shielding conditions occurred during a collision in the last few Ma.

**Thermal Resetting Events**

Both He and Ar contain a radiogenic contribution ($^4He$ and $^{40}Ar$). Past heating events are documented by K-Ar as well as U,Th-He ages. In samples N01-2b-7 and N01-2b-14 analyzed for cosmic-ray exposure age, the measured radiogenic $^4He$ and $^{40}Ar$ (Table 9) can be used to determine a K-Ar and U,Th-He age, when assuming L chondritic concentrations of K (825 ppm), U (13 ppm) and Th (43 ppm) (Wasson and Kallemeyn, 1988). The elemental concentrations of Th, U and K in Novato N01 measured at LNGS are listed in Table 8b. They agree well with the average concentrations given in Wasson and Kallemeyn (1988).

The U,Th-He age is determined to be between 200 and 630 Ma. When accounting for the suspected diffusive loss of He (8–23%), and assuming that radiogenic and cosmogenic He was similarly affected by this process, these ages increase to 240 and 680 Ma. The K-Ar ages of the samples are between 550 and 1,890 Ma. Some of these variations may be due to the small sample size, in which the K content may not have been homogeneously distributed. However, all shocked L chondrites examined by Korochantseva et al. (2007) were prone to partial Ar loss during the 470 Ma shock event, resulting in higher K-Ar ages. If Novato lost its radiogenic Ar in the same way, Ar was also not completely degassed during that event.

Novato does not contain a solar wind noble gas component as evident in the He and Ne isotope data and the He-Xe elemental ratios (Table 9). Hence, the initially selected samples of 2.3 and 2.5 mg were a bit too small to get precise values for trapped gas components. However, the subsequently measured larger samples of 16–18 mg yielded

sufficient gas amounts. The absence of any solar wind component shows that Novato is not a regolith breccia originating from the outermost layers of its parent body. Whereas regolith breccias are relatively rare among L chondrites (~3%; Bischoff and Schultz, 2004), fragmental breccias are not (22%; Rubin et al., 1983).

The trapped Kr and Xe isotopic composition is consistent with both phase Q (Busemann et al., 2000) and air composition. The $^{84}Kr/^{132}Xe$ ratios of all samples (~1–2) suggest that the trapped gas is Q-gas. The light/dark/90%-dark fragments show similar Ar-Xe abundances and isotope ratios including similar excesses in $^{129}Xe$ ($^{129}Xe/^{132}Xe$ ~1.1–1.3). None of the samples shows excess in $^{80,82}Kr$ and -Xe from an enhanced neutron fluence, converting Br and I into noble gases, suggesting again an origin of the Novato sample from deeper layers below the surface of the parent body, or low halogen abundances.

Anomalous Kr and Xe due to fission were not detected. Cosmogenic $^{83}Kr$ and $^{126}Xe$ could not be determined due to the small sample size, low target element concentrations and the relatively short exposure age. The low-trapped Kr and Xe concentrations are within the expected range for severely metamorphosed non-regolithic (gas-poor) ordinary chondrites. All samples show an excess of $^{129}I$-derived $^{129}Xe$, suggesting that the Xe-containing minerals in Novato were closed for Xe-loss while $^{129}I$ ($T_{1/2}$ ~ 15.7 Ma) was still alive and not inhomogeneously reset anytime after closure.

**More Recent Heating Events**

Novato experienced a relatively recent (< $10^5$ y) heating event (which did not erase the $^{129}I$-derived $^{129}Xe/^{132}Xe$ signature), according to thermoluminescence (TL) measurements at NASA Ames Research Center. A chip of dark lithology and a chip of light lithology were taken well clear of the fusion crust, and their TL properties (Sears et al., 2013) were measured for duplicate aliquots of each chip. The natural TL level of both light and dark lithologies was very low (Table 10), 6.6 ± 1.8 krad for the dark lithology and 12.8 ± 2.4 krad for the light lithology, compared to 50–100 krad more typical of fresh ordinary chondrites falls (Benoit and Sears, 1994). These natural TL values for Novato light and dark are not significantly different, given the uncertainties on these weak signals. They imply a reheating event (to about 200–300°C) within the last ~$10^5$ years, this being the time it typically takes for natural TL to reach equilibrium (Benoit and Sears, 1994). The cause of the heating is unclear. A small perihelion or atmospheric heating are clearly not the explanation, which leaves a recent shock event in space as most likely. This heating event may have caused the lower than expected abundance of some cosmogenic nuclides and might explain the slightly lower He cosmic ray exposure age.

The dark and light lithologies of the Novato meteorite had identical and low TL sensitivity, being the TL induced by a standard radiation exposure normalized to the same data for the Dhajala meteorite. The TL sensitivity of the dark lithology was 0.028 ± 0.007 (Dhajala = 1) while the TL sensitivity of the light lithology was 0.029 ± 0 .007 (Dhajala = 1). These values would be suggestive of a low petrographic type (type 3.2, Sears et al., 1980) but this is precluded by the mineralogy and petrology and by the temperature and width data of the induced TL peak. Instead, peak temperatures and width

values similar to those of both Novato lithologies are consistent with those of equilibrated ordinary chondrites.

Given that Novato is an equilibrated ordinary chondrite with an extremely low TL sensitivity, then the inevitable conclusion is that it has been heavily shocked, which is again generally consistent with petrographic data. In fact, the TL data suggests that the samples examined here are more heavily shocked than the sample examined petrographically and, perhaps surprisingly, that the light lithologies are as heavily shocked as the dark lithologies. Such a low TL sensitivity suggests a shock level of S5-S6 on the scale devised by Stöffler et al (1991). In fact, the TL sensitivity of Novato is similar to that of the Lubbock meteorite (0.035 ± 0.004, Dhajala = 1), a well-known shock-blackened L5 chondrite. The TL sensitivity value suggests shock levels in excess of 40 GPa (Hartmetz et al., 1986).

The shock-induced petrofabrics in Novato N05 and N06 are similar in both intensity and orientation (Fig. 12), indicating each experienced an identical (most recent) impact history. The orientation and intensity of foliation was derived from X-ray microtomography data collected at UC Davis (Fig. 2), using methods found in Friedrich et al. (2008, 2013). The metal grains within the tomographic volumes were digitally isolated and best-fit ellipsoids were drawn around each. The orientation of the foliation is shown in Fig. 12 as the direction of the long axis of each ellipsoid. To obtain a quantitative value for the intensity of foliation, we used a variation of the orientation tensor method: the natural logarithm of the ratio of major over minor eigenvalues of the ellipsoids is computed to yield a strength factor (Woodcock, 1977; Woodcock and Naylor, 1983). The higher the strength factor, the greater the common orientation of the metal grains in the sample and the greater the compaction/shock loading apparent in the material volume under investigation. The Novato N05 and N06 stones have extremely well developed petrofabric, with a slightly stronger strength factor than those seen for other ordinary chondrites of shock stage S4 (Fig. 13). Novato experienced a strong compaction and the most recent impact event recorded in them was quite intense.

## ORGANIC MATTER

Shocked ordinary chondrites are not expected to contain high levels of organic compounds, but experimental techniques today are sufficiently sensitive to detect trace amounts. Organic compounds illuminate the chemistry induced by thermal alteration of the rock, and depend on the mineral chemical composition, morphology, distribution of impurities, and the presence of structural and/or electronic defects (Schoonen et al., 2004; Kleber et al., 2007; Le Guillou et al., 2012). Novato N01 was recovered before exposure to rain. Since it has a low porosity, contamination by handling may not have penetrated deep into the stone, thereby making it a suitable target for organic analysis.

**Methanol Soluble Organics**

The organic analysis was performed on a 3.6 g freshly broken off fragment of Novato N01 at the Helmoltz Zentrum in Munich (N01-2, Fig. 1), immediately after gamma-ray counting of the whole rock was completed in late December. From the freshly fractured face, around 200 mg (N01-2a) was collected from both the light chondritic and the dark impact melt zones for destructive methanol solvent extraction of organics and analysis with desorption electrospray ionization (DESI) ion cyclotron resonance Fourier transform mass spectrometry (ICRFT/MS) and laser ablation ICP-MS imaging analysis (ICRFT/MS), as well as with nuclear magnetic resonance spectroscopy (NMR) as described in Schmitt-Kopplin et al. (2010) and Popova et al. (2013). The analysis of the fragments with imaging mass spectrometry techniques using DESI-ICR/FT/MS and LA-ICP/MS will be presented elsewhere. The method extracts preferentially the polar/protic molecules into methanol and results do not pertain to insoluble compounds such as PolyAromatic Hydrocarbons (PAHs).

Results from ultrahigh resolution mass spectrometry (resolution of 500,000 at m/z 400 with a mass precision of 0.1 ppm) show the typical aliphatic signatures in composition, with homologous series of hundreds of compounds (Fig. 14). The non-targeted organic structural spectroscopy (Hertkorn et al., 2007) identified thousands of ionizable polar compounds in the mass range from 140 to 2,000 amu. Aliphatic molecules were more abundant than aromatic molecules. However, the dark material contained relatively larger proportions of aromatic compounds (H/C lower than 1) than the light material. All fractions showed the highest intensity for CHO molecules, but CHOS and CHNO compounds also show strong signals (0.1 amu mass detail in Fig. 14). The dark material seems to comprise less CHOS compounds than the light material but larger proportions of more nitrogen-containing compounds, some of which with several nitrogen atoms, corresponding to the recent observations of the LL5 Chelyabinsk chondritic and melt impact materials (Popova et al., 2013).

Nuclear Magnetic Resonance ($^1$H NMR) spectra of the methanolic extracts (Fig. 15) provide further structural constraints and insight into the chemical environments of the organic compounds (Quirico et al., 2003). The $^1$H NMR spectra show a considerable diversity of purely aliphatic branched and some alicyclic compounds (CCC**H** units), with the presence of ~7% of cyclic and open chain carboxylic acids (according to the α-proton NMR integral). $^1$H NMR spectra of the dark and light lithologies indicated different ratios of key aliphatic branching motif units rather than a manifest chemical diversity of functional groups: the dark lithology extract showed higher proportions of methyl in branched, perhaps alicyclic molecules (i.e., on average smaller molecules than found in the chondritic extract) and carboxylic acids. The percentage ratio of CC**H**/OC**H**/$C_{sp2}$**H** units was found near 85/10/5, suggesting a higher abundance of pure compared to functionalized aliphatic environments. The olefin/aromatic NMR integral ratio was nearly equal; doubly fused and higher aromatics ($\delta_H$ > 7.3 ppm) dominated the aromatic $^1$H NMR signature. $^1$H NMR signatures of aliphatic OCH units differed for dark and light lithology extracts; however, the ether/hydroxyl ($\delta_H$ < 4 ppm) to ester ($\delta_H$ > 4 ppm) ratio ranged near 5:1 for both extracts.

Pronounced aliphatic branching (Remusat et al., 2005) was indicated by the larger proportions of methyl C-($C_2$)CH-C**H$_3$** adjacent to methylene groups than C-$CH_2$-C**H$_3$** (ethyl) groups in J-resolved (JRES) NMR spectra (Fig. 15c). Similarly, $^3J_{HH}$ double-doublet splittings of ether/hydroxyl with $\delta_H \approx 3.4–3.7$ ppm (Fig. 15c) and ester groups ($\delta_H \approx 4.2$ ppm) suggested the presence of CH-(O)C**H**-CH– units in possibly cyclic arrangements. Two sets of olefins ($\delta_H \approx 5.32$ and 5.34 ppm; 3% of $^1$H NMR integral) with opposite abundance ratios in light and dark lithology extracts were present. Here, the high frequency set showed Total Correlation Spectroscopy (TOCSY) cross peaks to aliphatic positions ($\delta_H \approx 2.05$ and 1.43 ppm), suggesting incorporation of a double bond in an aliphatic chain (Fig. 15b). A few cross peaks in $^1$H, $^{13}$C Heteronuclear Single Quantum Coherence (HSQC) NMR spectra indicated branched aliphatics also at $\delta_H \approx$ 1.28 ppm (polymethylene and branched aliphatics, with $\delta_C \approx 22–33$ ppm) and the presence of certain oxomethylene ($OCH_2$) groups with $\delta_C \approx 60–76$ ppm (Fig. 15d, Table 11).

**Amino Acids and PAHs**

The remains of the two Novato methanol extracts from ~50 mg samples of the N01 light and dark lithologies were subsequently analyzed at NASA Johnson Space Flight Center for amino acids as an indicator of terrestrial contamination of the meteorite samples in the period shortly after the fall. This targeted analysis of amino acids pertains to smaller molecules than analyzed above. Freshly fallen L chondrites typically have very low levels of soluble organics. The methanol extracts were dried under vacuum, acid hydrolyzed under 6M HCl vapor at 150°C for 3 hours, desalted by cation exchange chromatography, and derivatized with *o*-phthaldialdehyde/*N*-acetyl-L-cysteine (OPA/NAC) and then analyzed for amino acids with chiral separation using a liquid chromatography with fluorescence detection and time-of-flight mass spectrometry (LC-FD/ToF-MS) as previously described (Glavin et al., 2006; Glavin et al., 2011). Although the different extraction technique may affect the outcome, the Novato extracts had about 1000 times less of the non-protein α-aminoisobutyric acid abundance than that found in CM2 Murchison, and about the same low value found for a freshly collected H6 chondrite sample of Almahata Sitta (Burton et al., 2011). Results show that the amino acid distributions and enantiomeric ratios (D/L) in methanol extracts from the bright and dark lithologies were similar.

Several common terrestrial protein amino acids including glycine, serine, aspartic and glutamic acids, alanine, and valine were detected with relatively low D/L ratios ranging from ~0.06 to 0.25 (Table 12) suggesting that some terrestrial L-amino acid contamination of the samples has occurred. However, we cannot rule out the possibility that trace levels (~2–8 ppb) of the non-protein amino acids α-aminoisobutyric acid, DL-α-amino-*n*-butyric acid, and racemic DL-β-amino-*n*-butyric acid (Table 12), which are typically very rare on Earth, are indigenous to the Novato meteorite. Compound-specific stable isotope measurements are needed to firmly establish the origin of these non-protein amino acids in Novato.

The meteorite also contains non-soluble organic compounds in the form of polyaromatic hydrocarbons (PAH). A freshly broken fragment of Novato N01-1b (dark lithology) was

analyzed by laser desorption laser ionization mass spectrometry ($L^2MS$) (Wu et al., 2013) at Stanford University, a technique that involves no solvent. A rich mass spectrum of compounds was detected, as shown in Fig. 16. The mass spectrum shows an abundance of atoms and molecules having a low ionization potential. The peak at *m/z* = 26 indicates the existence of CN groups. Molecular weights of odd number are dominant, which suggests the presence of N atoms in the compounds. The signal at *m/z* = 91 is believed to be $C_7H_7^+$, which is commonly observed in PAHs. These results suggest that most of the low-ionization-energy compounds in Novato N01 are PAHs with either N atoms in the ring or in side chains. For example, the possible formula of molecules at *m/z* = 107 are $C_7H_9N$, which might be toluidine or N-methylaniline among other possibilities. Some elements are clearly observed also, such as $Na^+$ at m/z = 23, $Mg^+$ at 24, and $K^+$ at m/z = 39 and 41. The peaks at m/z = 206, 207, and 208 might arise from Pb as the intensity distribution fits well the expected isotope abundances of this element. Higher mass peaks than this are not observed.

**Macromolecular Carbon and Carbon and Nitrogen Isotopes**

In order to study the total carbon and nitrogen content and isotopic compositions, two fragments (one light, one dark) from Novato N01-1e (Fig. 1) were analyzed by Stepped Combustion – Gas Source Mass Spectrometry (SC-GC-MS) at the Open University, U.K. Results from the analyses are given in Table 13 and Fig. 17. The dark fractions of Novato contained 611.3 ppm carbon with weighted $\delta^{13}C \sim -39‰$. Carbon abundance in the light fraction was much lower, at 97.6 ppm with weighted $\delta^{13}C \sim -27‰$. Unfortunately, in both analyses, so much $SO_2$ was released at temperatures above 500°C (light fraction) and 700°C (dark fraction) that $CO_2$ isotope measurements were compromised, and could not be determined.

The carbon released from both fractions was mainly below 600°C, although in the dark fraction of N01-1e, there was a second maximum between 900°C and 1000°C (Fig. 17). The maximum combustion temperature of 600°C implies that most of the carbon occurs as an organic macromolecular component, or poorly graphitized carbon. Nitrogen was not affected by sulfur dioxide, and so both abundance and isotopic data were collected throughout the whole experiment. Again, there was a difference in the results for the two fractions, the dark having 13.9 ppm with $d^{15}N$ of ~ +4.8‰, whilst there were only 3.0 ppm nitrogen in the light fraction with $d^{15}N \sim -2.1‰$. In each sample, almost all the nitrogen was liberated by 600°C, implying its association with a carbonaceous host.

Looking at the individual profiles of Novato 01 (Fig. 16), and focusing only on the material which was released below 600°C, it is clear that there are at least two components in the dark fraction that combust in this temperature increment. Up to 400°C, 76.9 ppm carbon with $\delta^{13}C \sim -24‰$ is liberated. There is then a steep drop in isotopic composition, down to $\delta\ ^{13}C \sim -43‰$ for almost 440 ppm carbon. In contrast, although there are two separate maxima in nitrogen yield (at 200–400°C and 400–600°C), the isotopic composition of the nitrogen ($\delta\ ^{15}N \sim +2‰$) is almost constant across the temperature interval.

The lower temperature material (with atomic C/N ratio between 11 and 22) is likely to be terrestrial contamination. At least some of the nitrogen will be from adsorbed terrestrial atmosphere. The isotopically-light material has an atomic C/N ratio that extends to over 200, which is much higher than the estimated C/N ratio of macromolecular material in chondritic meteorites (ca. 50; Zinner, 1988). Values of such a magnitude are consistent with identification of the component as amorphous carbon, or even microcrystalline diamonds (Russell et al., 1991).

The light fraction of Novato 01 had a carbon combustion profile that was much more akin to the results from other equilibrated ordinary chondrites (Grady et al., 1989). Again, the lowest temperature material (this time with C/N of ~58) is possibly a terrestrial contaminant; the higher C/N ratio and lower $\delta^{15}N$ (about –4.4‰), implying that less atmosphere is adsorbed than in the dark fraction. C/N ratios of 10–60 are associated with land plants (Dai et al., 2005; Marchand et al., 2005). The second component identified in the dark fraction, with light carbon isotopic composition, seems to be absent from the light fraction.

Equilibrated ordinary chondrites contain very little indigenous carbon (Grady et al., 1989) or nitrogen (Hashizumi and Sugiura, 1995); any carbon present tends to be either poorly-crystallized to crystalline graphite or is dissolved in metal. Nitrogen is assumed to carried by these phases. The carbon and nitrogen data for the light lithology of Novato 01 fits into this picture. In contrast, the dark lithology displays characteristics that have more in common with unequilibrated ordinary chondrites: a higher abundance of carbon with a combustion temperature and C/N ratio that is consistent with identification of the component as amorphous to poorly-crystalline carbon, possibly even microcrystalline diamond. It is unlikely that this material is produced by conversion of indigenous carbon during the shock-blackening process, mainly because its abundance is more than an order of magnitude higher than that in the light fraction, which is taken to represent mean equilibrium ordinary chondrite carbon.

Overall, organic matter studies show an organic molecular complexity that mostly originates from chemistry in the meteoroid parent body. Further studies of organic molecular diversity within chondrites will help constrain the conditions of abiotic organic matter formation and evolution.

## DISCUSSION

### Possible Source Region in the Main Belt

Beside Novato, there are four other L chondrite falls with known orbital elements (Table 6b). From Jesenice (Spurny et al., 2010) to Innisfree (Halliday et al., 1978, 1981), to Novato (this work), to Villalbeto de la Peña (Llorca et al., 2007), to Park Forest (Brown et al., 2004), they form a sequence of increasing semi-major axis (a) and aphelion distance (Q), and decreasing eccentricity (e) and perihelion distance (q). All have their aphelion in the asteroid belt (Q = 2.5 to 4.3 AU). Novato and Jessenice have CRE ages very similar to the collisional lifetime, while Innisfree and Villalbeto de la Peña have

CRE ages that are much higher. The CRE age of Park Forest is unknown at present.

A large fraction (possibly all) shocked L chondrites were part of a ~100-km-sized parent body that experienced a collision event that re-set the K-Ar age by releasing Ar from the minerals 470 ± 6 Ma years ago (Korochantseva et al., 2007; Weirich et al., 2012). The event caused shock blackening and minerals to be melted and altered. Many L chondrites contain olivine grains with undulatory extinction, veins and cracks filled with metal and sulfide that are forced through them as melt, and other effects (Stöffler et al., 1988; Sears, 2004). Some high-pressure phases (e.g., ringwoodite, majorite) were also formed (e.g., Binns et al., 1969; Coleman, 1977). At about the same time, Earth experienced an increase in meteorite influx as indicated by fossil meteorites in Middle Ordovician deposits in Sweden dated to 467.3 ± 1.6 Ma (Schmitz et al., 2001).

Based on its dynamical age, Nesvorny et al. (2009) identified the Gefion asteroid family, located on the inside of the 5:2 mean-motion resonance, as the likely debris field from this collision. The nearby 5:2 resonance offered the initial low-efficiency but quick pathway to Earth in the Ordovician. The efficiency of this resonance is low because before the orbital eccentricity can be increased high enough to have Earth-intersecting orbits, the aphelion of the orbit evolves to cross Jupiter's orbit, as a result of which most meteoroids are deflected from hitting Earth.

A more efficient route is the 3:1 resonance, which has been proposed as the route through which small L-chondrite fragments of an ongoing collisional cascade find a path to Earth today. On their way towards evolving to the 3:1 resonance, the meteoroids can remain exposed to cosmic rays for a relatively long time, as a result of which this group does not show a sharp peak in the cosmic-ray exposure times (Nesvorny et al., 2009).

Based on the strongly shocked nature of Novato and the 460±220 Ma U,Th-He age, Novato appears to belong to this group of shocked L chondrites. The 550–1,890 Ma K-Ar age is higher, perhaps only because of Ar loss during the ~470 Ma event, which also affected other shocked L chondrites (Korochantseva et al., 2007). Ar-Ar age determinations are needed to be conclusive, but those could not be accomplished in time for this publication.

Does Novato's orbit still carry a signature of its source region? The collisional lifetime for near-Earth asteroids from collisions with main belt asteroids is about 1.4 $r^{1/2}$ My, with r the radius in cm (Bottke et al., 1993; Wetherhill, 1985; Farinella et al., 1998; Morbidelli and Gladman, 1998). From this, the collisional lifetime for Novato is about 5.9 Ma. As expected for a low-inclination source region that keeps the meteoroid crossing the main belt before impact on Earth, this value is similar to the measured CRE age of 9±1 Ma. In addition, Novato appears to have had a collision in only the last few Ma.

However, this cannot be the full story. Both Innisfree and Villalbeto de la Peña have CRE ages much higher than their nominal collisional lifetimes (Table 6c). This might suggest that these collisional lifetimes are underestimated for small meteoroids by about a factor of five. If so, the short CRE ages of Novato and Jesenice may still permit the current orbit

to trace the meteoroid to its source region.

Given the orbital elements a, e, and i of Novato (Table 6a-D, with 1-sigma uncertainty), the Bottke et al. (2002) model predicts a 45% probability that the meteoroid originated in the inner belt (ν6 resonance and Intermediate Mars Crossers), whereas the remaining 10% is shared between the 3:1 and the outer main belt. However, the Bottke et al. model applies to larger objects (> 100m), with source probabilities taken to be independent of size. Newer models, with source-dependent size distributions, show an increasing likelihood that meteoroids originate in the middle main belt when the size decreases.

A new model (Granvik et al., 2014) produced the dynamical timescales listed in Table 6c. The table lists the average transfer time (and standard deviation for a sample of such pathways) to go from the source resonance, to the orbit of one of the L chondrites. When a particle evolves to an orbit that fulfills the criterion that $|\Delta a|$, $|\Delta e|$, and $|\Delta i|$ are less than the observed 1-sigma error in the orbital elements, then the orbit is considered a match and the transfer time is recorded. To get sufficient statistics, the collection range for Novato was increased by a factor of 5.

The integrations started from an unbiased (to first order) distribution of main belt object orbits, which was forward integrated until the particles entered a sink (collision with the Sun or a planet, ejection from the inner solar system). The transfer time from the boundary between the NEO and MBO region to the impact orbit does not include non-gravitational forces. The main belt phase transfer times were calculated by Granvik et al. (2014) based on a Yarkovsky semimajor axis drift typical for much larger (100-m sized) objects and are not reported here.

We find that Novato, Jesenice, and Innisfree point to these meteoroids originating in the central belt, arriving to us from the 3:1 or the 5:2 mean-motion resonance. This scenario is consistent with these meteoroids originating from the Gefion family, but suggests that even today some shocked L chondrites may come to us directly from the 5:2 mean-motion resonance.

Villalbeto de la Peña has a CRE age much higher than the nominal collisional lifetime, showing that it managed to avoid collisions for a much longer period of time than the other L chondrites. Only a high-inclination source region such as the Hungaria or Phocaea regions would be consistent with this (Table 6c). Interestingly, Villalbeto de la Peña was recently reclassified as a hydrothermally metamorphosed polymict L-chondritic breccia (Bishoff et al., 2013), and in light of the long cosmic ray exposure age may therefore have a different source region.

**Pre-atmospheric Detection**

The orbit of Novato as shown in column D of Table 6a was also used to investigate the possibility that the small Novato meteoroid may perhaps have been detected in routine asteroid surveys prior to entry into Earth's atmosphere during the last hours before approach. 5,940,405 images were considered from the land-based CFHT, Spacewatch,

Catalina, Mount Lemmon, Siding Springs, Pan-STARRS, and LONEOS surveys, as well as the space-based WISE, NEOWISE, HST-WFPC2 and WFC3 infrared and visible images catalogues. No candidate detections were found. Aside from the small size, this object approached from southern latitudes, where asteroid surveys are infrequent. Assuming the estimated diameter of 30 cm and an albedo of 0.15, we calculate the absolute magnitude of the object at H=+35.1. Assuming a slope parameter of 0.15, the object's apparent magnitude was well above 24, the highest limiting magnitude of current sky surveys, until just 3 hours prior to contact. A contributing factor to Novato's high magnitude was its approach from an unfavorable sun angle, with a solar elongation of 67–68° and a phase angle of 111–112° in the days prior to contact. Novato's apparent magnitude decreased to +23.0 two hours prior to contact, was +21.5 one hour prior, and +20.1 30 minutes prior, finishing at magnitude +16.1 at atmospheric contact.

In order to search for potential survey images on prior Novato-Earth near approaches, 1000 test meteoroids were generated using Gaussian distributions over the atmospheric contact position and velocity uncertainties noted in column D of Table 6a. Each test meteoroid in this probability cloud was integrated back in time using a RADAU integrator (Everhart, 1985; Clark and Wiegert, 2011) accounting for gravitational influences of the Sun, major planets, and the Moon. Although the majority of the probability cloud dispersion over time is along the orbital path, the most recent nearest approach of the Earth and Novato that brought any test meteoroid within the local region of the Earth was in October 1993. This date is prior to readily available sky survey catalogues. Being 20 years prior to contact, the dispersion along the orbit is great, over 180° in solar longitude. The two closest approaches of test particles in a sparse portion of the probability result in apparent magnitudes of +23.8 and +24.7, near the limiting magnitude of today's most powerful surveys. Nevertheless, there was a slight possibility that the Novato meteoroid could have been imaged in 1993.

## CONCLUSIONS

A new meteorite fall in Novato, California, is reported, the second California fall of 2012. This meteorite was recovered when local resident Lisa Webber responded to a publication of the fireball trajectory and fall area calculated from observations by the Cameras for Allsky Meteor Surveillance (CAMS) program in the San Francisco Bay Area. An accurate pre-atmospheric orbit was derived. Arriving from a southern latitude, it was not detected in NEO surveys in the hours on approach to Earth, but there is a slight possibility that this 30-cm sized meteoroid was seen in space in 1993.

Mineral and petrochemical data and the 460 ± 220 Ma U,Th-He age point to this meteorite belonging to the shocked L chondrite group known to have had a fragmentation event ~470 Ma ago. Both light and dark lithologies experienced significant shock. The meteorite was slightly more compressed than other L6 chondrites of shock-stage S4. Novato is a fragmental breccia with solar-gas-free dark and light lithologies. Although the mixture of light and dark lithologies in Novato is similar to that of regolith breccias, Novato lacks solar gases and must have formed from materials that originated from somewhat deeper inside the L-chondrite parent body.

The cosmogenic radionuclide concentrations in Novato are consistent with a pre-atmospheric size of ~30 cm, as derived from the infrasound and optical measurements. The cosmogenic Ne composition of Novato indicates that the average size of this meteorite during its entire cosmic-ray exposure was larger than in the last ~1 Ma (as constrained by $^{26}$Al). The shielding corrected $^{21}$Ne/$^{26}$Al age of 9±1 Ma overlaps with a well-defined peak at ~10 Ma in the CRE age histogram of shocked L-chondrites with low $^{40}$Ar contents. However, the combination of cosmogenic radionuclides and noble gases suggests that Novato may have experienced a complex exposure history with a relatively long first-stage exposure under high shielding (resulting in the low $^{22}$Ne/$^{21}$Ne ratio) and a second-stage exposure under low shielding (resulting in the low radionuclide concentrations).

Thermoluminescence data show that a reheating event (to about 200–300$^{o}$C) occurred within the last ~0.1 Ma. The cause of the heating is unclear. A small perihelion or atmospheric heating are clearly not the explanation, which leaves a recent shock event in space as the most likely.

These heating events may have chemically altered the organic compounds in the meteorite, but did not completely oxidize and remove all such compounds. A rich array of methanol soluble compounds and insoluble PAHs were identified. Amino acid analysis points to a small level of terrestrial contamination, but some non-protein amino acids may be of extraterrestrial origin. The dark lithology has a higher abundance of carbon than the light lithology, with a combustion temperature and C/N ratio that is consistent with identification of the component as amorphous to poorly crystalline carbon, possibly even microcrystalline diamond.

Together with L chondrites Jesenice and Innisfree, the orbital data are consistent with dynamical lifetimes calculated for an origin in the central main belt, and driven toward Earth from the 3:1 or 5:2 mean-motion resonances. This is consistent with the proposed origin of shocked L6 chondrites in the Gefion family, but it suggests that even today these meteorites could come directly out of the 5:2 resonance. In contrast, recently reclassified hydrothermally metamorphosed polymict L-chondritic breccia Villalebeto de la Peña originated from a different, higher inclined, source region.

*Acknowledgments:* We thank Lynn Hofland of NASA Ames Research Center for performing the tensile strength measurements. This work was supported by the NASA Near Earth Object Observation and Planetary Astronomy programs (NNX08AO64G and NNX12AM14G to P.J.), the NASA Cosmochemistry program (NNG06GF95G to A.R., NNX11AJ51G to Q.Z.Y. & A.N.K., and NNX11AC69G to K.N.), and the Swiss National Science Foundation (STFC).

## REFERENCES


Arpesella C. 1996. A low background counting facility at Laboratori Nazionali del Gran Sasso, *Applied Radiation and Isotopes* **47**:991–996.

Baldwin B. and Sheaffer Y. 1971. Ablation and breakup of large meteoroids during atmospheric entry. *Journal of Geophysical Research* **76**:4653sical.

Bartol Neutron Monitors 2013. http://neutronm.bartol.udel.edu/

Beech M. 2001. Meteoroid rotation and fireball flickering: a case study of the Innisfree fireball. *MNRAS* **326**:937–942.

Bennett M. E. and McSween H. Y. 1996. Shock features in iron-nickel metal and troilite of L-group ordinary chondrites. *Meteoritics & Planetary Science* **31**:255–264.

Benoit P. H. and Sears D.W.G. 1994. A recent meteorite fall in Antarctic with an unusual orbital history. *Earth Planet. Sci. Lett.* **120**:463–471.

Bhandari N., Mathew K.J, Rao M. N., Herpers U., Bremer K., Vogt S., Wölfli W., Hofmann, H. J., Michel R., Bodemann R., and Lange H.-J. 1993. Depth and size dependence of cosmogenic nuclide production rates in stony meteoroids. *Geochimica Cosmochimica Acta* **57**:2361–2375.

Binns R. A., Davis R. J. and Reed S. J. B. 1969. Ringwoodite, natural $(Mg,Fe)_2SiO_4$ spinel in the Tenham meteorite. *Nature* **221**: 943–944.

Bischoff A., Schultz, L. 2004. Abundance and meaning of regolith breccias among meteorites. 67$^{th}$ Annual Meeting of the Meteoritical Society, abstr. 5118.

Bischoff A., Jersek M., Grau T., Mirtic B., Ott U., Kučera J., Horstmann M., Laubenstein M., Herrmann S., Randa Z., Weber M., Heusser G. 2011. Jesenice – A new meteorite fall from Slovenia. *Meteoritics & Planetary Science* **46**:793–804.

Bischoff A., Dyl K. A., Horstmann M., Ziegler K., Wimmer K., Young E. D. 2013. Reclassification of Villalbeto de la Peña - Occurrence of a winonaite-related fragment in a hydrothermally metamorphosed polymict L-chondritic breccia. *Meteoritics & Planetary Science* **48**:628–640.

Bottke W. F., Nolan M. C., Greenberg R. 1993. Collision lifetimes and impact statistics of near-Earth asteroids. *LPSC* **24**:159–160.

Bottke W. F., Morbidelli A., Jedicke R., Petit J.-M., Levison H. F., Michel P., Metcalfe T. S. 2002. Debiased orbital and absolute magnitude distribution of the Near-Earth Objects. *Icarus* **156**:399–433.

Bunch T. E., Keil K., Snetsinger K. G. 1967. Chromite composition in relation to chemistry and texture of ordinary chondrites. *Geochimica et Cosmochimica Acta* **31**:1569–1582.

Burton A. S., Glavin D. P., Callahan M. P., Dworkin J. P., Jenniskens P., Shaddad M. H. 2011. Heterogeneous distributions of amino acids provide evidence of multiple sources with the Almahata Sitta parent body, asteroid 2008 $TC_3$. *MAPS* **46**:1703–1712.

Brearley A. J. and Jones R. H. 1998. Chondritic meteorites. In: Planetary Materials (ed. J. J. Papike), Mineralogical Society of America, Washington, D. C., pp. 3-01–3-398.

Britt D. T. and Consolmagno G.J. 2003. Stony meteorite porosities and densities: A review of the data through 2001. *Meteoritics and Planetary Science* **38**:1161–1180.

Brown P., Pack D., Edwards W. N., Revelle D. O., Yoo B. B., Spalding R. E., Tagliaferri E. 2004. The orbit, atmospheric dynamics, and initial mass of the Park Forest meteorite. *Meteorit. Plan. Sci.* **39**:1781–1796.

Busemann H., Bauer H., Wieler R. 2000. Primordial noble gases in "phase Q" in carbonaceous and ordinary chondrites studied by closed-system stepped etching. *Meteorit. Plan. Sci.* **35**: 949–973.

Ceplecha, Z., Borovicka J., Elford W. G., Revelle D. O., Hawkes R. L., Porubcan V., Simek M. 1998. Meteor phenomena and bodies. *Space Science Review* **84**: 327–471.

Christie D. R. and Campus P. 2010. The IMS infrasound network: Design and establishment of infrasound stations. In: *Infrasound Monitoring for Atmospheric Studies* (eds., A. Le Pichon, E. Blanc and A. Hauchecorne), Dordrecht: Springer, pp. 29–75.

Clark D. and Wiegert P., 2011. A numerical comparison with the Ceplecha analytical meteoroid orbit determination method. *MAPS* **46**:1217–1225.

Clayton R. N. and Mayeda T. K. 1984. Oxygen isotopic compositions of enstatite chondrites and aubrites. *J. Geophy. Res.* **89**:C245–C249.

Clayton R. N., Mayeda T. K., Goswami J. N., Olsen E. J. 1991. Oxygen isotope studies of ordinary chondrites. *Geochimica et Cosmochimica Acta* **55**:2317–2337.

Clayton R. N. and Mayeda T. K. 1996. Oxygen isotope studies of achondrites. *Geochim. Cosmochim. Acta* **60**:1999–2017.

Clayton R. N. and Mayeda T. K. 1999. Oxygen isotope studies of carbonaceous chondrites. *Geochim. Cosmochim. Acta* **63**:2089–2104.

Coleman L. C. 1977. Ringwoodite and majorite in the Catherwood meteorite. *Canad. Mineral.* **15**: 97–101.

Consolmagno G. J., Britt D. T., Macke R. J. 2008. The significance of meteorite density and porosity. *Chemie der Erde* **68**:1-29.

Dai J., Sun M.-Y., Culp R. A. and Noakes J. E. 2005. Changes in chemical and isotopic signatures of plant materials during degradation: Implication for assessing various organic inputs in estuarine systems. *Geophys. Res. Lett.* **32**:L13608–.

Eberhardt P., Geiss J., and Lutz H. 1963. Neutrons in meteorites. In: Earth Science and Meteoritics, edited by Geiss, J. and Goldberg, E. D. Amsterdam: North Holland Publ. Co., p. 143-168.

Eberhardt P., Eugster O., Geiss J., and Marti K. 1966. Rare Gas Measurements in 30 Stone Meteorites. *Zeitschrift Naturforschung Teil A* **21**:414–426.

Ens T. A., Brown P. G. Edwards W. N., Silber E. A. 2012. Infrasound production of bolides: A global statistical study. *J. Atmosph. Solar Terr. Phys.* **80**:208–209.

Evans J. C., Reeves J. H., Rancitelli L. A., Bogard D. D. 1982. Cosmogenic nuclides in recently fallen meteorites – Evidence for galactic cosmic ray variations during the period 1967-1978. *Journal of Geophysical Research* **87:**5577-5587.

Everhart E. 1985. An efficient integrator that uses Gauss-Radau spacings. In: *Dynamics of Comets: Their Origin and Evolution.* A. Carus, & G. B. Valsecchi (Eds.) Proceedings of IAU Colloq. 83, held in Rome, Italy, June 11-15, 1984, **115**:185–202.

Evers L. G. and Haak H. W. 2001. Listening to sounds from an exploding meteor and

oceanic waves. *GRL* **28**:41–44.
Eugster O. 1988. Cosmic-ray production rates for He-3, Ne-21, Ar-38, Kr-83, and Xe-126 in chondrites based on Kr-81/Kr exposure ages. *Geochimica et Cosmochimica Acta* **52**:1649–1662.
Farinella P., Vokrouhlicky D., Harmann W. K. 1998. Meteorite delivery via Yarkovsky orbital drift. *Icarus* **132**:378–387.
Friedrich J. M., Wang M. and Lipschutz M. E. 2003. Chemical studies of L chondrites. V: compositional patterns for 49 trace elements in 14 L4-6 and 7 LL4-6 falls. *Geochimica et Cosmochimica Acta* **67**:2467–2479.
Friedrich J. M., Bridges J. C., Wang M.-S., Lipschutz M. E. 2004. Chemical studies of L chondrites. VI: Variations with petrographic type and shock-loading among equilibrated falls. *Geochimica et Cosmochimica Acta* **68**: 2889–2904.
Friedrich J. M., Wignarajah D. P., Chaudhary S., Rivers M. L., Nehru C. E., Ebel D. S. 2008. Three dimensional petrography of metal phases in equilibrated L chondrites – Effects of shock loading and dynamic compaction. *Earth and Planetary Science Letters* **275**:172–180.
Friedrich, J. M. and Rivers, M. L. 2013. Three-dimensional imaging of ordinary chondrite microporosity at 2.6 mm resolution. *Geochimica et Cosmochimica Acta* **116**:63–70.
Friedrich J. M., Ruzicka A., Rivers M. L., Ebel D. S., Thostenson J. O., Rudolph R. A. 2013. Metal veins in the Kernouvé (H6 S1) chondrite: Evidence for pre- or syn-metamorphic shear deformation. *Geochimica et Cosmochimica Acta* doi: 10.1016/j.gca.2013.01.009
Glavin D. P., Dworkin J. P., Aubrey A., Botta O., Doty III J. H., Martins Z. and Bada J. L. 2006. Amino acid analyses of Antarctic CM2 meteorites using liquid chromatography-time of flight-mass spectrometry. *Meteoritics & Planetary Science* **41**:889–902.
Glavin, D. P., Callahan, M. P., Dworkin, J. P. and Elsila J. E. 2010. The effects of parent body processes on amino acids in carbonaceous chondrites. *Met. Planet. Sci*. **45**: 1948–1972.
Göpel C. and Birck J.-L. 2010. Mn/Cr systematics: A tool to discriminate the origin of primitive meteorites? *Goldschmidt Conference Abstracts,* A348.
Grady M. M., Wright I. P. and Pillinger C. T. 1989. A preliminary investigation into the nature of carbonaceous material in ordinary chondrites. *Meteoritics* 24, 147-154.
Graf T., Baur H. and Signer P. 1990. A model for the production of cosmogenic nuclides in chondrites. *Geochimica et Cosmochimica Acta* **54:**2521–2534.
Granvik M., Morbidelli A., Jedicke R., Bolin B., Bottke W. F., Beshore E., Vokrouhlicky D., Nesvorny D., Michel P. 2014. *Icarus* (in prep.).
Haas J. R. and Haskin L. A. 1991. Compositional variations among whole-rock fragments of the L6 chondrites Bruderheim. *Meteoritics* 26:13-26.
Halliday I., Griffin A. A., Blackwell A. T. 1981. The Innisfree meteorite fall: A photographic analysis of fragmentation, dynamics and luminosity. *Meteorit. Planet. Sci.* **16**:153–170.
Halliday I., Blackwell A. T., Griffin A. A. 1978. The Innisfree meteorite and the Canadian camera network. *J. Roy Astron. Soc. Can.* **72**:15–39.
Hartmetz, C.P., Ostertag, R. and Sears, D.W.G. 1986. A thermoluminescence study of

experimentally shock-loaded oligoclase and bytownite. Proc. 17th Lunar and Planet. Sci. Conf., Part 1, *J. Geophys. Res.*, **91**: E263–E274.

Hashizume K. and Sugiura N. 1995. Nitrogen isotopes in bulk ordinary chondrites. *Geochim. Cosmochim. Acta* **59**: 4057–4069.

Hertkorn N., Ruecker C., Meringer M., Gugisch R., Frommberger M., Perdue E.M., Witt M., Schmitt-Kopplin Ph. 2007. High-precision frequency measurements: indispensable tools at the core of the molecular-level analysis of complex systems, *Analytical Bioanalytical Chemistry* **389**:1311–1327.

Heusser G., Hampel W., Kirsten T., Schaeffer O. A. 1978. Cosmogenic isotopes in recently fallen meteorites. *Meteoritics* **13**:492–493.

Irving A. J., Tanaka R., Steele A., Kuehner S. M., Bunch T. E., Wittke J. H., Hupé G. M. 2011. Northwest Africa 6704: a unique cumulate permafic achondrite containing sodic feldspar, awaruite and "fluid" inclusions, with an oxygen isotopic composition in the Acapulcoite-Lodranite field. *Annual Meteoritical Society Meeting,* #5231.

Jarosewich E. 1990. Chemical analyses of metorites: A compilation of stony and iron metorite analyses. *Meteoritics* **25**:323–337.

Jenniskens P., Gural P. S., Dynneson L., Grigsby B. J., Newman K. E., Borden M., Koop M., Holman D. 2011. CAMS: Cameras for Allsky Meteor Surveillance to establish minor meteor showers. *Icarus* **216**: 40–61.

Jenniskens P., Fries M. D., Yin Q.-Z., Zolensky, M., Krot, A. N., Sandford, S., Sears, D., Beauford, R., Ebel, D. S., Friedrich, J. M., Nagashima, K., Wimpenny, J., Yamakawa, A., Nishiizumi, K., Hamajima, Y., Caffee, M. W., Welten, K. C., Laubenstein, M., Davis, A. M., Simon, S. B., Heck, P. R., Young, E. D., Kohl, I. E., Thiemens, M., Nunn, M. H., Mikouchi, T., Hagiya, K., Ohsumi, K., Cahill, T. A., Lawton, J. A., Barnes, D., Steele, A., Rochette, P., Verosub, K., Gattacceca, J., Cooper, G., Glavin, D. P., Burton, A. S., Dworkin, J. P., Elsila, J. E., Pizzarello, S., Ogliore, R., Schmitt-Kopplin, P., Harir, P., Hertkorn, N., Verchovsky, A., Grady, M., Nagao, K., Okazaki, R., Takechi, H., Hiroi, T., Smith, K., Silber, E. A., Brown, P. G., Albers, J., Klotz, D., Hankey, M., Matson, R., Fries, J. A., Walker, R. J., Puchtel, I., Lee, C.-T. A., Erdman, M., Eppich, G. R., Roeske, S., Gabelica, Z., Lerche, M., Nuevo, M., Girten, B., and Worden., S. P. (the Sutter's Mill Meteorite Consortium) . 2012. Radar-enabled recovery of the Sutter's Mill meteorite, a carbonaceous chondrite regolith breccia. *Science* **338**:1583–1587.

Kleber M., Sollins P., Sutton R. 2007. A conceptual model of organo-mineral interactions in soils: self assembly of organic molecular fragments into zonal structures on mineral surfaces. *Biogeochemistry* **85**: 9–24.

Kohman T.P. and Bender M.L. 1967. Nuclide production by cosmic rays in meteorites and on the Moon. High-Energy Nuclear Reactions in Astrophysics, In: *High-Energy Nuclear Reactions in Astrophysics - A collection of articles*, edited by Shen B.S.P. and Benjamin W.A., New York, N.Y. pp. 169–245.

Korochantseva E. V., Trieloff M., Lorenz C. A., Buykin A. I., Ivanova M. A., Schwarz W. H., Hopp J., and Jessberger E. K. 2007. L-chondrite asteroid breakup tied to Ordovician meteorite shower by multiple isochron $^{40}$Ar-$^{39}$Ar dating. *Meteoritics & Planetary Science* **42**:113–130.

Le Guillou C., Rouzaud J.-N., Bonal L., Quirico E., Derenne S., Remusat L. 2012. High

resolution TEM of chondritic carbonaceous matter :Metamorphic evolution and heterogeneity. *Meteorit. Planet. Sci.* **47**: 345–362.

Leya I. and Masarik J. 2009. Cosmogenic nuclides in stony meteorites revisited. *Meteoritics & Planetary Sciences* **44**:1061–1086.

Llorca J., Trigo-Rodríguez J. M., Ortiz J. L., Docobo J. A., García-Guinea J., Catro-Tirado A. J., Rubin A. E., Eugster O., Edwards W., Laubenstein M., Casanova I. 2005. The Villalbeto de la Peña meteorite fall: I. Fireball energy, meteorite recovery, strewn field, and petrography. *Meteorit. Planet. Sci.* **40:** 795–804.

Lodders, K. 2003. Solar System Abundances and Condensation Temperatures of the Elements. *Astrophys. J*. **591:**1220–1247.

Marchand C., Disnar J.R., Lallier-Vergès E. and Lottier N. 2005. Early diagenesis of carbohydrates and lignin in mangrove sediments subject to variable redox conditions (French Guiana). *Geochim. Cosmochim. Acta* **69:** 131–142.

Marti K. and Graf T. 1992. Cosmic-Ray exposure history of ordinary chondrites. *Annual Review of Earth and Planetary Sciences* **20**: 221–243.

Masarik J., Nishiizumi K. and Reedy R. C. 2001. Production rates of cosmogenic helium-3, neon-21 and neon-22 in ordinary chondrites and the lunar surface. *Meteoritics & Planetary Science* 36:643-650.

Mason B. and Graham A. L., 1970. Minor and trace elements in meteoritic minerals. *Smithsonian Contr. to the Earth Sciences* **3**: 1-17

Meier M. M. M., Welten K. C., Caffee M. W., Friedrich J. M., Jenniskens P., Nishiizumi K., Shaddad M., Wieler R. 2012. A noble gas and cosmogenic radionuclide analysis of two ordinary chondrites from Almahata Sitta. *Meteoritics & Planetary Science* **47**:1075–1086.

Morbidelli A. and Gladman B., 1998. Orbital and temporal distributions of meteorites originating in the asteroid belt. *Meteoritics and Planetary Science* **33**: 999–1016.

Nesvorný D., Vokrouhlický D., Morbidelli A., and Bottke W. F. 2009. Asteroidal source of L chondrite meteorites. *Icarus* **200**:698–701.

Nishiizumi K., Regnier S., Marti K. 1980. Cosmic ray exposure ages of chondrites, pre-irradiation and constancy of cosmic ray flux in the past. *Earth Planet. Sci. Lett.* **50**:156–170.

Nishiizumi K. 2004. Preparation of $^{26}$Al AMS standards. *Nuclear Instruments and Methods in Physics Research* **B223–224**:388–392.

Nishiizumi K., Imamura M., Caffee M.W., Southon J.R., Finkel R.C., and McAninch J. 2007. Absolute calibration of $^{10}$Be AMS standards. *Nuclear Instruments and Methods in Physics Research* **B258**:403–413.

Ott U., Herrmann S., Haack H., Gau T. 2010. Noble gases in two meteorites that fell in Denmark and Slovenia in 2009. *LPSC* **41**: Abstract #1196.

Pérez-Ramírez J., Christensen C.H., Egeblad K., Christensen C.H., Groen J.C., 2008 - Hierarchical zeolithes: enhanced utilization of microporous crystals in catalysis by advances in materials design. *Chemical Society Reviews* **37**: 2530–2542.

Popova O. P., Jenniskens P., Emel'yanenko V., Kartashova A., Biryukov E., Khaibrakhmanov S., Shuvalov V., Rybnov Y., Dudorov A., Grokhovsky V. I., Badyukov D. D., Yin Q.-Z., Gural P. S., Albers J., Granvik M., Evers L. G., Kuiper J., Kharlamov V., Solovyov A., Rusakov Y. S., Korotkiy S., Serdyuk I., Korochantsev A. V., Larionov M. Y., Glazachev D., Mayer A. E., Gisler G.,

Gladkovsky S. V., Wimpenny J., Sanborn M. E., Yamakawa A., Verosub K., Rowland D. J., Roeske S., Botto N. W., Friedrich J. M., Zolensky M., Le L., Ross D., Ziegler K., Nakamura T., Ahn I., Lee J. I., Zhou Q., Li X.-H., Li Q.-L., Liu Y., Tang G.-Q., Hiroi T., Sears D., Weinstein I. A., Vokhmintsev A. S., Ishchenko A. V., Schmitt-Kopplin P., Hertkorn N., Nagao K., Haba M. K., Komatsu M., and Mikouchi T. (The Chelyabinsk Airburst Consortium), 2013. Chelyabinsk Airburst, Damage Assessment, Meteorite Recovery, and Characterization. *Science* **342**:1069–1073.

Qin L., Alexander C. M. O'D., Carlson R. W., Horan M. F., Yokoyama T. 2010. Contributors to chromium isotope variation of meteorites. *Geochim. Cosmochim. Acta* **74**:1122–1145.

Quirico E., Raynal P. I., Bourot-Denise M. 2003. Metamorphic grade of organic matter in six unequilibrated ordinary chondrites. *Meteorit. Plan. Sci.* **38**: 795–811.

Remusat L., Derenne S., Robert F. 2005. New insights on aliphatic linkages in the macromolecular organic fraction of Orgueil and Murchison meterorites through ruthenium tetroxide oxidation, *Geochimica et Cosmochimica Acta*, **69**,4377–4386.

Revelle D. O. and Ceplecha Z. 2001. Bolide physical theory with application to PN and EN fireballs. *ESA Special Publ.* **495**: 507–512.

ReVelle D. O. 2002. Fireball dynamics, energetics, ablation, luminosity, and fragmentation modeling. In *Proceedings of the Conference Asteroids, Comets, Meteors (ACM 2002)*, edited by Warmbein B. ESA SP-500. Noordwijk: European Space Research and Technology Research Center. pp. 127–136.

ReVelle D. O. 2007. NEO fireball diversity: Energetics-based entry modeling and analysis techniques. *Proceedings of the International Astronomical Union Symposium* **236**:95–106.

Rochette P., Sagnotti L., Bourout-Denise M., Consolmagno G., Folco L., Gattacceca J., Osete M. L., Pesonen L. 2003. Magnetic classification of stony meteorites: 1. Ordinary chondrites. *Meteoritics and Planetary Science* **38**: 251–268.

Rubin A. E., Peterson E., Keil K., Rehfeldt A., Jarosewich E. 1983. Fragmental breccias and the collisional evolution of ordinary chondrite parent bodies. *Meteoritics* **18**:179–196.

Rubin A. E. 1990. Kamacite and olivine in ordinary chondrites: Intergroup and intragroup relationships. *Geochim. Cosmochim. Acta* **54**, 1217–1232.

Rubin A. E. 1992. A shock-metamorphic model for silicate darkening and compositionally variable plagioclase in CK and ordinary chondrites. *Geochimica et Cosmochimica. Acta* **56**:1705–1714.

Rubin A. E. 2003. Chromite-plagioclase assemblages as a new shock indicator; Implications for the shock and thermal histories of ordinary chondrites. *Geochimica et Cosmochimica. Acta* **67**:2695–2709.

Russell S. S., Arden J. and Pillinger C. T. 1991. Evidence for Multiple Sources of Diamond from Primitive Chondrites. *Science* **254**:1188–1191.

Schmitt R. T., Deutsch A. and Stöffler D. 1993. Shock effects in experimentally shocked samples of the H6 chondrite Kernouvé (abstract). *Meteoritics* **28**:431–432.

Schmitt-Kopplin P., Gabelica Z., Gougeon R. D., Fekete A., Kanawati B., Harir M., Gebefuegi I., Eckel G., and Hertkorn N. 2010. High molecular diversity of

extraterrestrial organic matter in Murchison meteorite revealed 40 years after its fall. *Proceedings of the National Academy of Sciences of the United States of America* **107:** 2763-2768.

Schmitz B., Tassinari M., Peucker-Ehrenbrink B., 2001. A rain of ordinary chondritic meteorites in the early Ordovician. EPSL **194**:1–15.

Schneider D. M., Hartmann W. K., Benoit P. H., and Sears D. W. G. 2000. Fusion crust simulation and the search for Martian sediments on earth. Lunar Planet. Sci. XXXI, CD-ROM #1388.

Schoonen M., Smirnov A., Cohn C. 2004. A Perspective on the Role of Minerals in Prebiotic Synthesis. *Ambio* **33**,539–551.

Sears D. W. G. and Mills A. A. 1973. Temperature gradients and atmospheric ablation rates for the Barwell meteorite. *Nature Physical Science* **242**:25–26.

Sears D. W. G. 1979. *The nature and origin of meteorites*, Oxford UP, page 34–38.

Sears D. W. G., Grossman J. N., Melcher C. L., Ross L. M., Mills A. A. 1980. Measuring metamorphic history of unequilibrated ordinary chondrites. *Nature* **287**:791–795.

Sears D. W. G. 2004. *The Origin of Chondrules and Chondrites*. Cambridge University Press.

Sears D. W. G., Ninagawa K, Signhvi A. 2013. Luminescence studies of extraterrestrial materials: Insights into their recent radiation and thermal histories and into their metamorphic history. *Chemie der Erde* **73**:1–37.

Sharma P., Kubik P. W., Fehn U., Gove G. E., Nishiizumi K. and Elmore D. 1990. Development of $^{36}$Cl standards for AMS. *Nuclear Instruments and Methods in Physics Research* **B52:**410–415.

Sharma P., Bourgeous M., Elmore D., Granger D., Lipschutz M. E., Ma X., Miller T., Mueller K., Rickey F., Simms P. and Vogt S. 2000. PRIME lab AMS performance, upgrades and research applications. *Nuclear Instruments and Methods in Physics Research* **B172**:112–123.

Simon S. B., Grossman L., Clayton R. N., Mayeda T. K., Schwade J. R., Sipiera P. P., Wacker J. F., Wadhwa M. 2004. The fall, recovery, and classification of the Park Forest meteorite. *Meteorit. Plan. Sci.* **39**,625–634.

Slyuta E. N. 2010. Physical-mechanical anisotropy of ordinary chondrites and the shape of small rocky bodies. *LPSC abstract* #1103.

Spergel M. S., Reedy R. C., Lazareth O. W., Levy P. W., and Slatest L. A. 1986. Cosmogenic neutron-capture-produced nuclides in stony meteorites. *Journal of Geophysical Research* **91**:483–494.

Spurny P., Borovicka J., Kac J., Kalenda P., Atanackov J., Kladnik G., Heinlein D., Grau T. 2010. Analysis of instrumental observations of the Jesenice meteorite fall on April 9, 2009. *Meteorit. Planet. Sci.* **45**: 1392–1407.

Stöffler D., Bischoff A., Buchwald V., Rubin A. E. 1988. Shock effects in meteorites. In: Meteorites and the early solar system. Tucson, AZ, University of Arizona Press, p. 165–202.

Stöffler D., Keil K., Scott E. R. D. 1991. Shock metamorphism of ordinary chondrites. *Geochim. Cosmochim. Acta* **55**: 3845–3867.

Trinquier A., Birck J.-L., Allègre C. J. 2007. Widespread 54Cr heterogeneity in the inner solar system. *Astrophys. J.* **655**:1179–1185.

Trinquier A, Birck J.-L., Allègre C. J., Göpel C., and Ulfbeck D. 2008. $^{53}Mn$–$^{53}Cr$ systematics of the early Solar System revisited. *Geochimica et Cosmochimica Acta* 72:5146–5163

Troiano J., Rumble D. III, Rivers M. L., Friedrich J. M. 2011. Compositions of three low-FeO ordinary chondrites: indications of a common origin with the H chondrites. *Geochimica et Cosmochimica Acta* **75**: 6511–6519.

Van Schmus W. R. and Wood J. A. 1967. A chemical-petrologic classification for the chondritic meteorites. *Geochimica et Cosmochimica Acta* **31**:747–765.

Van Schmus W. R. and Ribbe P. H. 1968. The composition and structural state of feldspar from chondritic meteorites. *Geochimica et Cosmochimica Acta* **32**:1327–1342.

Wasson J.T. and Kallemeyn G.W. 1988. Compositions of Chondrites. Philosophical Transactions of the Royal Society of London. Series A, Mathematical and Physical Sciences: 325, No. 1587, *The Solar System: Chemistry as a Key to Its Origin*, 535–544.

Weirich J. R., Swindle T. D. Isachsen C. E., Sharp T. G., Li C., Downs R. T. 2012. Source of potassium in shocked ordinary chondrites. *Geochmicia et Cosmochimica Acta* **98**:125–139.

Weirich J. R., Swindle T. D., Isachsen C. E. 2012a. 40Ar-39Ar age of Northwest Africa 091: More evidence for a link between L chondrites and fossil meteorites. *MAPS* **47**:1324–1335.

Wetherhill G. 1985. Asteroidal source of ordinary chondrites. *Meteoritics* **20**:1–22.

Wieler R., Graf T., Pedroni A., Signer P., Pellas P., Fieni C., Suter M., Vogt S., Clayton R. N., and Laul J. C. 1989. Exposure history of the regolithic chondrite Fayetteville. II - Solar-gas-free light inclusions. *Geochimica et Cosmochimica Acta* **53**:1449–1459.

Woodcock N. H. 1977. Specification of fabric shapes using an eigenvalue method. *Geo. Soc. Am. Bull.* **88**:1231–1236.

Woodcock N. H. and Naylor M. A. 1983. Randomness testing in three-dimensional orientation data. *J. Struct. Geo.* **5**:539–548.

Wu Q., Pomerantz A., Mullins O., Zare R. N. 2013. Minimization of fragmentation and aggregation by laser desorption laser ionization mass spectrometry. J. Am. Soc. Mass Spectrometry **24**:1116–1122.

Yamakawa A., Yamashita K., Makishima A., Nakamura E. 2010. Chromium isotope systematics of achondrites: Chronology and isotopic heterogeneity of the inner solar system bodies. *Astrophys. J.* **720**:150–154.

Young E. D. and Russell S. S. 1998. Oxygen reservoirs in the early solar nebula inferred from an Allende CAI. *Science* **282**:452–455.

Zinner E. 1988. Interstellar cloud material in meteorites. In: *Meteorites and the Early Solar System* (eds. J. F. Kerridge and M. S. Mathews). University of Arizona Press, Tucson, pp. 956–983.

## FIGURES

Figure 1a. Recovered Novato meteorites, with sample identification chart for Novato N01 (scale in mm). Scale cubes are 1 cm in diameter, while the coin in the panel of N04 is a U.S. quarter. Scale for N06 (Fig. 1b) and N03 (Fig. 11) are shown elsewhere. Note fusion crust and manifestation of light and dark lithologies in individual meteorites.

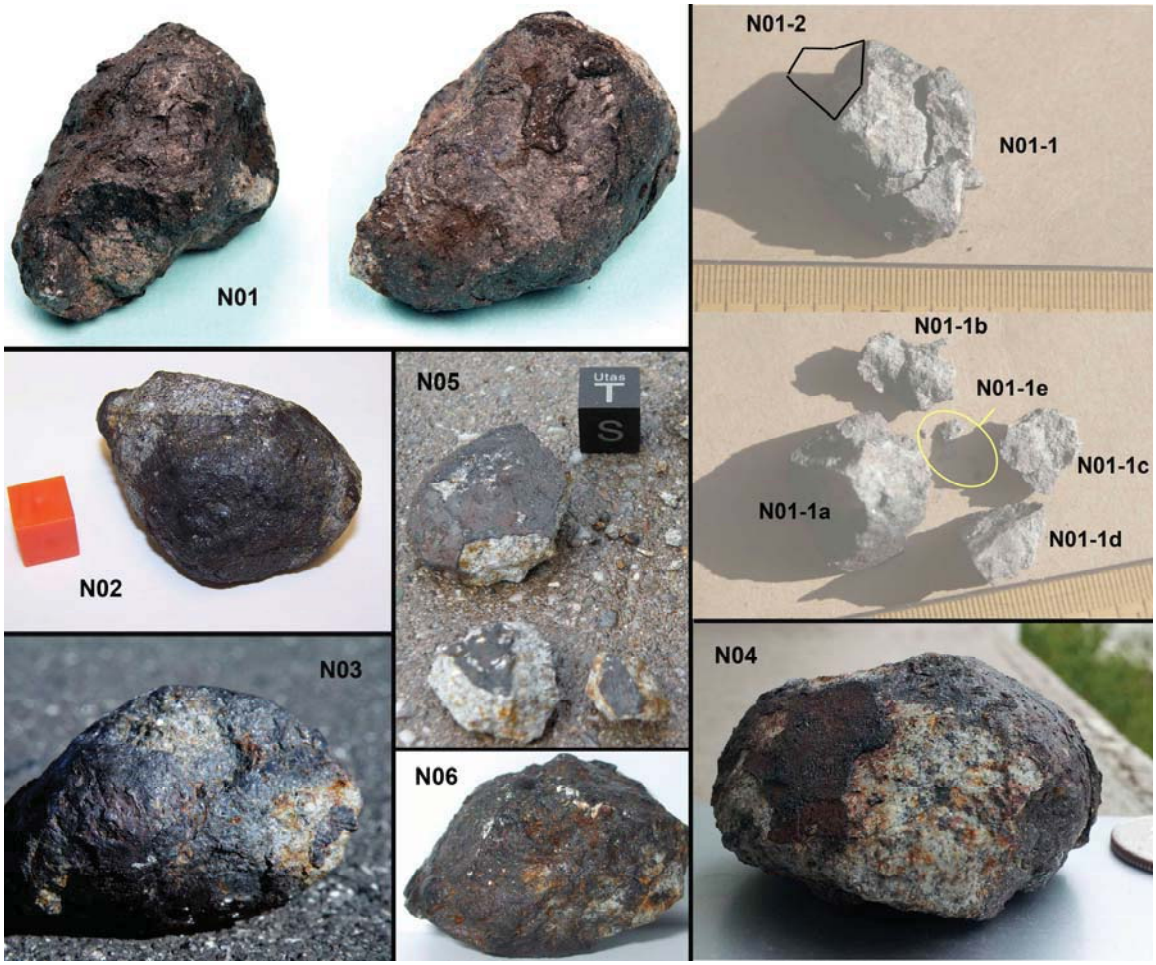

Figure 1b. Photographic images of cut Novato faces showing the brecciated chondritic texture with light and dark lithologies distributed unevenly. Boundaries between them can be sharp or gradual. (A) Contrast enhanced image of a slice of Novato N06. (B) Same for Novato N02, with cut marks at center top and in top left corner.


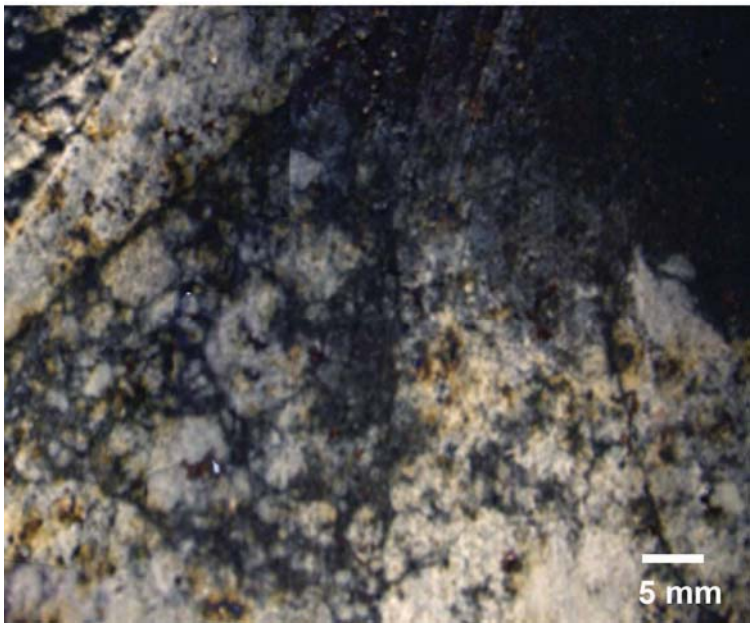

Fig 2. X-ray CT imagery of Novato N05 and N06, with light patches showing X-ray opague metal grains (FeNi) or sulfides (troilite, FeS). (A) A computer sliced X-ray view of the interior of N05 of pure light lithology, one of 1,824 X-ray CT slices in this view direction with a pixel size of 15.28 micron. (B) A computer sliced X-ray view of the interior of N06 of mostly dark lithology, one of 1,003 X-ray CT slices in this view direction with a pixel size of 44.12 micron. See the journal website for online 3D movie rendition of the two stones, full experimental details and movie captions at http://www.xxx.ccc .

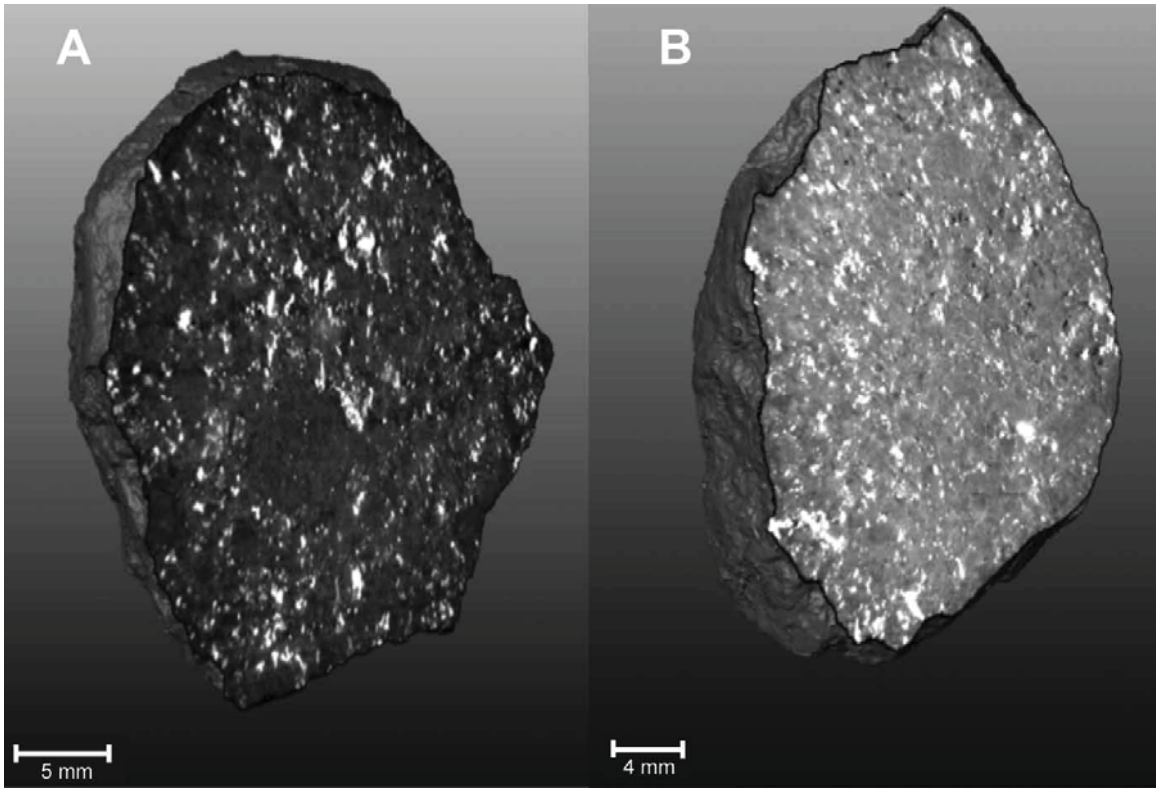

Figure 3a-f. Backscattering electron (BSE) images of Novato N06. The meteorite is extensively recrystallized during thermal metamorphism and contains abundant coarse grains of plagioclase, phosphates, and chromite. Only rare bared olivine chondrule can be recognized in BSE images. Abundant sulfide±metal veins crosscutting silicate and chromite grains suggest that the meteorite experienced extensive shock metamorphism after thermal metamorphism. The presence of plagioclase-chromite-phosphate pockets are also visible. chr = chromite; Cl-apt = Cl-apatite; met = Fe,Ni-metal; ol = olivine; pl = plagioclase; px = low-Ca pyroxene; sf = troilite; whit = whitlockite.

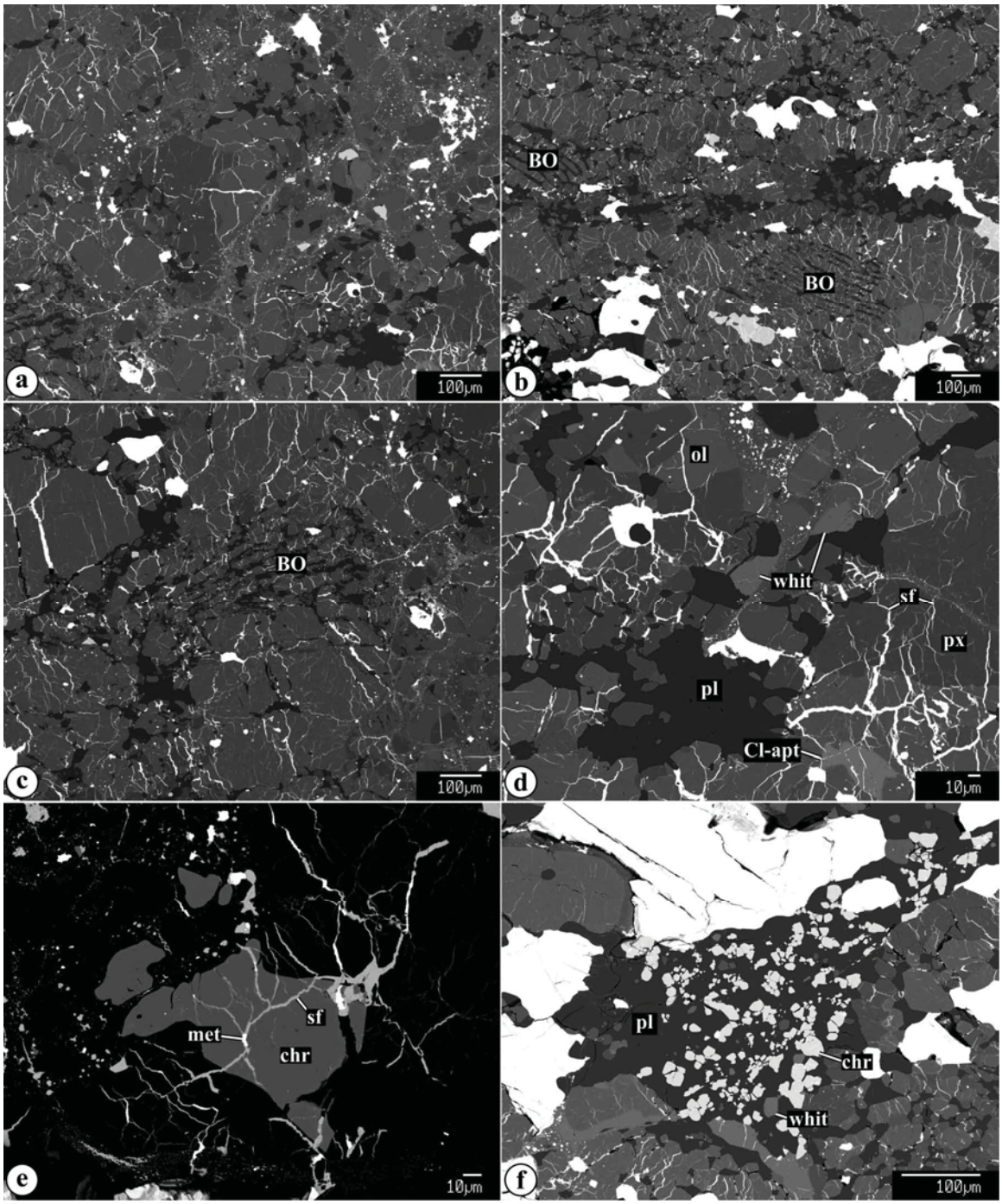

Figure 3g. Combined elemental maps of Novato N06 in Mg (red), Ca (green) and Al Kα X-rays (blue). ol = olivine; pl = plagioclase; ph = phosphate; px = low-Ca pyroxene.

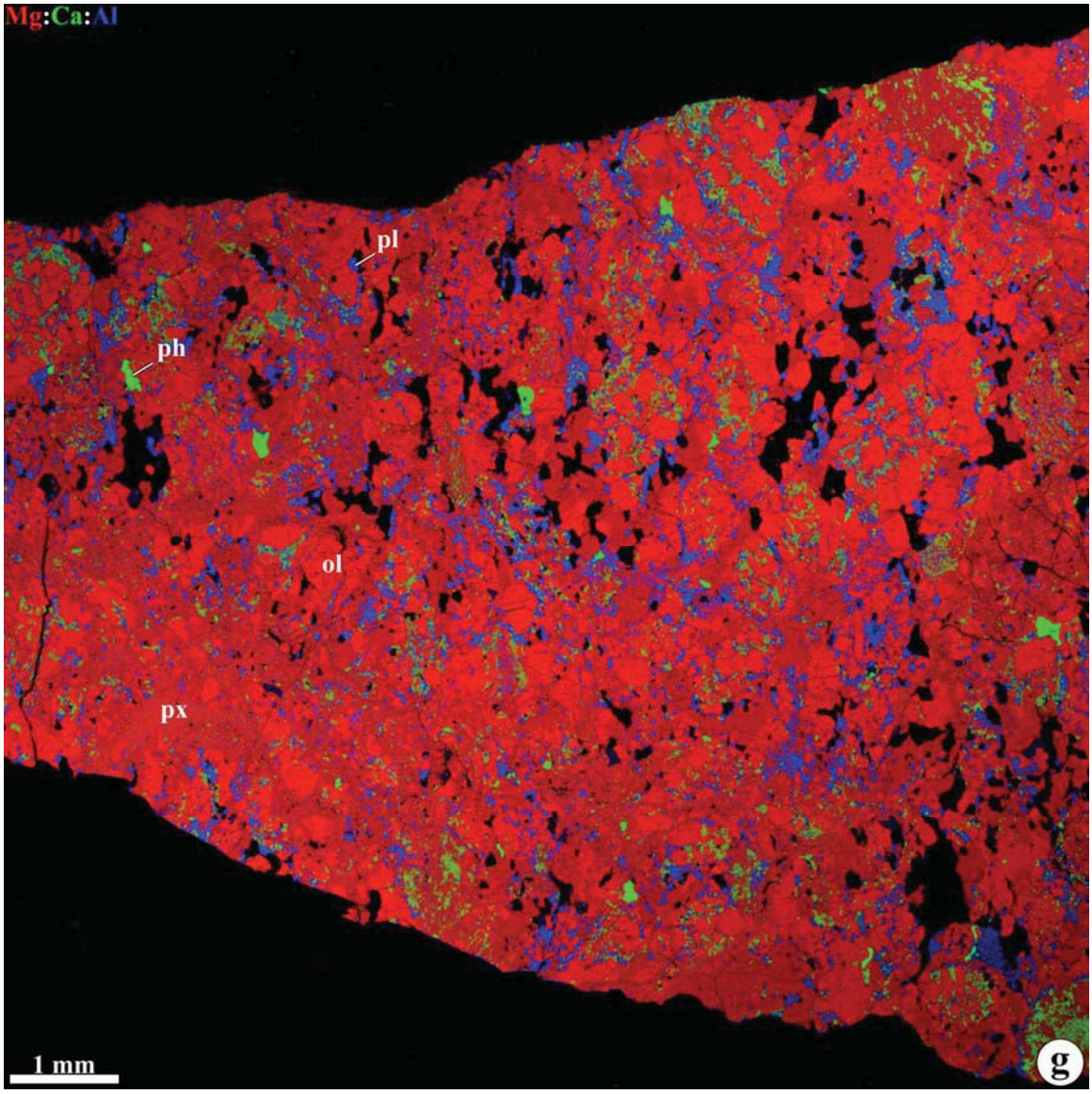

Figure 3h. Combined elemental maps of Novato N06 in P (red), Na (green) and Cl Kα X-rays (blue). Al-apt = Cl-apatite; whit = whitlockite.

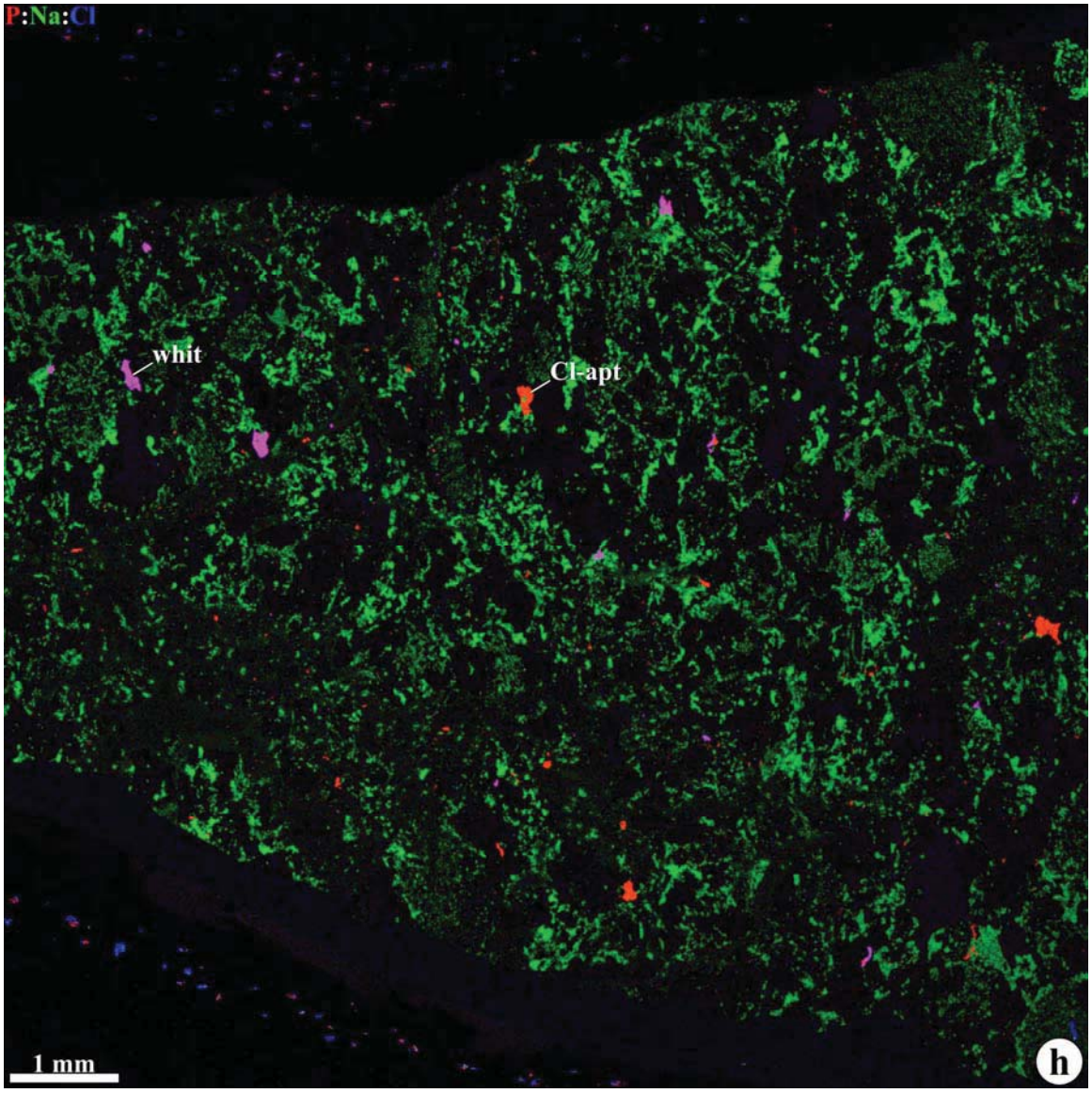

Figure 4a. Mean CI-normalized abundances of lithophiles, siderophiles and moderately volatile elements in Novato compared with average L chondrite compositions. Elements are organized by increasing putative volatility and similar geochemical character.

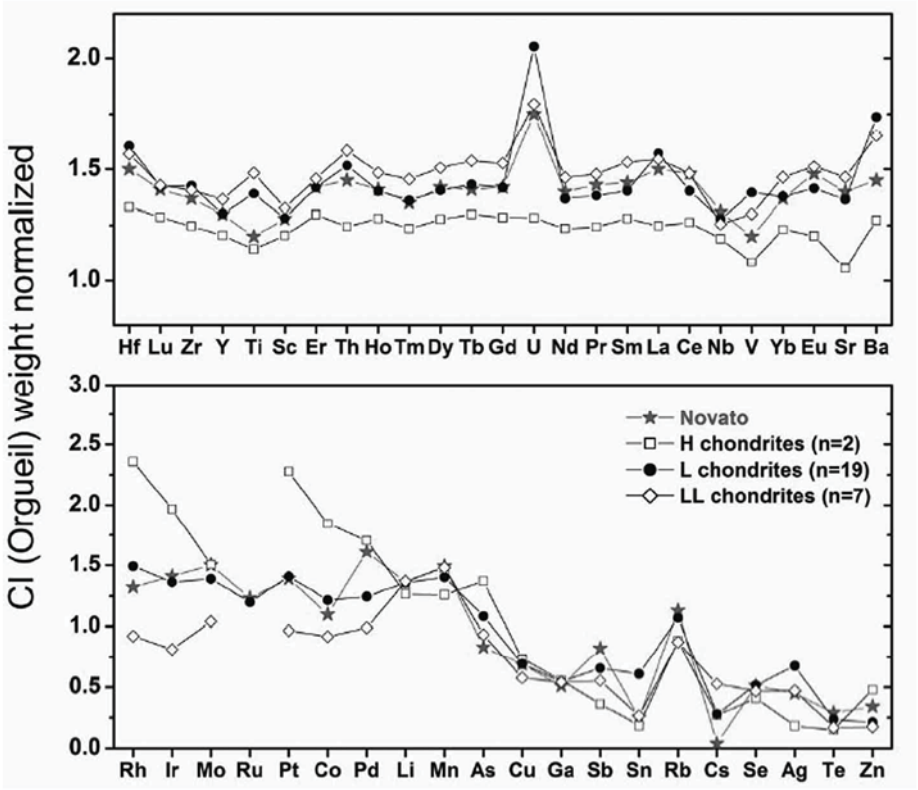

Figure 4b. CI-chondrite normalized REE pattern of fragments of Novato N01, N05 and N06. "Light" refers to light lithology, and "Dark" refers to dark lithology (as shown in Fig. 1b). Note that the pattern designated as “N01 Ave (F)” is an average of values from seven fragments of both light and dark lithologies (all from Novato 01, mostly dark lithologies).

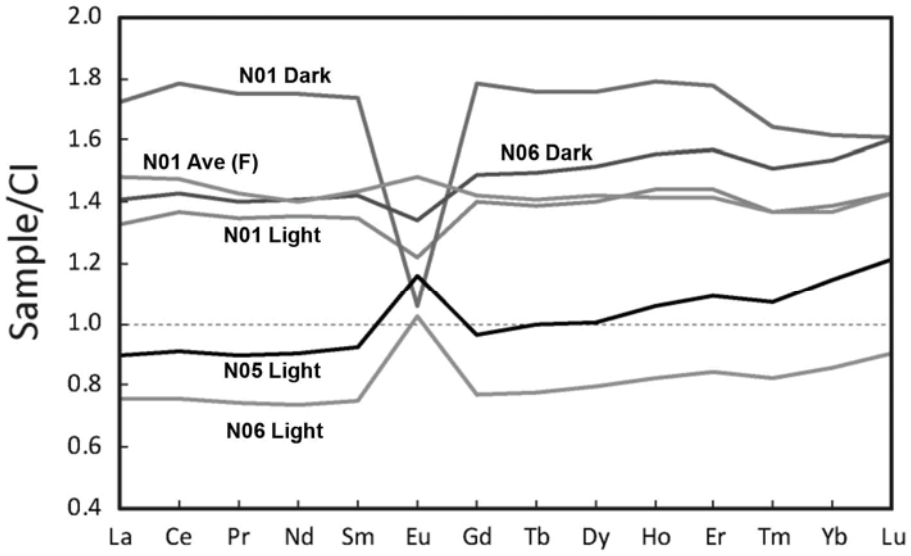

Figure 5. (**A**) Three oxygen-isotope diagram, showing Novato data together with H, L, and LL chondrites (Clayton et al., 1991). The inset shows the L and LL chondrites region with the Novato data in more details. (**B**) $\Delta^{17}O$ *vs.* Fa mol% of olivine in Novato, compared to other ordinary chondrites of type H, L, and LL (data source: Trioano et al., 2011 and references therein). (**C**) Variation of $\varepsilon^{54}Cr$ values among the various extraterrestrial materials. Novato dark lithology is identical to those of reported values for ordinary chondrites, whereas the light lithology of Novato shows a higher value, consistent with the higher $\Delta^{17}O$ value for the light lithology (Table 5, and panel D inset). Filled symbols represent data acquired at UC Davis. Open symbols are literature data: diamonds, inverted triangle and regular triangles are from Trinquier et al. (2007), Qin et al. (2010) and Yamakawa et al. (2010); (**D**) $\varepsilon^{54}Cr$ *vs.* $\Delta^{17}O$ for Novato, compared to the other major meteorite groups. Data sources for $\Delta^{17}O$ and $\varepsilon^{54}Cr$ are from Clayton and Mayeda (1984; 1996; 1999); Clayton et al. (1991); Young and Russell (1998); Jenniskens et al. (2012); Trinquier et al. (2007); Göpel et al. (2010) and Irving et al. (2011). Chelyabinsk data shown for comparison in all four panels are from Popova et al. (2013).

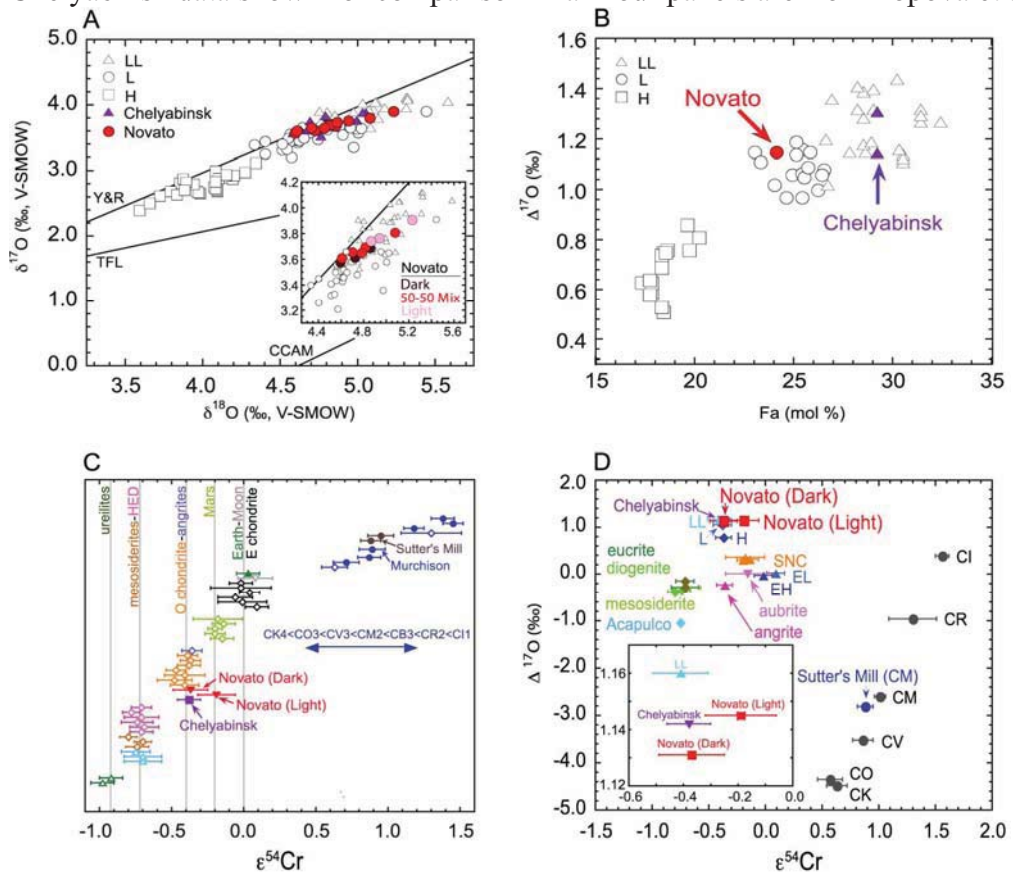


Notes: TFL refers to the terrestrial mass dependent fractionation line; CCAM refers to carbonaceous chondrite anhydrous mineral line (Clayton and Mayeda, 1999); Y&R refers a slope of 1 line defined by unaltered minerals from CV CAIs by Young and Russell (1998). Fa mol% is defined as mole ratio of Fe/(Fe+Mg) in olivine; $\Delta^{17}O$ is the deviation from the terrestrial fractionation line following the relationship $\Delta^{17}O=\delta^{17}O' - 0.528\times\delta^{18}O'$, where $\delta^{17,18}O' = ln(\delta^{17,18}O/10^3 + 1) \times 10^3$, $\delta^{17,18}O = [(^{17,18}O/^{16}O)_{sample} / (^{17,18}O/^{16}O)_{SMOW} - 1] \times 10^3$, and SMOW refers to standard mean ocean water.

Figure 6. Trajectory solution and station locations. Locations (a): Phil Terzain, (b) Wesley Jones, (c) Robert P. Moreno. Also shown are the location of the recovered meteorites and the possible fall area based on early CAMS results as published in the San Francisco Chronicle.

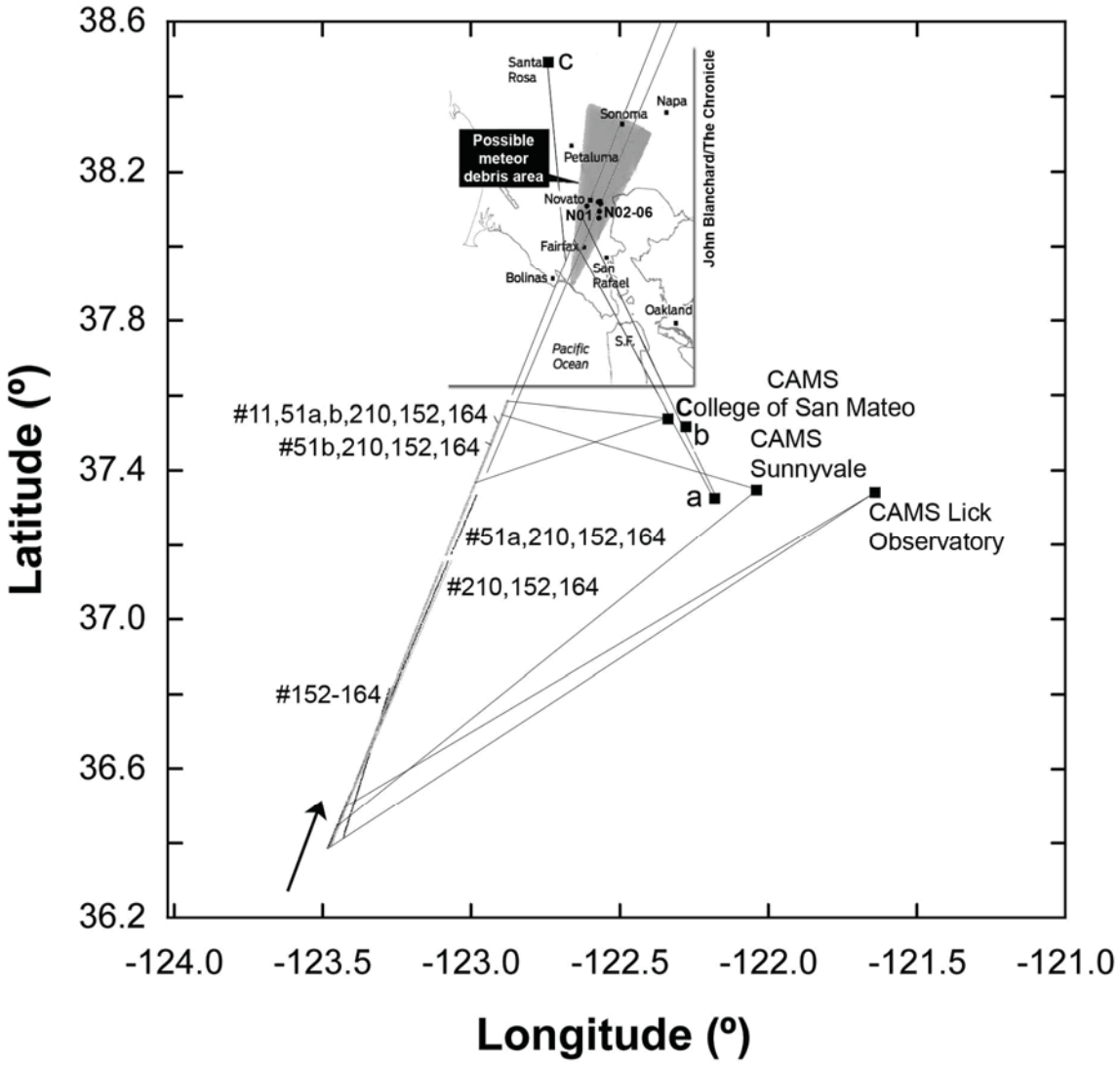

Figure 7. CAMS detections of the November 17 fireball, shown as the maximum pixel intensity for each pixel over an 8-second video sequence. (a) College of San Mateo maximum pixel image. (b) Same, but time-average data over same time interval.

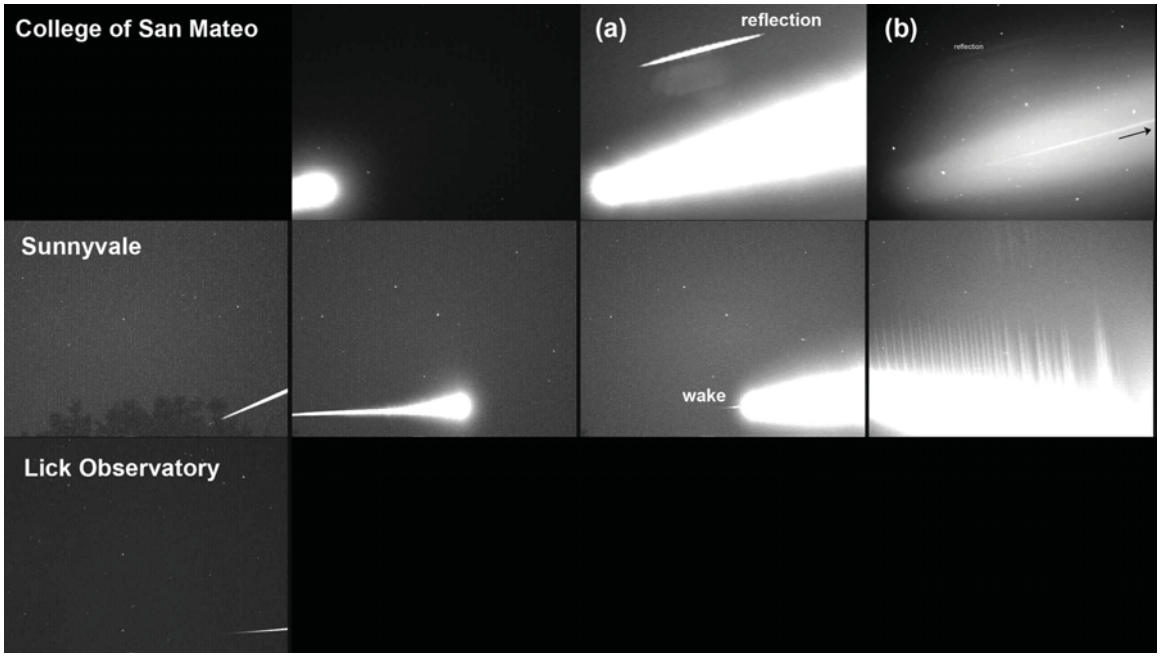

Figure 8. Novato fireball light curve normalized to a distance of 100 km, derived from CAMS video observations, an overlapping allsky image by James D. Wray, and a series of photographs by Robert P. Moreno Jr. (Fig. 7).

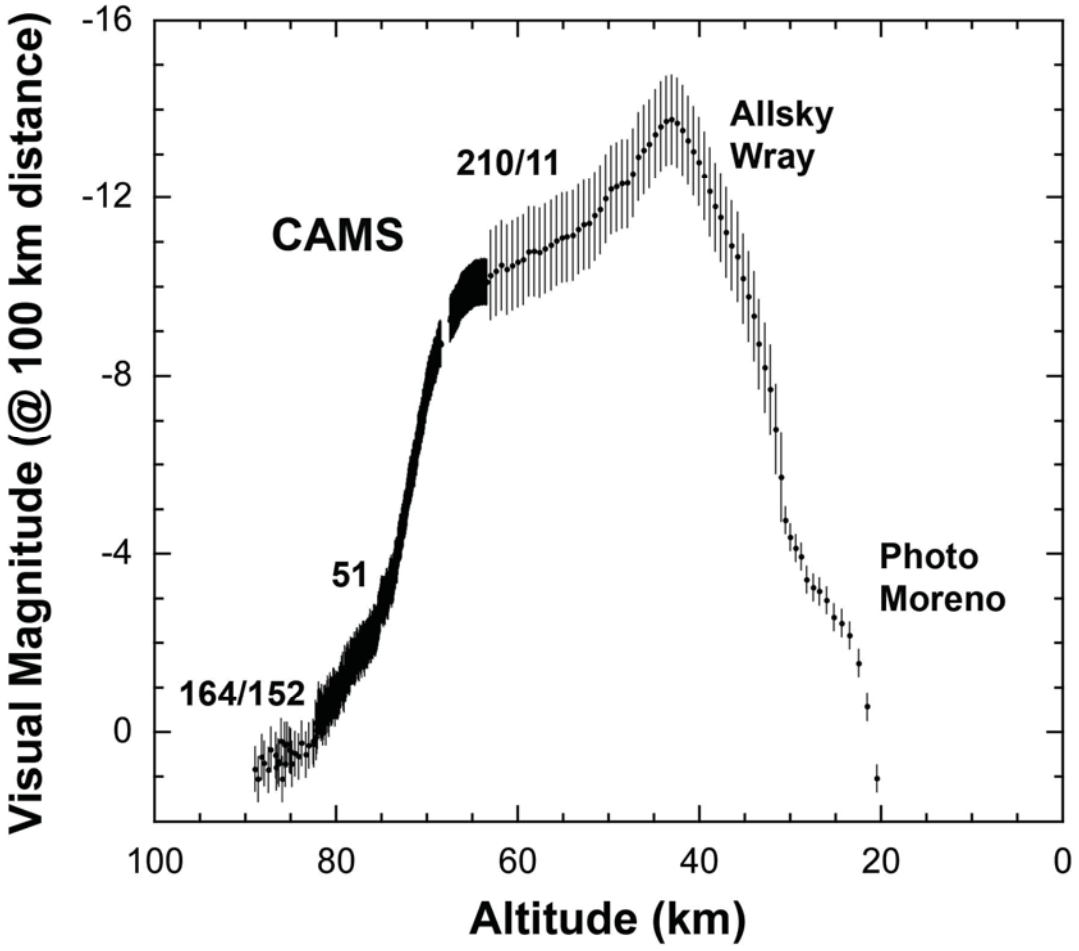

Figure 9. Doppler weather radar returns (KMUX 2:39:44 UT) from falling meteorites and location of the trajectory in Napa and Sonoma counties.

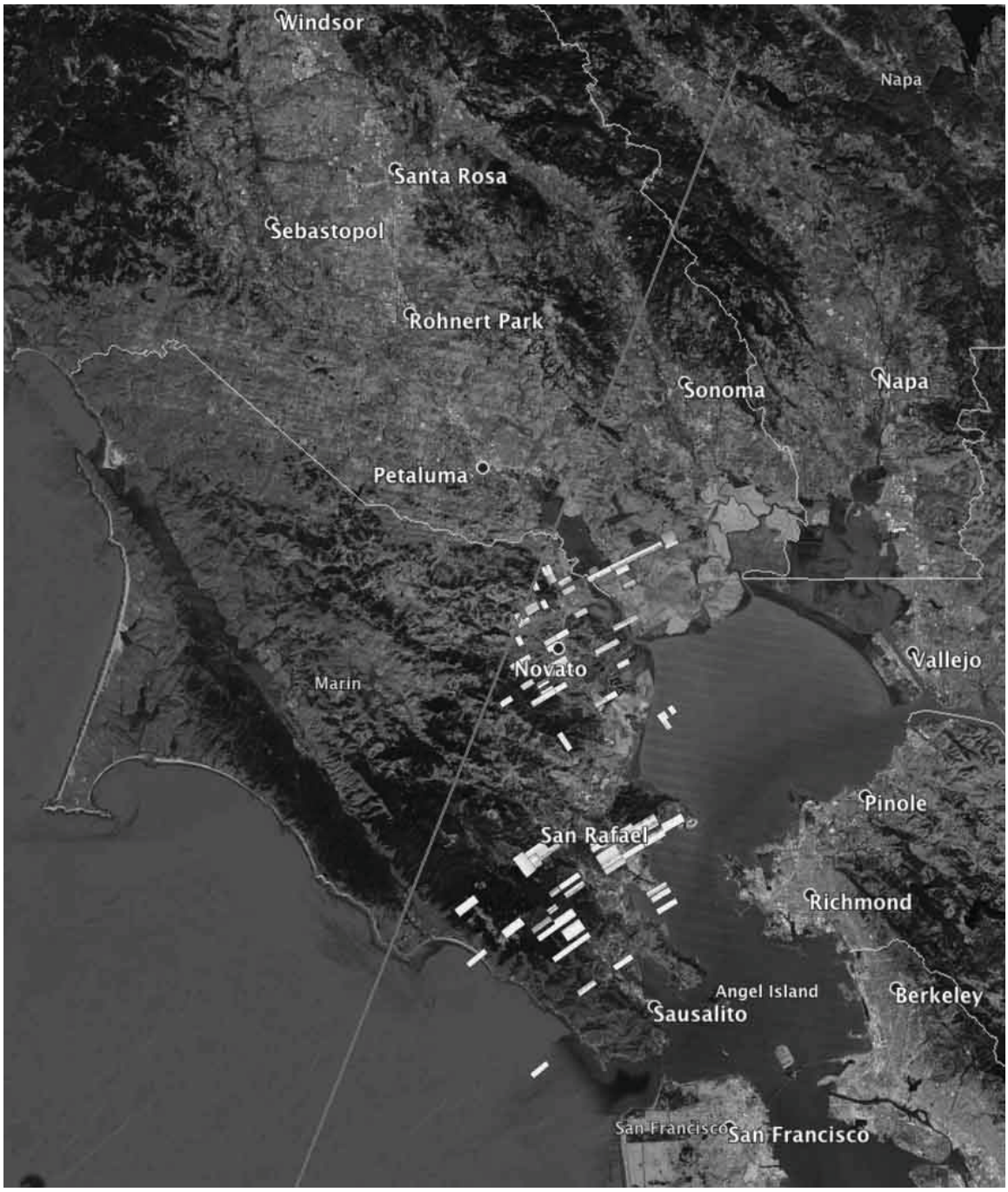

Figure 10. Fragmentation and relative deceleration at the end of the trajectory in a compilation of digital photographs of the October 17, 2012, fireball by Robert P. Moreno Jr. of Santa Rosa. Photos were taken a rate of 4 per second with a Canon EOS 7D camera. set at 200 mm focal length and F2.8 diaphragm, with 1/320s exposure time at ISO 1600.

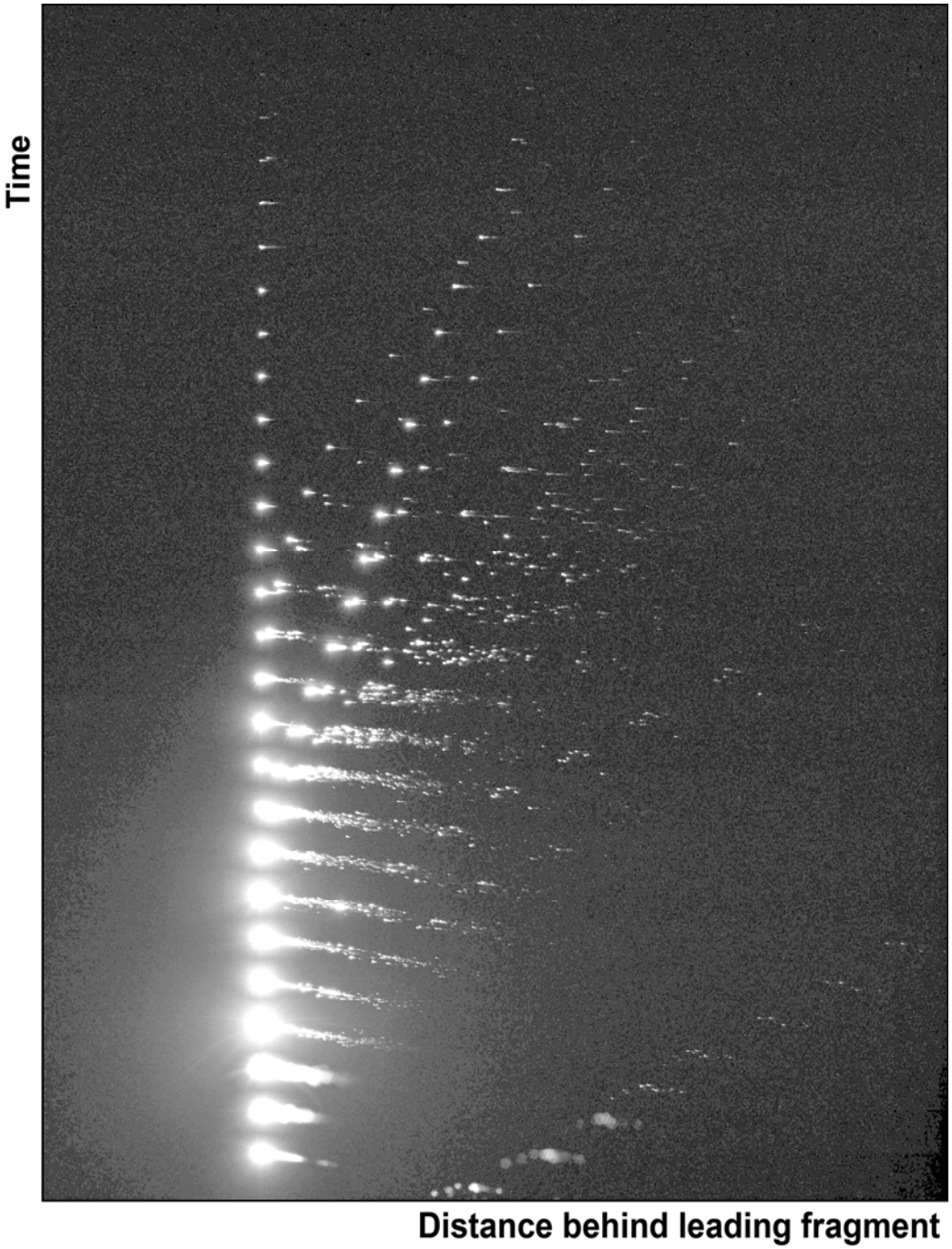

Figure 11. (A, B) Details of the fusion crust of N01, showing an area about 1 cm across. (C, D) Evidence for spallation in Novato N03, showing two sides of the meteorite as it was found. Cube is 1-cm sized.

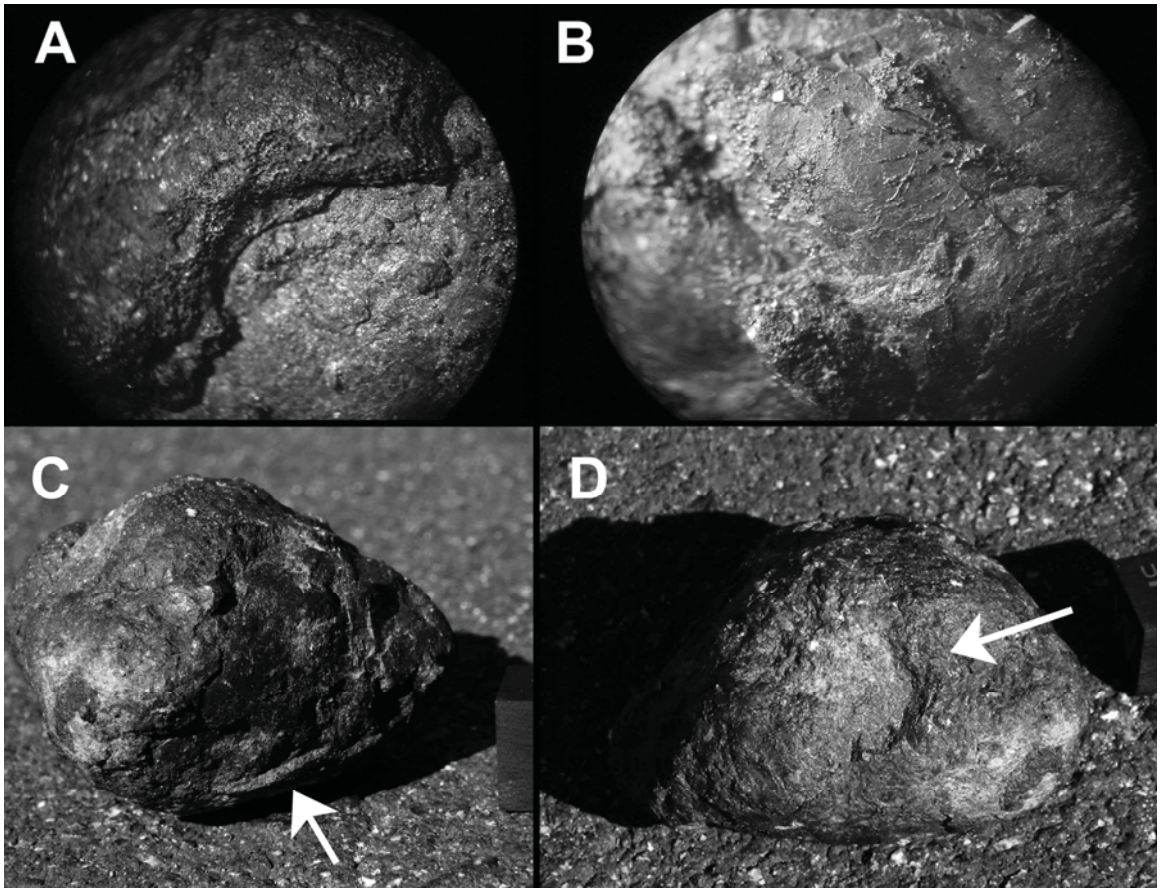

Figure 12. Stereoplot of major axis orientations of all individual metal grains in two different stones of the Novato L chondrite. The orientations of the stones in the meteoroid relative to one another are unknown. However, the intensity of foliation is nearly identical between the two fragments, suggesting that both experienced the same impact event.

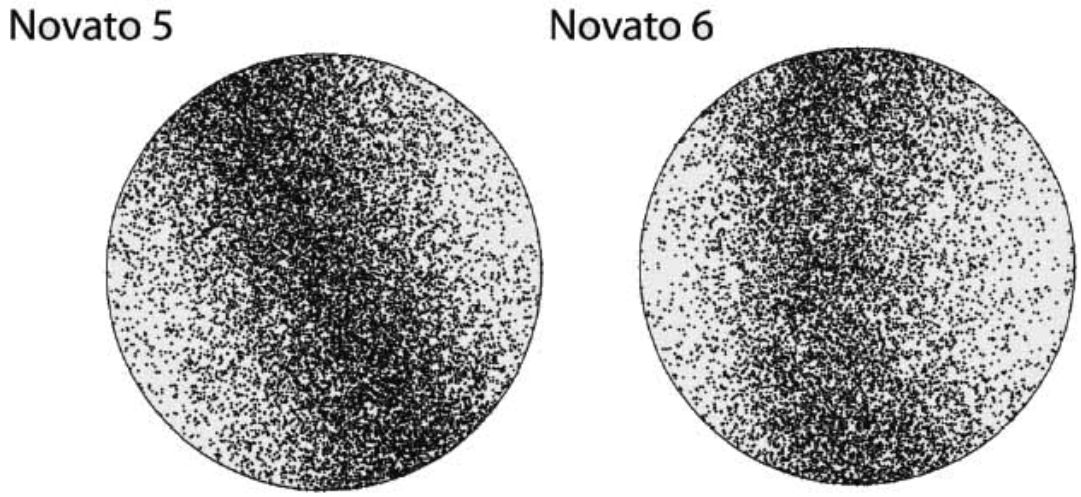

Figure 13. Degree of compaction, given by the strength factor determined from the collective orientation of metal grains in ordinary chondrites versus shock stage (Friedrich et al., 2008; 2013). Novato shows significant foliation in both samples examined.

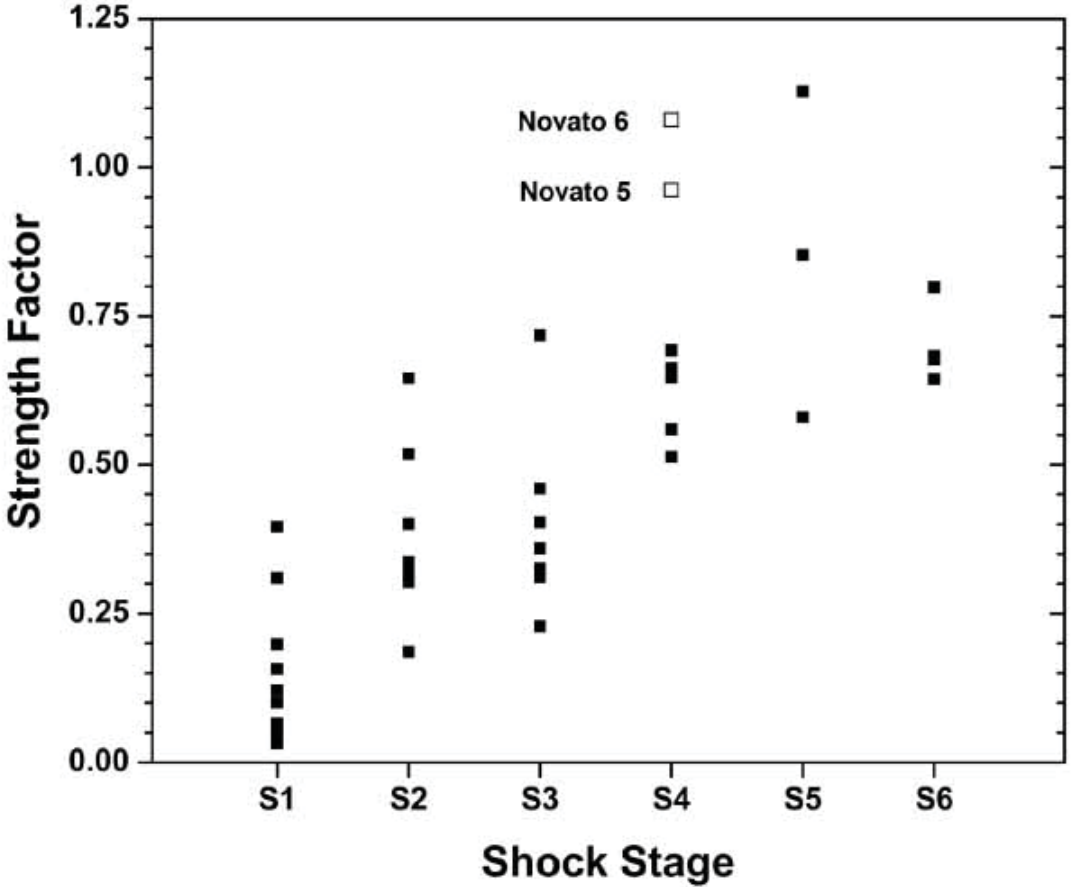

Figure 14. Visualization of the molecular content of the Novato light lithology (3,200 assigned compositions) and dark lithology (5,900 assigned) fractions as analyzed with ESI(-)-ICR/FTMS. The van Krevelen diagrams (A) show rather aliphatic type of structures with a prevalence of CHO and CHOS type molecules in the light material (left) and an increase in the count of CHNO compounds in the dark material (right); Diagrams (B) show how H/C changes by molecular mass and show the presence of regular homologous series up to higher masses. The area of each circle is proportional to the intensity of the detected mass peak. Colors mark compounds containing only CHO (blue), CHOS (green), CHNO (orange), or all CHNOS (red) molecules; (C) These 0.1 amu mass spectra (for m/z = 319.15 to 319.25) show the importance of the nitrogen compounds in the dark fraction and compares its specific organic signature and its complexity to Soltmany and Murchison meteorit extracts.

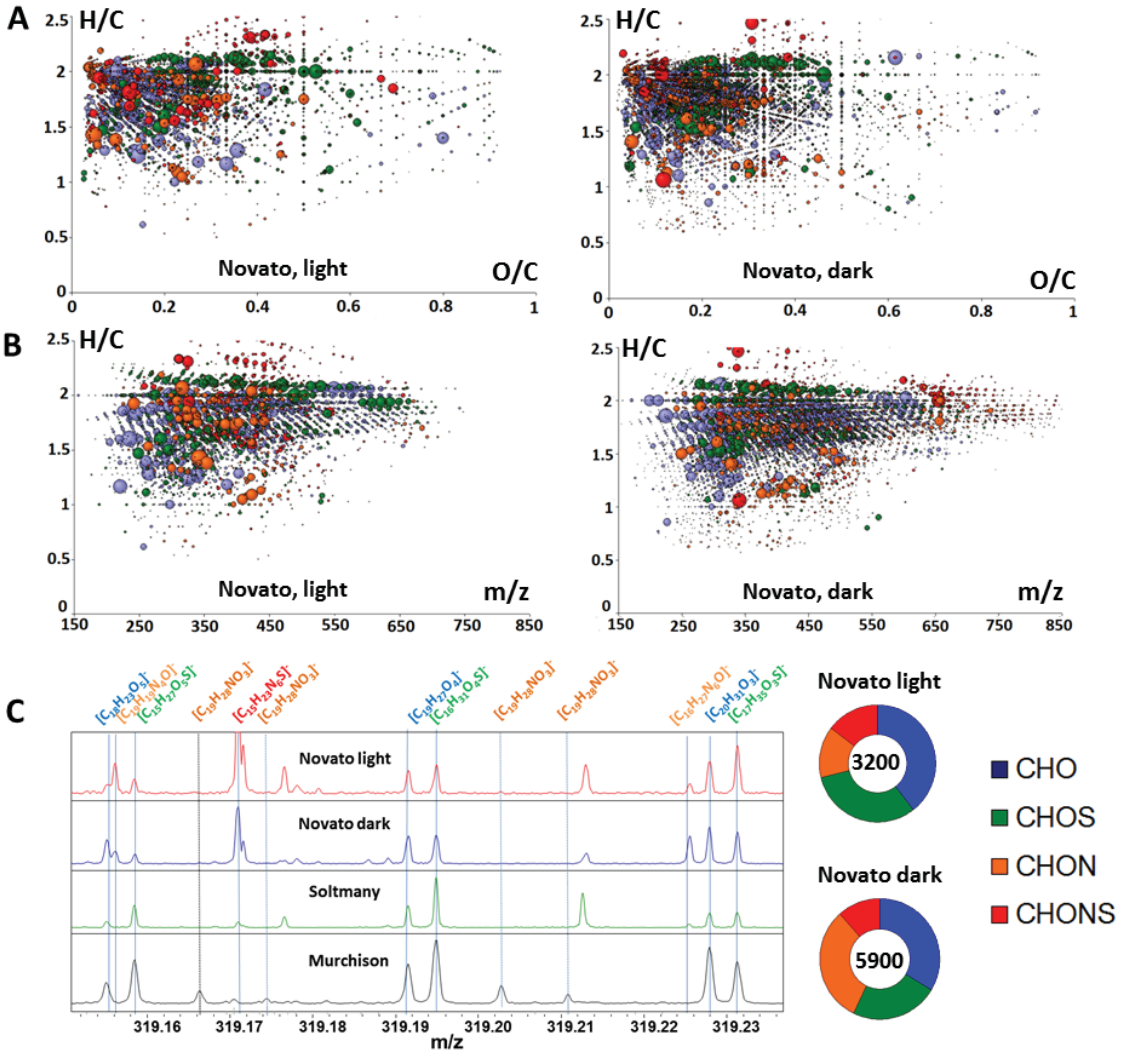

Figure 15. 2 Dimensional $^{1}H$, $^{13}C$ Nuclear Magnetic Resonance (NMR) spectra (800 MHz, $CD_3OD$) from dark lithology; the light lithology extracts vary in cross peak amplitudes rather than positioning. (A) $^{1}H$, $^{1}H$ Total Correlation Spectroscopy (TOCSY), with (A1) showing the C-C**H**-C**H**-C cross peaks, (A2) shows the O-C**H**-C**H**-C cross peaks, (A3) the O-C**H**-C**H**-O cross peaks and (A4) the C=C**H**-C**H**-C- cross peaks. The red dotted box denotes the $\mathbf{H}_3$C-C**H** cross peaks; (B) $^{1}H$, $^{1}H$ J-resolved NMR spectra of aliphatic protons; (C) same for OC**H** units; (D) same for CCC**H** units cross peaks; (E) same for $CH_2$-selective peaks (blue) and $CH_3$-selective peaks (red) of aliphatic cross peaks.

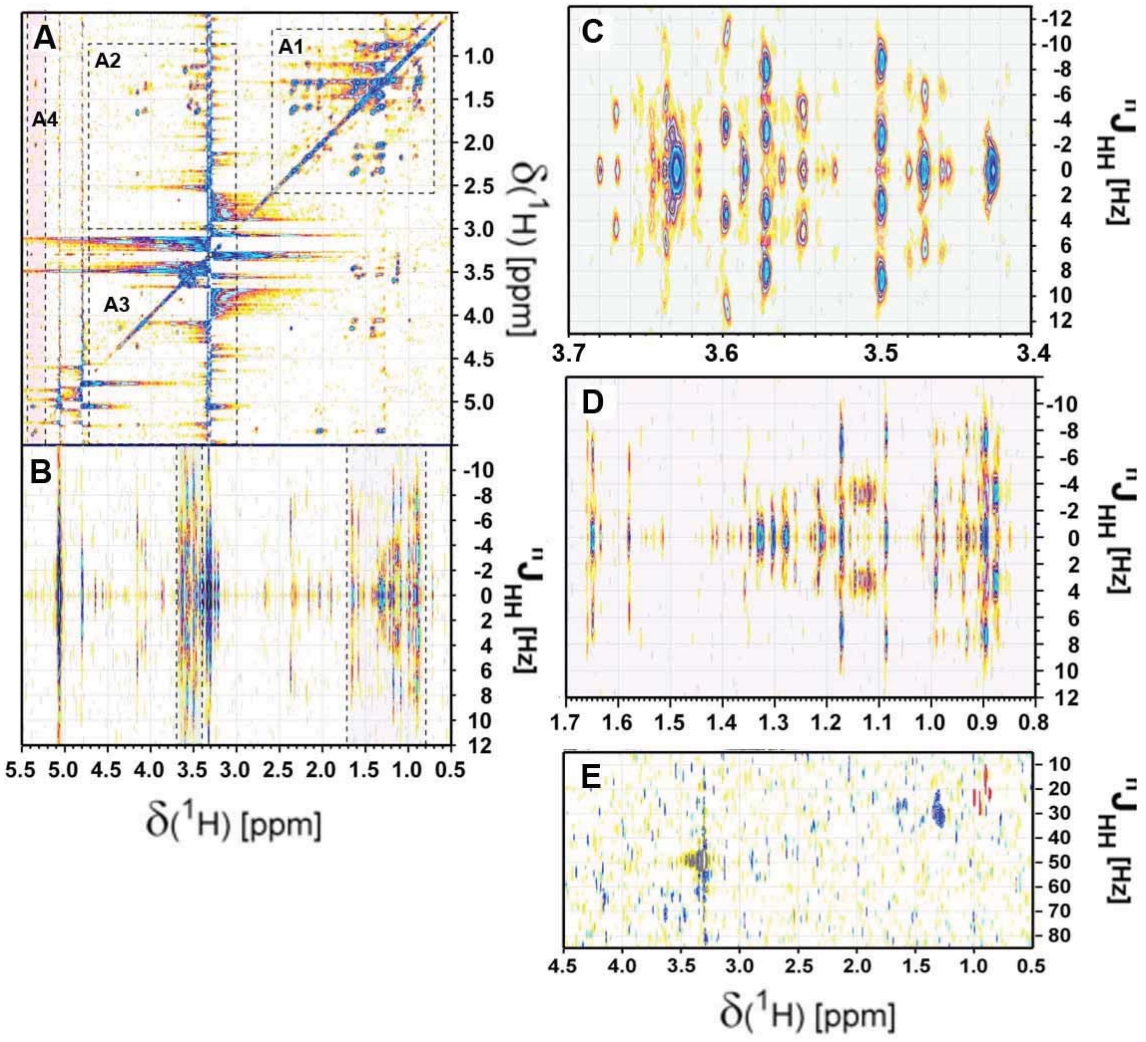

Figure 16. $L^2MS$ spectrum of Novato N01-1b. Inset shows an enlarged portion of the mass spectrum.

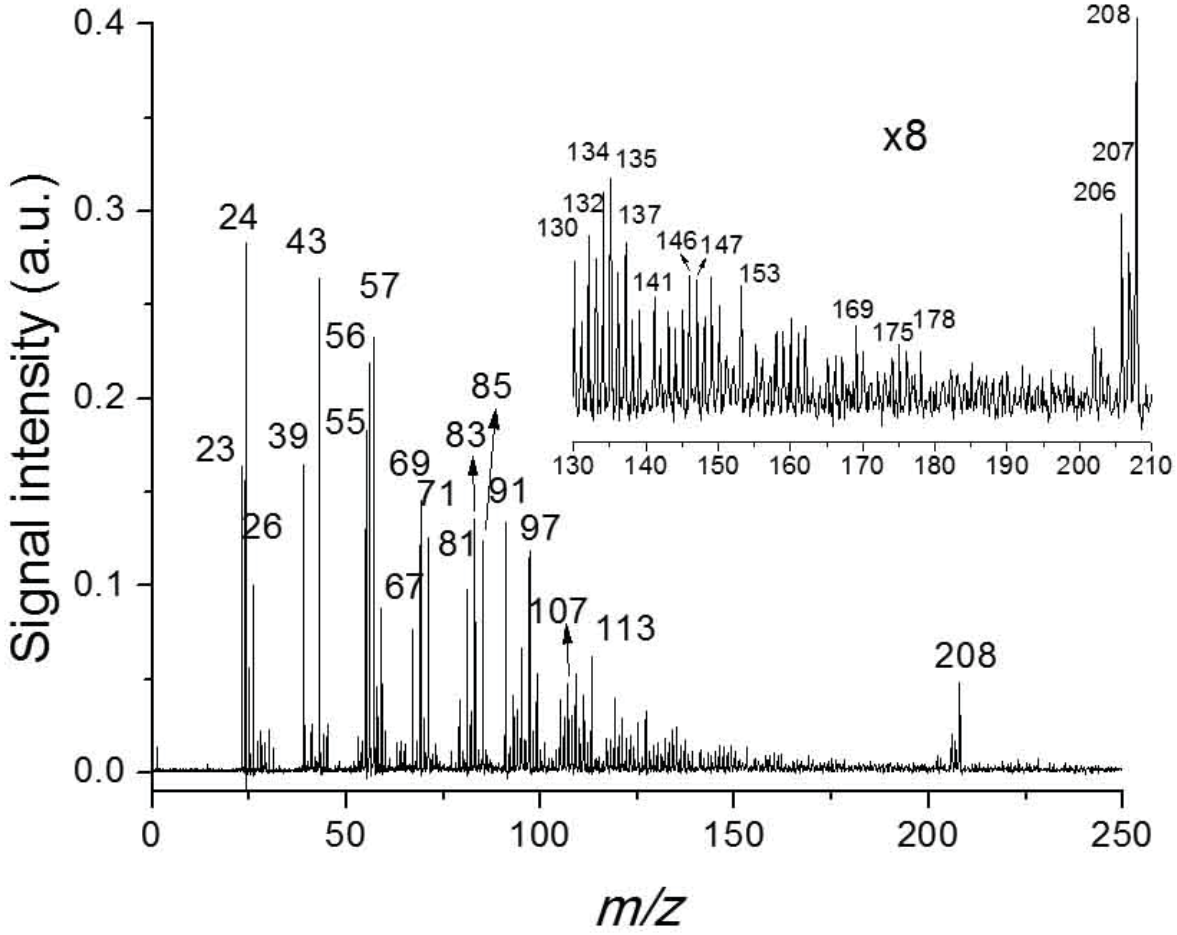

Figure 17. Data from stepped combustion-gas source-mass spectrometry of Light and Dark fragments from Novato 01-1e. (a) Carbon; (b) nitrogen; and (c) the atomic C/N ratio. Abundances of carbon and nitrogen are plotted as histograms and scaled on the left-hand axis. Isotopic compositions are plotted as lines and scaled on the right-hand axis. Errors in $\delta^{13}C$ and $\delta^{15}N$ are less than the size of the symbols.

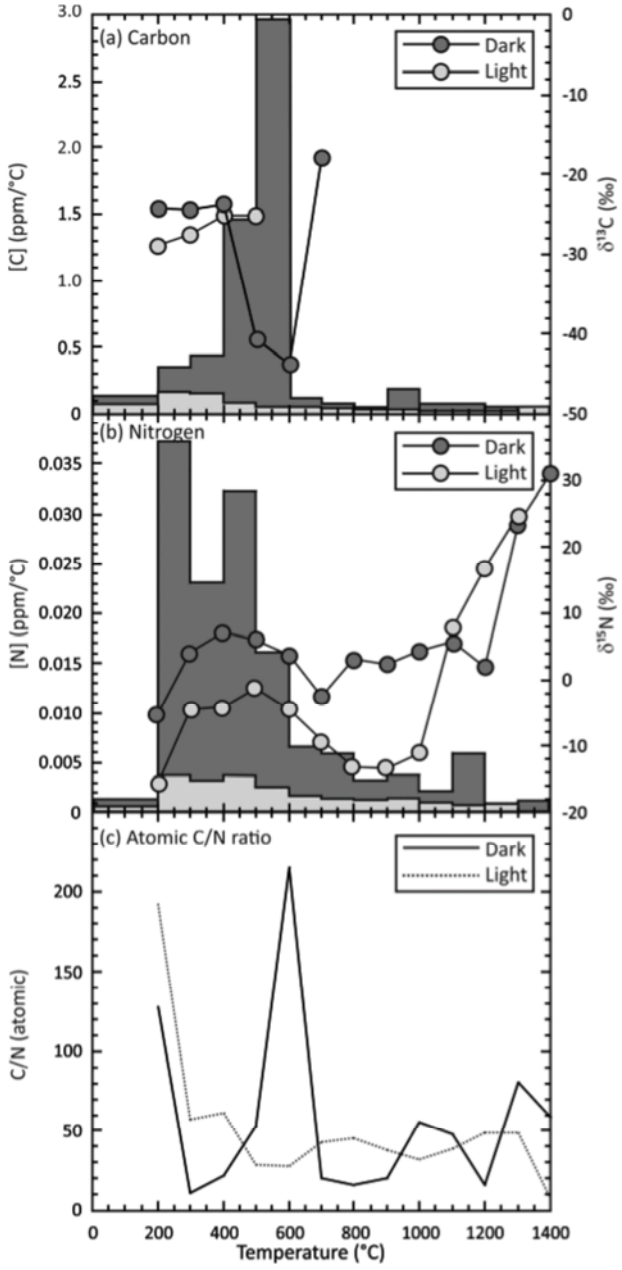

**TABLES**

Table 1. Overview of recovered meteorites.

| # | Mass (g) | log $\chi$ ($10^{-9}$ $kgm^3$) | Latitude (ºN) | Longitude (ºW) | Date of find | Finder |
|---|---|---|---|---|---|---|
| N01 | 61.9 | 4.20±0.02 | 38.1090 | 122.6105 | 10/20/2012 | Lisa Webber |
| N02 | 65.9 | 4.16±0.02 | 38.0941 | 122.5683 | 10/22/2012 | Brien Cook |
| N03 | 79.8 | -.- | 38.1152 | 122.5640 | 10/27/2012 | Jason Utas |
| N04 | 107 | -.- | 38.1217 | 122.5670 | 10/27/2012 | Robert Verish |
| N05 | 24.3 | 4.32±0.04 | 38.1195 | 122.5720 | 11/02/2012 | Jason Utas |
| N06 | 23.7 | 4.34±0.03 | 38.0768 | 122.5692 | 11/11/2012 | Darci Kane |

Table 2. Summary of XRF derived major elemental composition data for Novato N06 (slab), measured for areas with predominantly dark lithology and light lithology on the front and back of the slab.

| | Dark (Front) | | Dark (Back) | | Light (Front) | | Light (Back) | |
|---|---|---|---|---|---|---|---|---|
| | Mean | 1 σ | Mean | 1 σ | Mean | 1 σ | Mean | 1 σ |
| Si | 18.66% | 0.73% | 18.08% | 0.74% | 19.48% | 0.72% | 18.18% | 0.74% |
| Fe | 17.16% | 0.24% | 17.97% | 0.24% | 15.67% | 0.25% | 17.20% | 0.24% |
| Mg | 16.41% | 0.66% | 15.27% | 0.69% | 16.33% | 0.66% | 15.13% | 0.69% |
| Al | 1.70% | 2.66% | 1.77% | 2.60% | 2.05% | 2.39% | 1.92% | 2.48% |
| Ca | 1.33% | 1.74% | 1.24% | 1.81% | 1.46% | 1.67% | 1.50% | 1.65% |
| S | 1.25% | 1.99% | 1.76% | 1.67% | 1.67% | 1.73% | 1.67% | 1.72% |
| Na | 0.99% | 5.61% | 1.02% | 5.64% | 1.30% | 4.81% | 1.16% | 5.25% |
| Ni | 0.57% | 1.36% | 0.67% | 1.28% | 0.39% | 1.61% | 0.57% | 1.38% |
| Cr | 0.37% | 2.23% | 0.33% | 2.35% | 0.21% | 3.03% | 0.33% | 2.37% |
| Mn | 0.26% | 2.38% | 0.24% | 2.49% | 0.26% | 2.36% | 0.26% | 2.36% |
| P | 0.11% | 9.93% | -.- | -.- | 0.16% | 7.94% | 0.26% | 6.17% |
| K | 0.10% | 7.03% | 0.10% | 7.19% | 0.10% | 6.95% | 0.11% | 6.61% |
| Ti | 0.06% | 7.44% | 0.07% | 7.30% | 0.06% | 7.84% | 0.06% | 7.89% |

Table 3. Preliminary mean CI (Orgueil) weight normalized compositions of lithophiles, siderophiles, and moderately volatile trace elements in Novato, based on using Quadrupole ICP-MS measurements of Novato N01-2b.

| Sample | Lithophiles (n=25) | Siderophiles (n=6) | Mod. Vol. (n=14) |
|---|---|---|---|
| Novato N01-2b-4e (dark) | 1.41 ± 0.11 | 1.37 ± 0.17 | 0.67 ± 0.44 |
| Novato ~50/50 light/dark N01-2b-11,12,17 | 1.53 ± 0.38 | 1.50 ± 1.12 | 0.64 ± 0.43 |
| H chondrite (n=2) mean§ | 1.24 ± 0.07 | 1.94 ± 0.33 | 0.62 ± 0.44 |
| L chondrite (n=19) mean§ | 1.45 ± 0.16 | 1.33 ± 0.11 | 0.72 ± 0.40 |
| LL chondrite (n=7) mean§ | 1.48 ± 0.11 | 0.94 ± 0.08 | 0.65 ± 0.41 |

§ H chondrite mean from Troiano et al. (2011), L (shock stages S1-S3 only) and LL chondrite mean data from Friedrich et al. (2003 and 2004).

Table 4. Abundances of major, minor, and trace elements in the Novato L6 chondrite.

| | | Orgueil (CI Standard) | | UC Davis HR-ICP-MS | | | | | | Fordham Q-ICP-MS |
|---|---|---|---|---|---|---|---|---|---|---|
| | | UC Davis | Reference [a] | Novato 1 (L) | Novato 1 (D) | Novato 6 (L) | Novato 6 (D) | Novato 5 (L) | | Novato 01 (average of 7 fragments) |
| **Li** | ppm | 1.56 | 1.47 | 1.03 | 1.01 | 0.89 | 1.75 | 0.72 | | 1.6 |
| **Be** | ppm | 0.02 | 0.03 | 0.02 | 0.02 | 0.02 | 0.02 | 0.02 | * | |
| **Na** | Wt% | 0.51 | 0.50 | 0.79 | 0.65 | 0.76 | 0.75 | 0.79 | * | |
| **Mg** | Wt% | 9.65 | 9.58 | 14.86 | 12.31 | 12.81 | 15.63 | 14.83 | * | |
| **Al** | Wt% | 0.89 | 0.85 | 1.12 | 0.96 | 1.10 | 1.22 | 1.13 | | |
| **P** | Wt% | 0.12 | 0.10 | 0.11 | 0.14 | 0.07 | 0.13 | 0.09 | * | |
| **K** | Wt% | 0.05 | 0.054 | 0.07 | 0.06 | 0.07 | 0.06 | 0.07 | | |
| **Ca** | Wt% | 0.86 | 0.92 | 1.23 | 1.21 | 0.97 | 1.61 | 1.34 | * | |
| **Sc** | ppm | 6.11 | 5.90 | 8.21 | 7.46 | 6.36 | 10.40 | 9.29 | | 8.27 |
| **Ti** | Wt% | 0.05 | 0.05 | 0.06 | 0.06 | 0.06 | 0.07 | 0.07 | * | 0.056 |
| **V** | ppm | 75.9 | 54.3 | 56.1 | 51.2 | 73.6 | 70.8 | 56.4 | | 58 |
| **Cr** | ppm | 2464 | 2650 | 3098 | 1889 | 3943 | 3319 | 2286 | | |
| **Mn** | Wt% | 0.18 | 0.19 | 0.27 | 0.23 | 0.23 | 0.29 | 0.27 | * | 0.279 |
| **Co** | ppm | 503.3 | 506.0 | 544.5 | 316.8 | 1164.6 | 491.2 | 556.2 | * | 540 |
| **Fe** | Wt% | 20.29 | 18.50 | 20.67 | 19.79 | 27.52 | 21.97 | 21.52 | | |
| **Ni** | Wt% | 1.06 | 1.08 | 1.43 | 0.90 | 3.03 | 1.05 | 1.40 | * | |
| **Cu** | ppm | 137 | 131 | 78.0 | 71.9 | 135 | 53.7 | 70.0 | | 104 |
| **Zn** | ppm | 302 | 312 | 47.0 | 35.7 | 47.4 | 94.7 | 39.9 | | 105 |
| **Ga** | ppm | 9.21 | 9.80 | 5.11 | 2.74 | 4.90 | 4.07 | 4.23 | | 5.1 |
| **As** | ppm | | | | | | | | | 1.2 |
| **Se** | ppm | | | | | | | | | 9.6 |
| **Rb** | ppm | 2.34 | 2.31 | 2.58 | 2.04 | 2.47 | 2.57 | 2.37 | | 2.5 |
| **Sr** | ppm | 7.16 | 7.81 | 9.34 | 7.75 | 8.64 | 9.21 | 9.35 | | 9 |
| **Y** | ppm | 1.64 | 1.53 | 2.30 | 2.83 | 1.29 | 2.40 | 1.61 | | 2.32 |
| **Zr** | ppm | 4.30 | 3.62 | 5.73 | 5.06 | 4.37 | 6.97 | 5.60 | | 7.1 |
| **Nb** | ppm | 0.292 | 0.279 | 0.356 | 0.408 | 0.302 | 0.394 | 0.348 | | 0.47 |
| **Mo** | ppm | | | | | | | | | 2.1 |
| **Ru** | ppm | | | | | | | | | 1.4 |
| **Ag** | ppb | | | | | | | | | 90 |
| **Pd** | ppb | | | | | | | | | 860 |
| **Cd** | ppm | 0.618 | 0.674 | 0.016 | 0.021 | 0.017 | 0.345 | 0.017 | | |
| **Sn** | ppb | | | | | | | | | 370 |
| **Sb** | ppm | 0.160 | 0.130 | 0.083 | 0.052 | 0.140 | 0.066 | 0.093 | | 0.11 |
| **Te** | ppb | | | | | | | | | 650 |
| **Cs** | ppb | 0.183 | 0.189 | 0.003 | 0.004 | 0.004 | 0.015 | 0.004 | | 8 |
| **Ba** | ppm | 2.186 | 2.460 | 2.895 | 2.211 | 2.699 | 2.826 | 3.214 | | 3.1 |
| **La** | ppm | 0.240 | 0.246 | 0.319 | 0.414 | 0.181 | 0.339 | 0.215 | | 0.35 |

| | | | | | | | | | | |
|---|---|---|---|---|---|---|---|---|---|---|
| **Ce** | ppm | 0.665 | 0.600 | 0.909 | 1.187 | 0.502 | 0.950 | 0.604 | | 0.92 |
| **Pr** | ppm | 0.102 | 0.091 | 0.137 | 0.178 | 0.075 | 0.143 | 0.091 | | 0.14 |
| **Nd** | ppm | 0.479 | 0.464 | 0.648 | 0.838 | 0.352 | 0.674 | 0.434 | | 0.63 |
| **Sm** | ppm | 0.157 | 0.152 | 0.212 | 0.273 | 0.118 | 0.224 | 0.145 | | 0.22 |
| **Eu** | ppm | 0.061 | 0.058 | 0.074 | 0.064 | 0.062 | 0.081 | 0.070 | | 0.08 |
| **Gd** | ppm | 0.211 | 0.205 | 0.296 | 0.376 | 0.163 | 0.314 | 0.204 | | 0.29 |
| **Tb** | ppm | 0.041 | 0.038 | 0.056 | 0.071 | 0.032 | 0.061 | 0.040 | | 0.06 |
| **Dy** | ppm | 0.236 | 0.255 | 0.331 | 0.415 | 0.187 | 0.357 | 0.237 | | 0.30 |
| **Ho** | ppm | 0.061 | 0.057 | 0.088 | 0.109 | 0.050 | 0.095 | 0.064 | | 0.08 |
| **Er** | ppm | 0.166 | 0.163 | 0.240 | 0.295 | 0.140 | 0.261 | 0.181 | | 0.22 |
| **Tm** | ppm | 0.026 | 0.026 | 0.036 | 0.043 | 0.022 | 0.040 | 0.028 | | 0.04 |
| **Yb** | ppm | 0.158 | 0.169 | 0.219 | 0.255 | 0.135 | 0.242 | 0.181 | | 0.22 |
| **Lu** | ppm | 0.026 | 0.025 | 0.037 | 0.041 | 0.023 | 0.041 | 0.031 | | 0.04 |
| **Hf** | ppm | 0.098 | 0.106 | 0.137 | 0.123 | 0.104 | 0.172 | 0.140 | * | 0.17 |
| **Re** | ppb | | | | | | | | | 60 |
| **Ta** | ppm | 0.019 | 0.015 | 0.023 | 0.024 | 0.021 | 0.028 | 0.024 | * | |
| **Ir** | ppm | | | | | | | | | 610 |
| **Pt** | ppm | | | | | | | | | 1 |
| **Tl** | ppm | 0.121 | 0.142 | 0.001 | 0.001 | 0.001 | 0.002 | 0.001 | | |
| **Pb** | ppm | 2.644 | 2.630 | 0.060 | 0.045 | 0.069 | 0.062 | 0.045 | | |
| **Th** | ppm | 0.029 | 0.031 | 0.032 | 0.034 | 0.027 | 0.053 | 0.041 | | 0.047 |
| **U** | ppm | 0.008 | 0.008 | 0.006 | 0.005 | 0.013 | 0.017 | 0.050 | | 0.014 |

[a] Reference values for Orgueil taken from Lodders 2003 & 2009. * Calibrated using terrestrial standards, BCR-2, BHVO-2, AGV-2 and JP-1

Methods: At UC Davis, approximately 10-20 mg each of clean sample fragments from Novato 01 (light and dark lithologies, respectively), Novato 06 (light and dark lithologies, respectively), and a pure light lithology of Novato 05 were powdered in a clean agate mortar. Fusion crusts were carefully removed before crushing. The whole rock powders were dissolved in concentrated 3:1 HF-$HNO_3$ mixture, and heated in the oven using stainless steel bombs at 190°C for 96 hours, to ensure complete dissolution of refractory phases, such as chromites. Sample dilution factors were approximately 1,300 for trace element analyses and 45,000 for major element analyses, respectively. Limits of detection (3σ standard deviation of background) vary depending on the elements in question; REEs were in the ppq ($10^{-15}$) level, while higher blank elements such as Na, B, Ni, Cu, Zn, Mg and Ca were 0.1-0.5 ppb. Concentrations were calculated using a calibration curve composed of a number of known meteorite standards (Murchison (CM2), Allende (CV3)) and/or a suite of terrestrial standards (BCR-2, BHVO-2, AGV-2 and JP-1). These standards were measured together with the Novato and Orgueil meteorite samples. Accuracy was assessed by comparing our Orgueil (CI1) data with those of literature values (Lodders 2003 compilation).

Table 5a. Summary of oxygen isotope values for Novato. "n" marks the number of one set of mass spec analyses consisting of 20 cycles of standard-sample comparisons.

| 100% dark | Mass (mg) | Date | $\delta^{17}O'$ | $\delta^{18}O'$ | $\delta^{17}O'$ | $\Delta^{17}O'$ | n |
|---|---|---|---|---|---|---|---|
| N01-2b-1 | 1.3 | Dec. 12, 2012 | 3.688 | 4.856 | 3.688 | 1.124 | 2 |
| N01-2b-1 | 1.9 | Dec. 12, 2012 | 3.808 | 5.076 | 3.808 | 1.128 | 1 |
| N01-2b-1 | 1.9 | Dec. 13, 2012 | 3.577 | 4.593 | 3.577 | 1.152 | 2 |
| N01-2b-1 | 1.8 | Dec. 13, 2012 | 3.613 | 4.722 | 3.613 | 1.120 | 2 |
| N01-2b-15 | 1.2 | Dec. 12, 2012 | 3.695 | 4.813 | 3.695 | 1.154 | 1 |
| N01-2b-15 | 2.0 | Dec. 13, 2012 | 3.658 | 4.698 | 3.658 | 1.177 | 2 |
| N01-2b-15 | 1.7 | Dec. 13, 2012 | 3.611 | 4.605 | 3.611 | 1.180 | 2 |
| N01-2b-15 | 1.7 | Dec. 13, 2012 | 3.651 | 4.781 | 3.651 | 1.127 | 2 |
| N05-1 | 1.1 | Aug. 22, 2013 | 3.907 | 5.229 | 3.907 | 1.146 | 1 |
| N05-1 | 1.7 | Aug. 22, 2013 | 3.765 | 4.938 | 3.765 | 1.158 | 1 |
| N05-1 | 1.1 | Aug. 22, 2013 | 3.741 | 4.864 | 3.741 | 1.173 | 1 |

Table 5b. Summary of chromium isotope values for Novato, compared to mean values from other meteorites.

| | Type | $\varepsilon^{53}Cr$ | $\varepsilon^{54}Cr$ |
|---|---|---|---|
| Novato (Dark) | L6 | 0.23±0.04 | -0.37±0.12 |
| Novato (Light) | L6 | 0.20±0.04 | -0.19±0.13 |
| Chainpur | LL3.4 | 0.24±0.06[a] | -0.47±0.07[b] |
| Chelyabinsk | LL5 | 0.23±0.03[c] | -0.38±0.08[c] |
| Olivenza | LL5 | 0.23±0.06[a] | No data |
| Saint-Séverin | LL6 | 0.28±0.06[a] | -0.41±0.10[b] |
| Knyahinya | L5 | 0.15±0.06[a] | -0.38±0.08[b] |
| Ste.-Marguerite | H4 | 0.13±0.06[a] | -0.39±0.07[b] |
| Kernouvé | H6 | 0.19±0.06[a] | -0.37±0.07[b] |

[a] Trinquier et al. (2008)
[b] Trinquier et al. (2007)
[c] Popova et al. (2013)

Table 6a. Overview of Novato trajectory and orbit determinations (Equinox J2000). Atmospheric drag was ignored. Solutions A-C used the Schiaparelli's equation for correction from apparent to geocentric reference frame, while solution D integrated the orbit to a moment 2 months before impact.

| Novato | (A) 152+164 | (B) 11+210 | (C) All data - Schiaparelli | (D) All data - Integrated orbit |
|---|---|---|---|---|
| Date | 2012-10-18 | 2012-10-18 | 2012-10-18 | 2012-10-18 |
| Time | 02:44:29.88 | 02:44:29.88 | 02:44:29.88 | 02:44:29.88 |
| $RA_\infty$ (deg.) | 281.11±0.79 | 281.28 | 280.79±0.02 | 280.79±0.02 |
| $Dec_\infty$ (deg.) | –30.88±0.63 | –30.60 | –30.48±0.02 | –30.48±0.02 |
| $V_\infty$ (km/s) | 13.35±0.29 | 13.45 | 13.76±0.01 | 13.76±0.01 |
| Long. start (deg.) | 236.5995±0.0032 | <237.0040 | 236.5306±0.0007 | 236.5306±0.0007 |
| Lat. start (deg.) | +36.5357±0.0023 | <+37.3482 | +36.3917±0.0004 | +36.3917±0.0004 |
| H start (km) | 89.0±0.20 | >55.5 | 94.79±0.04 | 94.79±0.04 |
| H end (km) | <82.3 | <46.1 | <45.6 | <45.6 |
| $R.A._g$ (deg.) | 266.76±2.62 | 267.21 | 268.19±0.04 | -.- |
| $Dec_g$ (deg.) | -50.77±7.84 | -50.41 | -48.32±0.26 | -.- |
| $V_g$ (km/s) | 7.64±0.52 | 7.77 | 8.35±0.02 | -.- |
| Epoch (TD) | -.- | -.- | -.- | 2456158.61501 |
| a (AU) | 1.89±0.21 | 1.93 | 2.144±0.010 | 2.146±0.007 |
| q (AU) | 0.9882±0.0012 | 0.98824 | 0.98778±0.00003 | 0.98774±0.00002 |
| e | 0.476±0.059 | 0.4878 | 0.5392±0.0020 | 0.5396±0.0014 |
| i (deg.) | 5.57±1.35 | 5.58 | 5.467±0.053 | 5.461±0.005 |
| ω (deg.) | 347.15±0.76 | 347.26 | 347.333±0.014 | 347.323±0.015 |
| Node (deg.) | 24.942±0.002 | 24.9416 | 24.94129±0.00002 | 24.9871±0.0003 |
| M (deg.) | -.- | -.- | -.- | 304.644±0.023 |
| Convergence Angle (deg.) | 9.0 | 12.5 | 21.4 | 21.4 |

Table 6b. Overview of other known L chondrite falls with atmospheric trajectory and orbit determinations from photographic and video data (Equinox J2000).

| | Jesenice L6 | Innisfree L5 | Novato L6 | Villalbeto de la Peña L6 | Park Forest L5 |
|---|---|---|---|---|---|
| Date | 2009-04-09 | 1977-02-06 | 2012-10-18 | 2004-04-01 | 2003-03-27 |
| Solar Longitude (deg.) | 19.196 | 317.507 | 204.967 | 283.671 | 6.116 |
| Peak Brightness (visual magn. @ 100 km) | –15 | –12.1 | –14 | –18 | –21.7 |
| Kinetic Energy $E_{kin}$ (kt) | 0.004 | 0.0005 | 0.003 | 0.02 | 0.5 |
| Entry Speed $V_\infty$ (km/s) | 13.78±0.25 | 14.54 | 13.81 | 16.9 | 19.5±0.3 |
| Initial Mass (kg) | 170±80 | 12 | 80±35 | 760±150 | 10,000±4,000 |
| Initial Diameter (cm) | 40 | 20 | 30 | 70 | 180 |
| Entry Angle (deg.) | 40.6 | 67.8 | 17.9 | 29.0 | 29.0 |
| Altitude start (km) | 88 | >62 | 95 | >47 | 82 |
| Peak Brightness (km) | 26 | 36 | 43 | 28 | 28 |
| Altitude end (km) | ~18 | 21 | 20.5 | 22.2 | <18 |
| Final Speed (km/s) | 3.0 | 4.7 | -.- | 7.8 | -.- |
| Mass recovered (kg) | 3.61 | 4.58 | 0.4 | 4.6 | 5.2 |
| Semi-major Axis a (AU) | 1.75 ±0.07 | 1.872 ± 0.05 | 2.146 ±0.007 | 2.3 ±0.2 | 2.53 ±0.19 |
| Perihelion Distance q (AU) | 0.9965 ±0.0006 | 0.9862 ±0.0003 | 0.98774 ±0.00002 | 0.860 ±0.007 | 0.811 ±0.008 |
| Eccentricity e | 0.431 ±0.022 | 0.4732 ±0.015 | 0.540 ±0.001 | 0.63 ±0.04 | 0.680 ±0.023 |
| Inclination i (deg.) | 9.6 ±0.5 | 12.28 ±0.3 | 5.461 ±0.005 | 0.0 ±0.2 | 3.2 ±0.3 |
| Argument of Perihelion ω (deg.) | 190.5 ±0.5 | 177.97 ±0.4 | 347.32 ±0.02 | 132.3 ±1.5 | 237.5 ±1.6 |
| Ascending Node Ω (deg.) | 19.196 ±0.001 | 317.507 ±0.001 | 24.9871 ±0.0003 | 283.671 ±0.001 | 6.1156 ±0.0007 |
| K-Ar age (Ma) | 3,020–3,530 | 4,100±300 | 550–1890 | 700 | -.- |
| $^{40}$Ar-$^{39}$Ar age (Ma) | -.- | -.- | 700, 1000 | -.- | -.- |
| U,Th-He age (Ma) | 2,700–1,700 | -.- | 240–680 | -.- | -.- |
| Reference | [1] | [2] | This Work | [3] | [4] |

Notes: [1] = Spurny et al., 2010, Ott et al., 2010; [2] = Halliday et al., 1978; 1981, Beech, 2001 (uncertainty assuming speed uncertain by 0.1 km/s), Heusser et al., 1978; [3] = Llorca et al., 2005; [4] = Brown et al., 2004, Simon et al., 2004.

Table 6c. Overview of measured cosmic ray exposure (CRE) age, calculated collisional lifetime, and the dynamical lifetimes for different source regions. The dynamical lifetimes in bold are consistent with the measured CRE age.

| | Jesenice L6 | Innisfree L5 | Novato L6 | Villalbeto de la Peña L6 | Park Forest L5 |
|---|---|---|---|---|---|
| *CRE age (Ma)* | *3.8±0.3* | *28±3* | *9±1, with collision in last few Ma* | *48±5* | -.- |
| Collisional life time in main belt (Ma): | 6.3 | 4.3 | 5.9 | 8.9 | 11.3 |
| Dynamical time (Ma): | | | | | |
| *Inner belt:* | | | | | |
| Hungaria (i ~ 23º) | 52.4±1.8 | 58.1±2.2 | 19.8±3.2 | **31.6±3.9** | 29.9±2.4 |
| ν6 inner (a < 2.5; i < 4º) | 12.2±1.0 | **20.2±2.3** | **9.4±1.0** | 11.9±2.5 | 13.7±1.3 |
| ν6 inner (a < 2.5; i >4º) | 11.3±0.8 | 11.2±1.0 | **6.1±0.4** | 13.8±1.6 | 12.2±0.7 |
| 4:1 | **5.1±0.6** | 12.9±2.2 | **0.9±0.7** | 2.5±0.3 | 3.8±0.4 |
| 7:2 (a < 2.5 AU) | 21.5±2.3 | **18.9±2.1** | 28.1±8.9 | 15.3±1.2 | 16.3±0.6 |
| 7:2 (a > 2.5 AU) | 19.5±5.8 | 5.0±2.4 | **9.4±5.1** | 7.1±3.9 | 14.9±4.6 |
| ν6 inner (a > 2.5) | 27.8±22.8 | -.- | **15.8±14.8** | ~1.8 | 4.5±2.0 |
| 3:1 (a < 2.5 AU) | 7.0±1.1 | 11.1±2.6 | **3.5±1.8** | 1.2±0.1 | 0.9±0.2 |
| *Central belt:* | | | | | |
| ν6 outer (i ≤ 18º) | 7.1±3.0 | 8.7±1.1 | -.- | 4.4±1.4 | 6.8±1.2 |
| 3:1 (a > 2.5, i > 6º) | **48.1±39.2** | **21.1±16.8** | **2.0±0.6** | 6.8±3.5 | 1.8±0.4 |
| 3:1 (a > 2.5, i < 6º) | **11.1±5.9** | **13.9±7.3** | **2.7±0.9** | 0.8±0.2 | 0.7±0.1 |
| ν6 outer (i > 18º) | ~24.4 | **13.7±4.2** | -.- | -.- | 4.2±1.5 |
| Phocaea (i ~ 22º) | 83.2±14.6 | 78.6±12.7 | 36.9±15.8 | **82.8±38.2** | 37.2±8.2 |
| Teutonia | 7.5±1.3 | 12.0±2.4 | **3.7±0.4** | 1.3±0.1 | 0.7±0.1 |
| 8:3 | 17.7±7.3 | **12.5±6.4** | **0.9±0.5** | 1.0±0.3 | 2.4±0.7 |
| 5:2 | **7.3±3.4** | **9.3±7.7** | **6.3±3.7** | 0.5±0.1 | 0.4±0.1 |
| *Outer belt:* | | | | | |
| 2:1 | ~10.7 | ~10.6 | -.- | -.- | 0.7±0.5 |

Table 7. Summary of the infrasound signal measurements as recorded by I57US, located 310 km from the fireball trajectory terminal point.

| | Arrival 1 | Arrival 2 |
|---|---|---|
| Arrival time (UT) | 3:25:02 | 3:26:00 |
| Delay time (s) | 2348 | 2452 |
| Celerity (km/s) | 0.311 | 0.303 |
| Max. Amplitude (Pa) | 0.012±0.005 | 0.039±0.010 |
| Max peak-to-peak amplitude (Pa) | 0.020±0.011 | 0.054±0.020 |
| Period of maximum Amplitude (s) | 0.7±0.0 | 0.6±0.1 |
| Frequency at Maximum PDS (Hz) | 1.48 | 1.58 |
| Period at Maximum PSD (s) | 0.7 | 0.6 |
| Total Duration (s) | 45 | 90 |
| Trace Velocity (km/s) | 0.363 | 0.363 |
| Observed Back Azimuth (deg.) | 309.6 | 309.6 |

Table 8a. Massic activities (corrected to the time of fall) of cosmogenic radionuclides (in dpm $kg^{-1}$) in the 60.1 g specimen of the Novato L6 chondrite measured by non-destructive gamma-ray spectroscopy. Errors include a 1σ uncertainty of ~10% in the detector efficiency calibration.

| Nuclide | Half-life | Activity |
|---|---|---|
| $^{52}$Mn | 5.591 d | 20 ± 9 |
| $^{48}$V | 16.0 d | 20 ± 3 |
| $^{51}$Cr | 27.7 d | 35 ± 7 |
| $^{7}$Be | 53.1 d | 81 ± 12 |
| $^{58}$Co | 70.9 d | 9 ± 1 |
| $^{56}$Co | 77.3 d | 6 ± 1 |
| $^{46}$Sc | 83.8 d | 9 ± 1 |
| $^{57}$Co | 271.8 d | 14 ± 2 |
| $^{54}$Mn | 312.3 d | 104 ± 11 |
| $^{22}$Na | 2.60 y | 108 ± 10 |
| $^{60}$Co | 5.27 y | < 1.4 |
| $^{44}$Ti | 60 y | < 2.8 |
| $^{26}$Al | $7.05 \times 10^5$ y | 61.1 ± 5.4 |

Table 8b. Concentrations of U, Th and K (ng $g^{-1}$ for U and Th and in μg $g^{-1}$ for K) in the 60.1 g specimen of the Novato L6 chondrite based on the measured activities of their long-lived radioactive isotopes measured by non-destructive gamma-ray spectroscopy. Errors include a 1σ uncertainty of ~10% in the detector efficiency calibration.

| Element | Concentration |
|---|---|
| U (ppb) | 13 ± 2 |
| Th (ppb) | 44 ± 5 |
| K (ppm) | 901 ± 92 |

Table 9a. Noble gas (He, Ne, Ar) analysis of two samples, 22.8 mg of N01-2b-7 and 47.8 mg of N01-2b-14.

| # | Mass | $^{3}He/^{4}He$ | $^{4}He$ | $^{20}Ne/^{22}Ne$ | $^{21}Ne/^{22}Ne$ | $^{22}Ne$ | $^{36}Ar/^{38}Ar$ | $^{40}Ar/^{36}Ar$ | $^{36}Ar$ |
|---|---|---|---|---|---|---|---|---|---|
| 2b-7 | 22.80±0.05 | 0.0748±0.0001 | 130.0±0.3 | 0.894±0.005 | 0.918±0.004 | 2.75±0.01 | 2.98±0.01 | 424±1 | 1.69±0.06 |
| 2b-14 | 47.80±0.10 | 0.0621±0.00009 | 150.0±0.3 | 0.913±0.003 | 0.918±0.03 | 2.69±0.008 | 0.583* | 611* | n.d. |
| light small | 2.52±0.010 | 0.0833±0.0013 | 123±2 | 0.87±0.18 | 0.927±0.017 | 2.9±0.8 | 2.0±0.8 | | 0.9±0.3 |
| light | 16.16±0.02 | 0.0906±0.0005 | 107.8±0.4 | 0.864±0.009 | 0.9214±0.0026 | 2.58±0.04 | 1.215±0.012 | 477±16 | 0.417±0.003 |
| dark small | 2.31±0.010 | 0.0774±0.0013 | 131±2 | 0.75±0.21 | 0.933±0.020 | 2.7±1.1 | 1.6±0.8 | 1659±772 | 0.8±0.3 |
| 90% dark | 18.50±0.10 | 0.0686±0.0006 | 141.5±0.9 | 0.891±0.008 | 0.907±0.003 | 2.66±0.04 | 2.903±0.019 | 470±11 | 1.544±0.009 |
| dark | 18.47±0.01 | 0.0449±0.0002 | 228.8±0.5 | 0.878±0.007 | 0.9104±0.0023 | 2.71±0.03 | 2.503±0.019 | 1042±27 | 1.014±0.005 |

| | $^{3}He_{cos}$ | $^{21}Ne_{cos}$ | $^{38}Ar_{cos}$ | $3/21_{cos}$ | $22/21_{cos}$ | T3** | T21** | T38** | He-loss |
|---|---|---|---|---|---|---|---|---|---|
| 2b-7 | 9.69±0.03 | 2.52±0.33 | 0.284±0.003 | 3.84±0.51 | 1.09±0.005 | 4.93 | 6.45 | 5.91 | 20% |
| 2b-14 | 9.34±0.02 | 2.47±0.32 | n.d. | 3.78±0.49 | 1.09±0.003 | 4.76 | 6.32 | n.d. | 25% |
| light small | 10.27±0.06 | 2.67±0.07 | 0.33±0.17 | 3.85±0.10 | 1.079±0.020 | 5.23 [6.31] | 6.81 [6.92] | (6.83) ([6.79]) | 23% |
| light | 9.77±0.04 | 2.376±0.010 | 0.312±0.005 | 4.110±0.024 | 1.085±0.003 | 4.98 [6.02] | 6.07 6.36] | 6.48 [6.50] | 21% |
| dark small | 10.16±0.06 | 2.56±0.08 | 0.40±0.26 | 3.97±0.12 | 1.072±0.023 | 5.17 [6.23] | 6.53 [6.37] | (8.34) ([8.20]) | 21% |
| 90% dark | 9.70±0.07 | 2.410±0.017 | 0.279±0.007 | 4.03±0.04 | 1.103±0.004 | 4.94 [6.00] | 6.15 [7.01] | 5.81 [5.98] | 17% |
| dark | 10.27±0.04 | 2.465±0.009 | 0.247±0.005 | 4.168±0.023 | 1.0984±0.028 | 5.23 [6.35] | 6.29 [7.03] | 5.14 [5.25] | 8% |

| | $^{4}He_{rad}$ | $^{40}Ar_{rad}$ | R4*** | R40*** |
|---|---|---|---|---|
| 2b-7 | 76.3 | 719 | 287 | 1450 |
| 2b-14 | 99.1 | 611 | 370 | 1300 |
| light small | 65±5 | 680±410 | 245 | (1400) |
| light | 53±4 | 205±8 | 200 | 550 |
| dark small | 74±5 | 1510±960 | 280 | (2310) |
| 90% dark | 87±4 | 726±18 | 325 | 1460 |
| dark | 171±5 | 1074±27 | 630 | 1890 |

Notes: All concentrations are given in $10^{-8}$ $cm^3$ STP/g. Typical errors for samples 7 and 14 are ~3% for concentrations and ~0.5% for ratios. The samples, wrapped in an aluminum foil, were exposed to ultra-high vacuum for several days and pre-heated at ~90ºC. The gases were extracted by pyrolysis in a Mo crucible in a single temperature step at ~1800°C (extraction for 30 min). Complete release of Kr and Xe was checked with a re-extraction step at the same temperature, which contributed 18–23% of the totally released Kr and 8-15% of the Xe. Argon was separated from He and Ne using a charcoal cooled with liquid nitrogen.

*For N1-14, $^{36}Ar$ was not measured. The concentrations of $^{38}Ar$ and $^{40}Ar$ are given instead of the $^{36}Ar/^{38}Ar$ and $^{40}Ar/^{36}Ar$ ratios, respectively. The radiogenic 4He is based on a cosmogenic $^{4}He/^{3}He$ ratio of 5.5.

** Cosmic-ray exposure age in Ma, calculated with the following production rates derived from Leya and Masarik (2009), in $10^{-8}$ $cm^3$STP/gMa: $^{3}He$ = 1.96; $^{21}Ne$ = 0.392;

$^{38}Ar = 0.0481$.

***Gas-retention age in Ma, calculated assuming L chondritic abundances of K, U, Th (Wasson and Kallemeyn, 1988). The two “small” samples of 2.3 and 2.5 mg, respectively, were measured initially to verify the presence of solar noble gases that could otherwise harm the detectors. The small samples released sufficiently abundant He and Ne but the Ar, K and Xe abundances were too small for precise measurements.

Table 9b. Krypton abundances and isotope ratios ($^{84}Kr = 100$) in Novato samples.

| Sample | $^{84}Kr$ | $^{78}Kr/^{84}Kr$ | $^{80}Kr/^{84}Kr$ | $^{82}Kr/^{84}Kr$ | $^{83}Kr/^{84}Kr$ | $^{86}Kr/^{84}Kr$ |
|---|---|---|---|---|---|---|
| light small | 1.7±0.6[a] | 1.1±0.8 | 5.3±2.0 | 18±8 | 23±14 | 36±18 |
| light | 1.00±0.14[b] | 0.68±0.16 | 4.5±0.8 | 20±4 | 20±4 | 29±5 |
| dark small | 1.4±0.6[a] | n.d. | 7±3 | 20±12 | 31±22 | 35±23 |
| dark | 1.56±0.10[c] | 0.52±0.10[d] | 4.2±0.5 | 20.3±1.7 | 20.7±1.9 | 30±3 |
| 90% dark | 1.95±0.10[c] | 0.53±0.07 | 4.1±0.4 | 20.9±1.8 | 21.2±1.8 | 31.9±2.6 |

[a] no Kr detected in re-extraction.

[b] no check for complete degassing by re-extraction, 20±3% added based on $^{84}Kr$ amount released in re-extraction of the "dark" and "90% dark" samples.

[c] the re-extraction steps of "dark" and "90% dark" released 23% and 18%, respectively, of each total. Isotope abundances of both extraction steps were added - where detected.

[d] peak $^{78}Kr$ in re-extraction step not correctly centered and not considered to calculate ratio.

n.d. = not detected, concentrations are given in $10^{-10}$ $cm^3$ STP/g.

Table 9c. Xenon abundances and isotope ratios ($^{132}$Xe = 100) in Novato samples.

| Sample | $^{132}$Xe | $^{124}$Xe /$^{132}$Xe | $^{126}$Xe /$^{132}$Xe | $^{128}$Xe/ $^{132}$Xe | $^{129}$Xe /$^{132}$Xe | $^{130}$Xe /$^{132}$Xe | $^{131}$Xe /$^{132}$Xe | $^{134}$Xe /$^{132}$Xe | $^{136}$Xe/ $^{132}$Xe |
|---|---|---|---|---|---|---|---|---|---|
| light small | 0.66±0.06 | 0.5±0.4 | n.d. | 5.7±1.2 | 127±14 | 14.3±1.7 | 82±13 | 41±7 | 33±5 |
| light | 1.00±0.04 | 0.52±0.03 | 0.425±0.028 | 8.1±0.4 | 112±6 | 16.1±0.9 | 81±5 | 36.5±2.0 | 31.8±1.8 |
| dark small | 0.99±0.07 | n.d. | 0.79±0.27 | 8.1±1.1 | 119±10 | 16.1±1.4 | 88±8 | 36±5 | 33±4 |
| dark | 1.252±0.025 | 0.474±0.028 | 0.427±0.027 | 8.2±0.3 | 108±4 | 16.4±0.7 | 80±3 | 38.0±1.5 | 31.6±1.3 |
| 90% dark | 0.959±0.025 | 0.44±0.03 | 0.38±0.04 | 8.0±0.4 | 114±6 | 15.5±0.9 | 82±4 | 38.7±2.0 | 31.7±1.7 |

n.d. = not detected, concentrations are given in $10^{-10}$ cm$^3$ STP/g.

Table 10. Thermoluminescence data for the light and dark lithologies of the Novato meteorite*.

| | NTL (krad) | TL sens (Dhajala=1) | Tp ($^{o}$C) | Wp ($^{o}$C) |
|---|---|---|---|---|
| Novato dark lithology | 6.6±1.8 | 0.028±0.007 | 180±20 | 155±15 |
| Novato light lithology | 12.8±2.8 | 0.029±0.007 | 187±14 | 153±18 |

* Uncertainties are one sigma based on triplicates.

Table 11. Summary of $^{1}H$ NMR section integrals for chondritic and melt crust methanolic extracts

| $\delta(^{1}H)$ [ppm] | Novato light | Novato dark |
|---|---|---|
| 10.0 - 5.0 | 4.4 | 6.1 |
| 5.0 - 3.1 | 11.5 | 9.9 |
| 3.1 - 1.9 | 10.3 | 9.8 |
| 1.9 - 1.35 | 16.1 | 19.7 |
| 1.35 - 1.25 | 31.9 | 25.8 |
| 1.25 - 1.0 | 10.6 | 13.8 |
| 1.0 - 0.5 | 15.2 | 15.0 |
| SUM | 100.0 | 100.0 |

Table 12. Summary of the amino acid analysis of the light and dark lithologies from methanol spray sampling of the Novato N01-2a meteorite.

| Amino Acid | Novato light (ppb) | D/L ratio | Novato dark (ppb) | D/L ratio |
|---|---|---|---|---|
| D-Aspartic acid | 53 ± 2 | 0.19 ± 0.01 | 23 ± 4 | 0.25 ± 0.05 |
| L-Aspartic acid | 281 ± 1 | | 90 ± 8 | |
| D-Glutamic acid | 83 ± 5 | 0.11 ± 0.01 | 47 ± 9 | 0.15 ± 0.03 |
| L-Glutamic acid | 768 ± 54 | | 316 ± 5 | |
| D-Serine | < 4 | < 0.01 | < 2 | < 0.01 |
| L-Serine | 444 ± 13 | | 199 ± 54 | |
| Glycine | 398 ± 152 | -.- | 111 ± 17 | -.- |
| β-Alanine | < 3 | -.- | < 3 | -.- |
| γ-Amino-n-butyric acid | 9 ± 2 | -.- | 7 ± 1 | -.- |
| D-Alanine | 18 ± 2 | 0.15 ± 0.09 | 9 ± 1 | 0.12 ± 0.04 |
| L-Alanine | 120 ± 71 | | 76 ± 25 | |
| D-β- Amino-n-butyric acid | 3 ± 2[b] | ~ 1 | 2 ± 1[b] | ~1 |
| L-β- Amino-n-butyric acid | 3 ± 2[b] | | 2 ± 1[b] | |
| α-Aminoisobutryic acid | 6 ± 2[b] | -.- | 7 ± 3[b] | -.- |
| DL-α-Amino-n-butyric acid[c] | 6 ± 5[b] | nd | 8 ± 5[b] | nd |
| DL-Isovaline | < 5 | nd | < 5 | nd |
| ε-Amino-n-caproic acid | 8 ± 6 | -.- | 15 ± 2 | -.- |
| D-Valine | 9 ± 3 | 0.06 ± 0.02 | < 6 | < 0.19 |
| L-Valine | 144 ± 2 | | 32 ± 7 | |

Notes: [a]Novato N01-2a meteorite methanol extracts (light and dark lithologies) were analyzed by OPA/NAC derivatization (15 min.) and LC separation with UV fluorescence (LC-FD) and time of flight mass spectrometry (TOF-MS) detection. For the LC-FD/TOF-MS data, the fluorescence peaks and the mono-isotopic masses of each protonated OPA/NAC amino acid derivative ($M + H^+$) was used for quantification and final peak integrations included background level correction using a procedural blank and a comparison of the peak areas with those of an amino acid standard run on the same day. The final values were normalized using the desalting and derivatization recoveries of an internal D,L-norleucine standard (recoveries ranged from 60-70% for the meteorite extracts). The uncertainties (δx) are based on the standard deviation of the average value of three separate measurements (n) with a standard error, $\delta x = \sigma_x \cdot (n-1)^{-1/2}$.

[b]Tentatively detected above blank levels.

[c]Enantiomers could not be separated under the chromatographic conditions.

Table 13. Carbon and Nitrogen stepped combustion data from Novato N01-1e.

| Temp. (°C) | | Total (< 1400) | | | 200-400 | | | 400-600 | | |
|---|---|---|---|---|---|---|---|---|---|---|
| | **Wt. (mg)** | **[C] (ppm)** | **$\delta^{13}C$ (‰)** | **C/N (at)** | **[C] (ppm)** | **$\delta^{13}C$ (‰)** | **C/N (at)** | **[C] (ppm)** | **$\delta^{13}C$ (‰)** | **C/N (at)** |
| Dark | 4.788 | 611.3 | -39 | -.- | 76.9 | -24 | 11-22 | 439.5 | -43 | 53-215 |
| Light | 6.089 | 97.6 | -27 | -.- | 33.8 | -26 | 58 | 14.9 | -25 | 28 |
| | | **[N] (ppm)** | **$\delta^{15}N$ (‰)** | | **[N] (ppm)** | **$\delta^{15}N$ (‰)** | | **[N] (ppm)** | **$\delta^{15}N$ (‰)** | |
| Dark | 4.788 | 13.9 | +4.8 | | 6.0 | +1.9 | | 4.8 | +2.0 | |
| Light | 6.089 | 3.0 | -2.1 | | 0.7 | -4.4 | | 0.6 | -2.6 | |

Note: Experimental procedures were as follows. Uncrushed chips of material were weighed into platinum foil, then loaded into the Finesse SC-GC-MS system. The samples were heated under pure oxygen for ~ 40 minutes at each temperature; the resulting combustion products were then cryogenically separated for analysis into carbon dioxide and nitrogen. Sulfur dioxide and water were also produced and separated, but not analyzed. The temperature program for the experiments was of increments of 100°C from room temperature to 1400°C. $CO_2$ and $N_2$ were analyzed on separate triple collector gas-source mass spectrometers. Errors on the analyses were ± 1 ‰ for $CO_2$, with the minimum amount of gas measured ~ 1 ng. For nitrogen, the error on the analysis was ± 0.5 ‰, and minimum sample size was ~ 0.5 ng.